

UCSF

UC San Francisco Electronic Theses and Dissertations

Title

The role of the MADS domain transcription factor MEF2C in cardiac and skeletal muscle metabolism

Permalink

<https://escholarship.org/uc/item/7p54s4qh>

Author

Anderson, Courtney Meghan

Publication Date

2010

Peer reviewed|Thesis/dissertation

The role of the MADS domain transcription factor MEF2C in
cardiac and skeletal muscle metabolism

by

Courtney Meghan Anderson

DISSERTATION

Submitted in partial satisfaction of the requirements for the degree of

DOCTOR OF PHILOSOPHY

in

Biomedical Sciences

in the

GRADUATE DIVISION

of the

UNIVERSITY OF CALIFORNIA, SAN FRANCISCO

Dedication:

This work is dedicated to my parents, Michael and Sheila Brown. I owe everything I am to them.

Acknowledgments:

First and foremost, I would like to thank my graduate advisor, Brian Black. He has been an exceptional mentor to me throughout my graduate career. The first thing that appealed to me about working in Brian's lab was his unparalleled enthusiasm for science. He has a thirst for data and science unlike any other PI I have come across, and that excitement motivated me tremendously. He taught me to be a rigorous scientist, think critically, and delve deeply into the biology. I know I was not the easiest of students for him to deal with and I struggled with the rigors of graduate school, but Brian always had faith in me and kept pushing me to strive for more. I am truly grateful to him for all that I have learned over the years in graduate school, and I will never forget all of the lessons, in science and in life, that he has taught me.

Brian also has developed a fantastic workplace environment. He has selected an amazing group of scientists, both intellectually and socially. The Black Lab is the most collaborative, intelligent, and humorous collection of scientists I have encountered. It has been such a pleasure to work alongside these wonderful people, and it has been an honor to call them not only my colleagues, but also my friends. There are several lab members in particular I would like to acknowledge who have helped with the work presented in this thesis. Analeah Heidt, who was a tremendous help in getting me started in the lab and was a collaborator on the skeletal muscle knockout project, has been a wonderful friend and role model. I am also extremely thankful for Jillian Jarrett and all of her hard work in maintaining our mouse colony and keeping the lab so well organized.

My thesis committee members, Robert J. Farese Jr. and Roger Cooke, have been instrumental in guiding me throughout my graduate career, and I thank them for providing valuable insight and perspective on my thesis work. I also would like to acknowledge the Biomedical Sciences (BMS) program administrators, especially Lisa Magargal, who has been an immense help in guiding students through the program.

My graduate work really and truly took a turn for the better after I met my husband, Sean Anderson. It is not easy being married to a scientist – the late nights, numerous weekends, and grossly underestimating how long an experiment will take as they wait in the car all require a tremendous amount of patience from a spouse. Sean has been an amazing husband in dealing with all of this, and I am extremely grateful to have him by my side. I look forward to our future together, and will work on minimizing the wait time in the car!

I would have never even made it to San Francisco, let alone graduate from UCSF, if it were not for the constant love and support (and financial help!) from my wonderful family back on the East Coast. It was difficult to leave them, but they were always there for me to listen to my struggles and celebrate my triumphs. In particular, my mother, Sheila Brown, has been an amazing source of inspiration and love. Her own struggles in life motivated me to work as hard as possible and make her proud. I cannot thank her enough for all that she has sacrificed for me, and I promise to continue making her proud.

Last, but certainly not least, I would like to thank my father, Michael Brown. He was the one who first inspired me to study biology. My father may still not be with us, but I know somewhere he is looking down at me and smiling. I promised him I would become a doctor, and now I am.

Abstract:

**The role of the MADS domain transcription factor MEF2C in
cardiac and skeletal muscle metabolism**

by

Courtney Meghan Anderson

The MADS domain transcription factor family MEF2 is a critical regulator of a number of diverse developmental programs, including cardiovascular, skeletal muscle, neural crest, vasculature, and bone development. One isoform of MEF2, MEF2C, plays a particularly critical role in the formation of the heart and the differentiation of skeletal muscle.

MEF2C is a signal-dependent transcription factor that can function as either an activator or a repressor, depending on cofactor interactions and posttranslational modifications. Recently, an isoform of the SAP domain protein Myocardin, Myocardin-935, has been identified as a potent coactivator of MEF2C activity, yet the targets of MEF2C-Myocardin and the transcriptional mechanisms that control Myocardin coactivation of MEF2C remain unresolved. In chapter 2, we identified a highly conserved transcriptional enhancer from the *Ampkα2* gene that is sufficient to direct expression exclusively to the myocardium during development and in adulthood. *Ampkα2* encodes a subunit of the 5'-AMP-activated protein kinase (AMPK), an energy-sensing enzyme that maintains cellular energy homeostasis and controls cardiac metabolism by regulating fatty acid oxidation, glycolysis, and glucose uptake. We show that the *Ampkα2*

myocardial enhancer requires a MEF2C-Myocardin complex for activity *in vivo* and *in vitro*, and that this complex regulates *Ampkα2* expression through two essential, highly conserved MEF2 sites in the enhancer.

In addition to regulating genes in the heart, MEF2C is also a potent transcriptional co-activator of many genes and proteins in skeletal muscle, such as GLUT4 and PGC1 α . In chapter 3, we sought to determine the requirement of *Mef2c* in skeletal muscle by generating a conditional knockout mouse. Using two independent, transgenic Cre lines, we determined that *Mef2c* is required in skeletal muscle for overall body size. Mice lacking *Mef2c* also have defective fiber type composition and mild glycogen accumulation, but these impairments do not have an effect on exercise abilities. Lastly, we show that MEF2C may function downstream of insulin receptor signaling through a p38 MAPK signaling pathway in skeletal muscle.

Table of Contents:

Dedication.....iii

Acknowledgements.....iv

Abstract.....vi

List of Figures and Tables.....ix

Chapters:

1. General Introduction.....1

2. A MEF2C-Myocardin complex directly regulates the cardiac metabolic master
regulatory gene *Ampk α 2* through a conserved myocardial-specific enhancer.....13

3. MEF2C function in skeletal muscle is required for normal growth and glucose
metabolism.....55

4. General Conclusions.....104

5. Materials and Methods.....108

6. References.....142

List of Figures and Tables:

Figure 2-1: A highly conserved noncoding element resides within the intronic region of <i>Ampkα2</i>	41
Figure 2-2: The <i>Ampkα2-lacZ</i> transgene is expressed in the myocardium throughout development and postnatally in line 931.....	42
Figure 2-3: The <i>Ampkα2-lacZ</i> transgene is expressed in the myocardium throughout development and postnatally in line 932.....	43
Figure 2-4: <i>Ampkα2</i> is expressed in the heart during the earliest stages of cardiac development and maintains expression throughout development and postnatally.....	43
Figure 2-5: Deletional analysis of the <i>Ampkα2</i> myocardial enhancer identifies a highly conserved element that is necessary and sufficient for enhancer function <i>in vivo</i>	44
Figure 2-6: Sequence analysis of the <i>Ampkα2</i> myocardial enhancer reveals conserved binding sites for MEF2, NKX, and GATA transcription factors.....	45
Figure 2-7: The <i>Ampkα2</i> myocardial enhancer contains a high-affinity GATA binding site that is not required for activity of the enhancer.....	46
Figure 2-8: The <i>Ampkα2</i> myocardial enhancer contains a high-affinity NKE binding site that is not required for activity of the enhancer.....	47
Figure 2-9: The <i>Ampkα2</i> myocardial enhancer is dependent on two high-affinity MEF2 binding sites.....	48
Figure 2-10: The <i>Ampkα2</i> myocardial enhancer is dependent on both conserved MEF2 sites for function <i>in vivo</i>	50
Figure 2-11: MEF2C is required in <i>trans</i> for activation of the enhancer, but not for endogenous <i>Ampkα2</i> expression.....	51
Figure 2-12: MEF2C and Myocardin may form a ternary complex and synergistically activate the <i>Ampkα2</i> myocardial enhancer.....	52
Figure 2-13: The synergistic activation of the <i>Ampkα2</i> myocardial enhancer and other MEF2-dependent reporters by MEF2C and Myocardin requires the Myocardin leucine-zipper motif	53
Figure 2-14: A model for the regulation of MEF2-dependent genes by MEF2C and Myocardin.....	54

Figure 3-1: The <i>Myogenin</i> -1565-Cre transgene directs Cre expression exclusively in skeletal muscle	84
Figure 3-2: Generation of skeletal-muscle specific <i>Mef2c</i> conditional knockout mice...	85
Figure 3-3: Both the <i>Mef2c</i> -73K-Cre transgene and the <i>Myogenin</i> -1565-Cre transgene efficiently delete <i>Mef2c</i> from skeletal muscle.....	86
Figure 3-4: Mice lacking <i>Mef2c</i> in skeletal muscle are viable but are significantly smaller during the weaning period.....	88
Figure 3-5: Mice lacking <i>Mef2c</i> in skeletal muscle remain smaller in size during adulthood and have smaller organ size.....	90
Figure 3-6: Deletion of <i>Mef2c</i> in skeletal muscle results in shorter tibia length.....	92
Figure 3-7: Deletion of <i>Mef2c</i> in skeletal muscle by the <i>Myogenin</i> -1565-Cre transgene, but not by the <i>Mef2c</i> -73K-Cre transgene, results in smaller muscle and fiber size.....	93
Figure 3-8: Mice lacking <i>Mef2c</i> in skeletal muscle have fewer slow-twitch skeletal muscle fibers.....	95
Figure 3-9: Mice lacking <i>Mef2c</i> in skeletal muscle do not have impairments in voluntary running ability.....	96
Figure 3-10: Deletion of <i>Mef2c</i> in skeletal muscle by the <i>Mef2c</i> -73K-Cre transgene results in accumulation of glycogen in vacuoles in muscle fibers post-exercise.....	98
Figure 3-11: Deletion of <i>Mef2c</i> in skeletal muscle by the <i>Mef2c</i> -73K-Cre transgene, but not by the <i>Myogenin</i> -1565-Cre transgene, results in increased glycogen accumulation in the muscle fibers post-exercise.....	99
Figure 3-12: Deletion of <i>Mef2c</i> in skeletal muscle by the <i>Mef2c</i> -73K-Cre transgene results in better tolerance of glucose but has no effect on insulin resistance.....	101
Figure 3-13: Activation of MEF2C by insulin receptor stimulation.....	102
Figure 3-14: Insulin-stimulated myofiber hypertrophy requires p38-MAPK phosphorylation.....	103
Table 1: <i>Mef2c</i> skeletal muscle conditional knockout phenotypes.....	71
Table 2: List of EMSA probes.....	124

Chapter 1: General Introduction

MEF2 family of transcription factors

The myocyte enhancer factor 2 (MEF2) family of transcription factors plays an important role in cardiac and skeletal muscle development and metabolism. MEF2 proteins have a MADS (MCM1, agamous, deficiens, serum response factor) domain and a MEF2 domain at their N-termini, through which dimerization, DNA binding, and cofactor interactions occur (Black and Olson, 1998). MEF2 proteins can homodimerize or heterodimerize and bind to the consensus DNA sequence YTAWWWWTAR (Black and Olson, 1998). The C-terminal regions function as transcriptional activation domains, and can undergo posttranslational modifications that either activate or repress MEF2 proteins (Black and Cripps, 2010).

There are four vertebrate *Mef2* genes, *Mef2a*, *-b*, *-c*, and *-d*. *Mef2c* is the earliest to be expressed in the mouse heart, with expression beginning around embryonic day E7.5 in cardiac mesoderm (Edmondson et al, 1994). *Mef2c* is crucial for cardiac development, as mice that lack *Mef2c* die by E9.5 due to cardiac looping defects and as a consequence have a single ventricle (Lin et al, 1997). *Mef2c* is also expressed in skeletal muscle precursors within the somites of the mouse embryo beginning at E9.0 (Edmondson et al, 1994). A recent study examining the requirement of *Mef2c* in skeletal muscle in inbred mice showed that *Mef2c* is required for sarcomere integrity and postnatal muscle maturation (Potthoff et al, 2007c). However, because these mice die by postnatal day 2, the role of *Mef2c* in adult muscle function in the mouse has not been determined previously. In zebrafish, MEF2C and MEF2D are required together for thick

filament assembly but not for differentiation or thin filament formation (Hinitz and Hughes, 2007).

One way in which the activity of MEF2 proteins is regulated is through their interaction with class II HDACs. Increases in cytoplasmic calcium result in the activation of the phosphatase calcineurin, which then activates calcium/calmodulin-dependent kinases (CaMK) I, II, and VI. Class II HDACs (HDAC4, -5, -7, and -9) reside in the nucleus, where they are bound to MEF2 transcription factors and repress MEF2 activity (Miska et al, 1999; Lu et al, 2000a). Upon phosphorylation by CaMK, class II HDACs interact with 14-3-3 proteins and are shuttled out of the nucleus (McKinsey et al, 2000; Choi et al, 2001; McKinsey et al, 2001), leading to the derepression of MEF2 proteins and activation of MEF2 target genes (Zhang et al, 2002).

MEF2 proteins also undergo extensive posttranslational modifications, which can affect their function as transcriptional activators or repressors (reviewed in Black and Cripps, 2010). There are several signaling pathways involved in MEF2 modifications. In particular, MEF2 proteins are phosphorylated by MAP kinase (MAPK) signaling pathways, in which the MAP3Ks phosphorylate the MAP2Ks MKK6 and MKK3, which then phosphorylate and activate p38 MAPK (Keren et al, 2006). Activated p38 MAPK then directly phosphorylates MEF2A and MEF2C at specific residues, promoting MEF2 proteins as transcriptional activators (Han et al, 1997; Ornatsky et al, 1999; Zhao et al, 1999; Khiem et al, 2008).

MEF2 proteins generally require interaction with co-factors to regulate transcription of MEF2 target genes (Black and Cripps, 2010). These co-factors can be other transcription factors that bind DNA and interact with MEF2, or they can be non-

DNA-binding proteins that regulate MEF2 activity solely through protein-protein interactions, such as the SAP domain protein Myocardin (Black and Cripps, 2010). Alternative splicing of Myocardin produces two isoforms: a short form, Myocardin-856, which is expressed in smooth muscle, and a long form, Myocardin-935, which is expressed in cardiac muscle (Creemers et al, 2006). Myocardin-935 interacts with MEF2C through its N-terminal domain, and synergizes with MEF2C to activate transcription of MEF2-dependent genes (Creemers et al, 2006). Furthermore, Myocardin molecules dimerize with each other through their leucine zipper (LZ) domains (Wang et al, 2003). In smooth muscle, Myocardin preferentially activates genes with two CaRG boxes bound by serum response factor (SRF) by dimerization through the LZ domain (Wang et al, 2003).

Heart development

The heart is the first organ to form in the vertebrate, beginning around E6.5 in the mouse embryo (reviewed in Buckingham et al, 2005). Cardiac progenitor cells originate in the primitive streak and are derivatives of the mesodermal germ layer. These cells migrate away from the primitive streak to form the cardiac crescent and differentiate at E7.5. The crescent then fuses at the midline to form a linear heart tube at E8.0, and then undergoes cardiac looping around E8.5. By E9.5 the four chambers of the heart become evident, and by E14.5 the chambers are separated and the heart is essentially fully formed (Buckingham et al, 2005). The developing heart consists of two population of cells: the first heart field, which will give rise to the left ventricle and atria and contribute some cells to the right ventricle, and the second heart field, which will give rise to the right

ventricle and outflow tract, as well as contribute some cells to the atria and inflow pole of the heart (Buckingham et al, 2005). Our lab has identified an enhancer for *Mef2c* that directs transgene expression to the second heart field and its derivatives in the right ventricle and outflow tract and is regulated by GATA4 and ISL1-1, a known marker of the second heart field (Cai et al, 2003; Dodou et al, 2004).

The heart has one of the highest energy demands of any organ in the body. Energy in the form of ATP is required in order to sustain contractile function and continually supply blood to the rest of the body (Lopaschuk and Jaswal, 2010). Interestingly, there are practically no energy reserves in the heart and it must constantly produce energy in the form of adenosine triphosphate (ATP) (Lopaschuk et al, 2010). The heart has several ways to maintain constant ATP production. In the early embryo, the developing cardiac precursor cells use glycolysis as a source of energy (Chung et al, 2010). However, upon differentiation and maturation into a cardiomyocyte, the mature cell predominantly uses mitochondrial oxidation of fatty acids to produce ATP (Chung et al, 2007), which is a more efficient method for generating energy and allows for greater oxygen consumption and increased ATP production by the heart (Lopaschuk and Jaswal, 2010).

The master metabolic switch, AMPK

5'-adenosine monophosphate-activated protein kinase (AMPK) is one of the key molecules regulating cardiac energy metabolism because it can increase ATP production in the heart by stimulating glucose uptake, glycolysis, and fatty acid oxidation (Arad et al, 2007). AMPK is a heterotrimeric enzyme composed of three subunits: $\alpha 1$ and $\alpha 2$ are the catalytic subunits; $\beta 1$ and $\beta 2$, and $\gamma 1$, $\gamma 2$, and $\gamma 3$ are the regulatory subunits (Arad et

al, 2007). In energy-depleted states where there is a high AMP/ATP ratio, binding of AMP to the γ subunits activates the kinase (Cheung et al, 2000). Upon binding, AMP activates the kinase in three ways: allosteric activation, conformational change that allows for phosphorylation of the critical residue Thr 172 on the α subunit by the kinases LKB1 and calmodulin-dependent protein kinase kinase (CaMKK), and inhibition of Thr 172 dephosphorylation by protein phosphatases (Arad et al, 2007). While the regulation of AMPK activity has been well studied, its transcriptional regulation has not been examined previously.

The AMPK subunits are transcriptionally expressed in a variety of tissues (Viollet et al, 2009). In the heart, the predominant forms expressed are $\alpha 2$, $\beta 2$, and $\gamma 2$. Transgenic and knockout mouse models have demonstrated a critical role for the $\alpha 2$ subunit in cardiac metabolism, particularly glucose transport and glycolysis, ischemic tolerance, and mitochondrial biogenesis (Viollet et al, 2009). *Ampk $\alpha 2$ ^{-/-}* mice have exacerbated cardiac hypertrophy in response to β -adrenergic receptor stimulation with isoproterenol, demonstrating a protective role for *Ampk $\alpha 2$* in the development of cardiac hypertrophy (Zarrinpashneh et al, 2008). In another study, it was shown that *Ampk $\alpha 2$ ^{-/-}* mice have 25% less mitochondrial cardiac cardiolipin content, the main functional phospholipid of the mitochondrial inner membrane in the heart, demonstrating that the $\alpha 2$ subunit plays a role in controlling mitochondrial respiration in the heart (Athea et al, 2007). Furthermore, mice with a dominant negative form of the $\alpha 2$ subunit display exacerbated ATP depletion under hypoxic conditions (Xing et al, 2003), and mice with a kinase dead form of the $\alpha 2$ subunit showed that AMPK is necessary for glucose uptake and glycolysis during ischemia (Russell et al, 2004). All of these mouse models demonstrate that the $\alpha 2$ subunit

is necessary for maintaining myocardial energy homeostasis during cardiac stress and energy depletion. However, despite its importance, the transcriptional regulation of *Ampkα2* in the heart has not been investigated.

It has been implicated that AMPK may activate MEF2 proteins through the p38 MAPK pathway (Al-Khalili et al, 2004; Holmes et al, 2005). Stimulation of AMPK activity by aminoimidazole carboxamide ribonucleotide (AICAR) in primary human myotubes results in increased DNA binding of MEF2 proteins, and this binding is inhibited by an AMPK inhibitor and a p38 MAPK inhibitor (Al-Khalili et al, 2004). In rats treated with AICAR, MEF2 binding activity is increased, however AMPK cannot directly phosphorylate MEF2 proteins, suggesting that perhaps AMPK is working through another kinase such as p38 MAPK to activate MEF2 (Holmes et al, 2005).

Skeletal muscle development

Skeletal muscle is one of the largest organ systems in the body, comprising 40-50% of total body mass (Stump et al, 2006), and is another major source of ATP production and utilization. In the mouse embryo, most skeletal muscle originates from progenitor cells located in the somites, which segment from the paraxial mesoderm and line the sides of the neural tube, beginning around E8.0 (Lyons and Buckingham, 1992). Muscle progenitor cells migrate away from the somites and proliferate to form the muscle of the body wall and limbs (Buckingham, 2001). The first muscle fibers, known as primary fibers, appear between E11-E14, and the secondary fibers form around E14-E16, when innervation is beginning (Ontell and Kozeka, 1984; Buckingham et al, 2003). Primary fibers acquire characteristics of Type I or slow twitch fibers, which utilize

oxidative metabolism as an energy source, are high in mitochondria, and are slow to fatigue (Pette and Spamer, 1986). Secondary fibers become Type II or fast twitch fibers, which utilize glycolysis as an energy source, are fast contracting, and fatigue easily (Pette and Spamer, 1986).

Skeletal muscle remodeling

Skeletal muscle is unique in that, despite having a set pattern and specification of fiber type during development, adult myofibers can remodel, or switch, fiber types in response to cues such as exercise, contraction, and motor neuron activity (Garry et al, 1996). Two major pathways involved in fiber type switching are the calcineurin-NFAT pathway and the MEF2-HDAC pathway. Calcineurin is a protein phosphatase that is activated by calcium binding to calmodulin, and it dephosphorylates nuclear factor of activated T cells (NFAT) (Crabtree, 1999). This results in translocation of NFAT from the cytoplasm to the nucleus, where it can activate calcium-dependent target genes (Crabtree, 1999). Calcineurin is important in establishing Type I fibers, as demonstrated by the increase in slow fibers in mice overexpressing calcineurin (Naya et al, 2000) and the reduction in Type I fibers in mice lacking calcineurin (Parsons et al, 2003).

The MEF2-HDAC pathway has also been shown to regulate Type I fiber formation by using mice harboring a multimerized MEF2 reporter transgene driving *lacZ* expression (Naya et al, 1999). These mice show that MEF2 is chronically active only in Type I fibers. Furthermore, the over expression of MEF2C results in increased formation of Type I fibers (Potthoff et al, 2007b). Lastly, class II HDACs are degraded in Type I

fibers, augmenting the ability of MEF2 to activate the slow myofiber gene program (Potthoff et al, 2007b).

Several target genes of MEF2 in fiber type formation have been identified, in particular peroxisome proliferator-activated receptor γ coactivator-1 α and β (PGC-1 α and β). PGC-1 α is a transcriptional coactivator that regulates mitochondrial biogenesis and oxidative metabolism, and is preferentially expressed in Type I fibers (Puigserver et al, 1998; Lin et al, 2002). Overexpression of PGC-1 α in skeletal muscle results in a dramatic increase in Type I fibers (Lin et al, 2002). Furthermore, PGC-1 α directly interacts with MEF2C (Michael et al, 2001) and co-activates MEF2C to drive activity of Type I fiber promoters (Lin et al, 2002). On the other hand, PGC-1 β is involved in Type II fiber formation. Overexpression of PGC-1 β in skeletal muscle induces fibers with Type IIx characteristics via coactivation of MEF2D (Arany et al, 2007).

IGF signaling pathway in skeletal muscle

Following birth, skeletal muscle fibers are normally post-mitotic and increase in size mainly through hypertrophic growth of the individual muscle fibers (Glass, 2005; Gundersen, 2010). This occurs primarily through the IGF/Akt/mTOR pathway, in which IGF-1 binding activates the IGF-1 receptor (IGFR), a receptor tyrosine kinase (Glass, 2005). IGFR recruits IRS, which leads to activation of two signaling pathways: the Ras-Raf-MEK-ERK pathway, which is essential for proliferation and survival, and the PI3K/Akt pathway, which induces skeletal muscle hypertrophy (Moelling et al, 2002; Rommel et al, 1999). Overexpression of IGF in skeletal muscle induces muscle hypertrophy (Coleman et al, 1995; Musaro et al, 2001) and expression of activated Akt in

C2C12 cells results in hypertrophic growth of myotubes (Rommel et al, 1999).

Overexpression of Akt in the skeletal muscle of mice induces rapid hypertrophy of muscle fibers, along with activation of the p70S6K protein synthesis pathway (Lai et al, 2004).

MEF2 responds to IGF-1 signaling to induce cardiac hypertrophy. IGF-1 activates MEF2C via induction of p38 MAPK phosphorylation in rat cardiomyocytes, and this in turn activates genes such as *Nppa* and *Acta1* that are hallmarks of cardiac hypertrophy (Munoz et al, 2009). In addition, cardiomyocyte stretch-induced activation of IGF-1 activates the p38 MAPK and MEF2 pathway (Shyu et al, 2005). In C2C12 myoblasts, IGF-1 can overcome the inhibitory effects of HDAC4, which normally represses MEF2 proteins, to induce myotube hypertrophy (Lu et al, 2000b).

Insulin signaling pathway in skeletal muscle

Insulin signaling also plays a critical role in skeletal muscle hypertrophy. In normal insulin signaling (Stump et al, 2006; Gallagher et al, 2010), insulin is released from pancreatic β cells in response to glucose. The secreted insulin travels through the bloodstream and binds to the insulin receptor on its target tissues (Stump et al, 2006).

Insulin receptor stimulation increases intracellular tyrosine kinase activity, which phosphorylates insulin receptor substrates (IRS-1 and -2) (Stump et al, 2006).

Phosphorylated IRS-1 associates with the p85 regulatory subunit of PI3K and activates the p110 catalytic subunit of PI3K (Stump et al, 2006). PI3K activation can then activate either the Akt pathway, which leads to the phosphorylation of transcription factors such as FOXO1 that are involved in gluconeogenesis and glucose transporter translocation

(Stitt et al, 2004), or the MAPK pathway (Sweeney et al, 1999), which leads to the phosphorylation of transcription factors such as MEF2C, which are involved in cell growth (Keren et al, 2006). Insulin stimulation increases the DNA binding capabilities of MEF2C in cell culture models, and this can be blocked by the p38 inhibitor SB203580 (Al-Khalili et al, 2004).

In muscle tissues, the insulin signaling pathway also mobilizes the glucose transporter GLUT4 from the intracellular compartment to the plasma membrane (Slot et al, 1991). This translocation of GLUT4 to the cell surface allows for glucose uptake by muscle cells, which is then phosphorylated by hexokinase and directed to either oxidative (aerobic) or non-oxidative (anaerobic) pathways to provide energy in the form of ATP to the muscle (Stump et al, 2006). The GLUT4 promoter contains a MEF2 site that is necessary for activation of the promoter *in vitro* and *in vivo* (Liu et al, 1994; Thai et al, 1998), and MEF2 DNA binding is reduced in muscle tissue from diabetic mice, which also have a reduction in GLUT4 expression (Thai et al, 1998). In addition, MEF2A interacts with the GLUT4 enhancer factor GEF to synergistically regulate the GLUT4 promoter (Knight et al, 2003).

The metabolic syndrome

In 2006 approximately 34% of the United States population was characterized as having metabolic syndrome, which is a result of poor diet, lack of physical exercise, and genetic predisposition (Gallagher et al, 2010). Metabolic syndrome is a collection of risk factors such as abdominal obesity, high blood pressure, low high-density lipoprotein (HDL) cholesterol, insulin resistance, and hyperglycemia that ultimately lead to the

development of Type 2 diabetes and cardiovascular disease (Gallagher et al, 2010). The hallmark of this syndrome is defective insulin activity. Increasing evidence implicates skeletal muscle as a major contributor to the pathophysiology of the syndrome, as muscle is the most abundant insulin-sensitive tissue in the body.

Insulin resistance leads to decreased insulin signaling and, in turn, decreased expression of GLUT4 at the plasma membrane and subsequent decreased glucose transport, limiting the fuel available to muscle for contraction (Kelley et al, 1996). Impaired insulin signaling also causes abnormal accumulation of lipids in skeletal muscle and reduced mitochondrial function and ATP production in insulin-resistant muscle (Schrauwen and Hesselink, 2004; Stump et al, 2006). Furthermore, impaired insulin signal transduction and defects in GLUT4 translocation are associated with skeletal muscle insulin resistance in Type 2 diabetic patients (Krook et al, 2000; Ryder et al, 2000). Lastly, it has been reported that insulin-stimulated glucose transport directly relates to the percent of Type I fibers, and that obese patients with Type 2 diabetes have fewer Type I fibers, suggesting that reduced Type I fibers may be involved in the development of insulin resistance (Hickey et al, 1995). Because skeletal muscle is crucial to maintaining normal insulin signaling and energy production, it is important to understand the molecular mechanisms underlying skeletal muscle metabolism.

Summary

The work presented in this thesis examines the transcription factor MEF2C in cardiac and skeletal muscle metabolism. In chapter 2, I investigate the transcriptional regulation of *Ampk α 2* in the heart. We demonstrate that a MEF2C-Myocardin complex

directly regulates the cardiac metabolic master regulatory gene *Ampkα2* through a conserved myocardial-specific enhancer. The data presented in this chapter are the first to establish the transcriptional regulation of *Ampkα2* in the heart, and also the first to show a MEF2C-Myocardin complex regulating cardiac metabolic gene transcription through two MEF2 sites. In chapter 3, I examine the function of MEF2C in skeletal muscle. Although MEF2C has been implicated in skeletal muscle metabolism, its role has not been tested genetically, nor has the requirement of *Mef2c* in adult skeletal muscle been fully examined. My results show that MEF2C is required for normal growth and glucose metabolism, and are the first to suggest that MEF2C maintains energy homeostasis *in vivo*. Taken together, this work uncovers novel roles for MEF2C in cardiac gene regulation and skeletal muscle metabolism.

Chapter 2: A MEF2C-Myocardin complex directly regulates the cardiac metabolic master regulatory gene *Ampkα2* through a conserved myocardial-specific enhancer

Because alterations in cardiac metabolism have been implicated in the development of many cardiomyopathies (Taha and Lopaschuk, 2007), it is important to understand the transcriptional regulation of genes involved in cardiac energy production. Despite the prominent role that AMPK plays in cardiac muscle metabolism and the breadth of information on the kinase activity of AMPK, the transcriptional regulation of AMPK in the heart has not been investigated. Therefore, in this chapter, I sought to identify the regulatory elements controlling the transcriptional activation of AMPK in the heart.

A highly conserved noncoding element resides within the intronic region of *Ampkα2* and directs *lacZ* expression to the myocardium

To identify regulatory elements that control expression of the catalytic $\alpha 2$ subunit of AMPK, we compared mouse and human sequences from the *PRKAA2* (also known and from herein referred to as *Ampkα2*) locus using BLAST and VISTA analyses (Altschul et al, 1990; Mayor et al, 2000) over a region spanning from -10kb from the transcriptional start site to +10kb from the 3'UTR of the mouse *Ampkα2* locus (Fig. 2-1A). We identified a 930bp noncoding region located downstream of the transcriptional and translational start sites between exons 1 and 2 that is highly conserved between mouse and human (Fig. 2-1A). Given that this sequence of DNA has been conserved throughout evolution, we hypothesized that this region may be important for the

transcriptional regulation of *Ampkα2*. To test this hypothesis, this conserved noncoding sequence from *Ampkα2* was cloned into the HSP68-*lacZ* reporter (Kothary et al, 1989) (Fig. 2-1B) to generate transgenic mouse embryos and analyze the enhancer activity pattern during development and into adulthood.

From this construct, two transgenic mouse lines were generated: line 931 (Fig. 2-2) and line 932 (Fig. 2-3). Both lines demonstrated *lacZ* expression in the heart, however line 931 had more robust expression than line 932. In line 931, whole mount β-galactosidase (β-gal) staining revealed that this 930bp conserved noncoding region was sufficient to direct expression to developing myocardial progenitors as early as embryonic day 7.5 (E7.5) when the myocardial precursor cells are beginning specification and differentiation (Fig. 2-2A), and the *Ampkα2* enhancer remained active in this line throughout cardiac development and in the postnatal and adult heart (Fig. 2-2B-H). Because the heart is composed of many cell types, we wanted to identify the specific cell population in which the enhancer was active. Therefore, we examined β-gal stained transgenic embryos by transverse section at various developmental stages. Section analyses (Fig. 2-2B'-H') demonstrate that *lacZ* expression was highly specific to the myocardium, and there was a complete absence of staining in the epicardium and endocardium (Fig. 2-2E'). Line 932 transgenic embryos and postnatal hearts also had myocardial *lacZ* expression (Fig. 2-3), albeit weaker than line 931.

These findings demonstrate that we have identified an enhancer for *Ampkα2* that is active during the earliest stages of cardiac development, is highly specific for the myocardium.

***Ampkα2* is expressed in the heart during the earliest stages of cardiac development and maintains expression throughout development and postnatally**

While the kinase activity of AMPK has been well characterized, as well as the expression pattern of the AMPK subunits in adult tissues (reviewed in Arad et al, 2007), the mRNA transcript pattern for *Ampkα2* during development has not been determined. To verify that the *Ampkα2* enhancer activity follows the pattern of endogenous *Ampkα2* expression, we conducted *in situ* hybridizations on whole mount embryos at various stages of development (Fig. 2-4). Indeed, the enhancer pattern matched the endogenous pattern of *Ampkα2* expression closely. Endogenous *Ampkα2* transcript was detectable as early as E7.75 in the cardiac precursor cells of the cardiac crescent (Fig. 2-4A). *Ampkα2* expression was maintained throughout cardiac development and in the postnatal and adult heart (Fig. 2-4B-F). These data demonstrate that not only is *Ampkα2* expressed during the earliest stages of cardiac development, but that the endogenous pattern of *Ampkα2* expression matches the activity of the *Ampkα2* enhancer.

Deletion analyses of the *Ampkα2* myocardial enhancer identifies a highly conserved element that is necessary and sufficient for enhancer function *in vivo*

To identify the minimal region of the *Ampkα2* 930bp enhancer that was sufficient to maintain *lacZ* expression in the heart and define the transcriptional pathways upstream of *Ampkα2*, we tested a series of deletion fragments within the 930bp enhancer for their ability to direct expression to the heart in transgenic embryos (Fig. 2-5). Fig. 2-5A depicts the constructs we used and their nucleotide positions relative to the full-length enhancer (Frag. #1). Using conservation as a guide to determine which region to focus

on, we first tested a 407bp region from within the 930bp fragment that was deeply conserved between mouse and human (Frag. #2). This 407bp fragment between nucleotides 443 and 849 was sufficient to direct expression to the heart (Fig. 2-5C) and recapitulated the expression of the full-length fragment in 4 out of 6 independently generated transgenic embryos.

To determine if an even smaller, deeply conserved region could direct expression to the heart, we tested a 200bp fragment within this region containing nucleotides 443-642 (Frag. #3). Indeed, this fragment followed the expression of the full-length fragment in the heart in 4 out of 6 independently generated transgenic embryos (Fig. 2-5D), demonstrating that the 200bp region was sufficient to direct *lacZ* expression in the heart. To determine if the 200bp fragment was necessary for enhancer function, we deleted this region from the 930bp context (Δ 443-642) (Frag. #4). There was a complete absence of X-gal staining in the heart in all 5 independently generated transgenic embryos (Fig. 2-5E), demonstrating that the 200bp region was necessary for *Ampk α 2* myocardial enhancer function *in vivo*. Taken together, these data demonstrate that a 200bp deeply conserved, noncoding region from the *Ampk α 2* locus is necessary and sufficient to direct activity of the *Ampk α 2* enhancer to the developing heart.

Sequence analyses of the *Ampk α 2* myocardial enhancer reveals conserved binding sites for MEF2, NKX2-5, and GATA transcription factors

To identify potential regulatory elements and binding sites for transcription factors that may activate the enhancer, we examined the sequence of the 200bp minimal region from the *Ampk α 2* locus (Fig. 2-6). A ClustalW analysis (Thompson et al, 1994)

was performed to compare the mouse and human sequences for evolutionary conservation. This analysis revealed the presence of two perfectly conserved MEF2 consensus binding sites, located 54bp apart, which is interesting because the MEF2 family of transcription factors is essential for cardiac development (Lin et al, 1997; Naya et al, 2002). The analysis also revealed the presence of binding sites for GATA and NKX2-5 transcription factors, both of which are expressed early in the heart and are necessary for cardiac development (Brewer and Pizzey, 2006; Bartlett et al, 2009).

Identification of two putative MEF2 consensus binding sites, as well as GATA and NKE sites, within the *Ampkα2* enhancer suggests that MEF2, GATA, and NKX2-5 proteins might regulate the *Ampkα2* gene.

The *Ampkα2* myocardial enhancer contains high-affinity GATA and NKE binding sites, but they are not required for activity of the enhancer

GATA proteins are zinc-finger transcription factors that recognize the consensus binding site (T/A)GATA(A/G) (Orkin, 1992). GATA factors 1, 2, and 3 are associated with hematopoiesis (Zon et al, 1991), whereas GATA factors 4, 5, and 6 are associated with cardiac development and endoderm formation (Laverriere et al, 1994). Because the *Ampkα2* enhancer contains a GATA site, we tested the hypothesis that GATA proteins may bind to the site and regulate activity of the enhancer. Indeed, GATA4 protein bound to the site in EMSA (Fig. 2-7A). Recombinant GATA4 protein was used with a radiolabeled double-stranded oligonucleotide encompassing either a control site (lanes 2-6) or the *Ampkα2* GATA site (lanes 8-12). GATA4 efficiently bound to the *Ampkα2* GATA site (lane 8), and this binding was competed by an excess of unlabeled *Ampkα2*

GATA probe (lane 11), but not by an excess of unlabeled mutant *Ampkα2* GATA probe (lane 12).

To test whether the GATA site was required *in vivo* for activity of the enhancer, a transgene containing a mutation in the GATA site in the 930bp context was used to generate transgenic embryos. The wild-type *Ampkα2* enhancer transgene construct (Fig. 2-7B) as well as the mutant GATA construct (Fig. 2-7C) directed *lacZ* expression to the heart. We cannot rule out that mutation of the GATA site may have caused a quantitative reduction in enhancer activity. However, these data demonstrate that, despite the ability of GATA4 to bind to the *Ampkα2* GATA site, the *Ampkα2* myocardial enhancer is not dependent on this site for function *in vivo*.

NKX2-5 is a transcription factor that is part of the homeodomain-containing family NK-2 and recognizes the NK element (NKE) T(C/T)AAGTG (Chen and Schwartz, 1995). Targeted disruption of *Nkx2.5* in mice resulted in failure of cardiac looping and embryonic lethality by E9-10, demonstrating that NKX2-5 is important for cardiac development (Lyons et al, 1995). Because the *Ampkα2* enhancer contains an NKE site, we tested whether NKX2-5 could bind to this site *in vitro* (Fig. 2-8A). Recombinant NKX2-5 protein was used in EMSA with a radiolabeled double-stranded oligonucleotide encompassing either a control site (lanes 2-6) or the *Ampkα2* NKE site (lanes 8-12). NKX2-5 efficiently bound to the *Ampkα2* NKE site (lane 8), and this binding was competed by an excess of unlabeled *Ampkα2* NKE probe (lane 11), but not by an excess of unlabeled mutant *Ampkα2* NKE probe (lane 12).

To test whether the NKE site is required *in vivo* for activity of the enhancer, a transgene containing a mutation in the NKE site in the 930bp context was used to

generate transgenic embryos. The wild-type *Ampkα2* enhancer transgene construct (Fig. 2-8B) as well as the mutant NKE construct (Fig. 2-8C) directed *lacZ* expression to the heart. These data demonstrate that the *Ampkα2* myocardial enhancer is not dependent on the NKE site for function *in vivo*.

The *Ampkα2* myocardial enhancer is dependent on two high-affinity MEF2 binding sites for activity *in vivo*

The MEF2 family of transcription factors binds the consensus site (C/T)TA(A/T)₄TA(A/G) (Black and Olson, 1998) and has been shown to play a critical role in cardiac development (Lin et al, 1997; Naya et al, 2002). Furthermore, the expression pattern of MEF2C in the heart overlaps with the expression pattern of *Ampkα2* in the heart (Edmondson et al, 1994). To determine whether the MEF2 consensus binding sites found within the *Ampkα2* enhancer are bona fide MEF2 sites, we tested each site to see if they can bind MEF2C by EMSA (Fig. 2-9A). Recombinant MEF2C protein was used with a radiolabeled double-stranded oligonucleotide encompassing either the *Ampkα2* MEF2 site 1 (lanes 2-6) or the *Ampkα2* MEF2 site 2 (lanes 8-12). MEF2C bound to both the *Ampkα2* MEF2 site 1 and site 2 (lanes 2 and 8, respectively). Binding of MEF2C to each of these sites was specific because this binding was competed away when an excess of unlabeled self probe was added to the reaction (lanes 5 and 11), and restored when an unlabeled probe with mutated MEF2 sites was added (lanes 6 and 12). This data demonstrates that MEF2C specifically binds to the MEF2 consensus sites identified within the *Ampkα2* enhancer.

To test whether MEF2C could bind to the *Ampkα2* enhancer *in vivo*, chromatin immunoprecipitation (ChIP) was performed (Fig. 2-9B). The pluripotent P19 mouse embryonal carcinoma cell line clonal derivative P19CL6 was used for ChIP experiments. These cells can efficiently differentiate into functioning cardiomyocytes upon differentiation by treatment with 1% DMSO for 7 days (Habara-Ohkubo, 1996). Differentiated P19CL6 cells were transfected with MEF2C expression plasmid and subjected to ChIP using anti-MEF2C antibody. Anti-MEF2C antibody specifically precipitated DNA fragments encompassing the MEF2 sites in the endogenous *Ampkα2* enhancer (Fig. 2-9B), and this product was specific for MEF2C, since the absence of antibody did not result in detection of the *Ampkα2* enhancer (Fig. 2-9B). Taken together with the EMSA results, these data demonstrate that MEF2C directly interacts with the *Ampkα2* enhancer both *in vitro* and *in vivo*.

Because MEF2C bound to the MEF2 sites within the *Ampkα2* enhancer, we next wanted to know whether MEF2C could transactivate the enhancer. To test this hypothesis, we transfected P19CL6 cells with a β-gal reporter plasmid containing the 200bp fragment from the *Ampkα2* enhancer fused with a minimal promoter from the *thymidine kinase* gene (*Ampkα2*-TK-β-gal). The enhancer exhibited minimal baseline activity in these cells (Fig. 2-9C), providing a silent background to test the ability of MEF2 proteins to transactivate the *Ampkα2* enhancer. MEF2C alone transactivated the enhancer, albeit weakly, and this activation was dependent on the presence of two intact MEF2 sites in the enhancer (Fig. 2-9C).

While MEF2 proteins can function independently as transcriptional regulators, they typically require co-factors to activate or repress gene transcription (reviewed in

Black and Cripps, 2010). There are a multitude of potential co-factors for MEF2, so to test if MEF2C might require a co-factor for the activation of the *Ampkα2* enhancer, we used the herpes simplex virus VP16 constitutively active transcriptional activation domain fused to MEF2C to overcome the need for a co-activator. We tested the ability of an expression plasmid containing MEF2C (amino acids 1–141) fused to the VP16 domain (pCDNA1-MEF2C-VP16) to transactivate the *Ampkα2* enhancer. MEF2C-VP16 robustly transactivated the *Ampkα2* enhancer, with more than 2000-fold activation of the enhancer (Fig. 2-9D). Strong activation required only a single intact MEF2 site; mutation of both MEF2 sites completely abolished MEF2C-VP16 transactivation of the enhancer.

These data demonstrate that MEF2C binds to the MEF2 consensus binding sites in the *Ampkα2* myocardial enhancer *in vitro* and *in vivo*. Furthermore, MEF2C by itself weakly transactivates the enhancer, while an activated form (MEF2C-VP16) robustly transactivates the enhancer, suggesting that a co-factor may be involved in transactivation of the *Ampkα2* myocardial enhancer by MEF2C.

The *Ampkα2* myocardial enhancer is dependent upon both conserved MEF2 sites for function *in vivo*

To determine if MEF2 is required for activation of the *Ampkα2* enhancer *in vivo*, we first tested the requirement of the cis-acting elements by mutating the MEF2 sites within the 930bp fragment from *Ampkα2*. We generated transgenic embryos and X-gal stained the embryos for *lacZ* expression. As shown previously, the wild-type *Ampkα2* construct directed expression to the heart at E11.5 (Fig. 2-10A). Mutation of either of the MEF2 sites appeared to reduce activity (Fig. 2-10B, C). However, double mutation of the

MEF2 sites resulted in complete loss of *lacZ* expression in every transgenic founder (Fig. 2-10D). Furthermore, *lacZ* expression in the double MEF2 site mutant remained off in the adult transgenic heart (Fig. 2-10H).

To see if there was a measurable, quantitative reduction in enhancer activity due to the loss of one or both MEF2 sites, we quantified the amount of β -gal activity from each of the wild-type and mutant transgenic constructs (Fig. 2-10E, F). Multiple, independent transgenic founder embryos were generated from each *Ampk α 2* enhancer construct. Hearts were isolated from F0 transgenic embryos at E11.5 and cellular extracts were generated to quantify β -gal activity. Quantification of β -gal for each transgenic heart demonstrated that mutation of a single MEF2 site resulted in reduced β -gal activity, while mutation of both MEF2 sites completely abolished activity of the enhancer (Fig. 2-10E). When depicted on a log₁₀ scale (Fig. 2-10F), the data demonstrated that this reduction in activity by the loss of either a single MEF2 site or both MEF2 sites in combination is significant compared to WT hearts. Furthermore, these results support the qualitative results shown in Fig. 2-10A-D, which suggested a reduction in activity with the loss of a single MEF2 site and absence of β gal activity with the loss of both MEF2 sites.

Taken together, these results demonstrate that the MEF2 binding sites found within the *Ampk α 2* enhancer are required for its activation, suggesting that MEF2 is necessary in *cis* for activity. A single MEF2 site is sufficient for weak activation, but both MEF2 sites are required for robust enhancer activity.

MEF2C is required in *trans* for activation of the enhancer, but not for endogenous *Ampk α 2* expression

To determine if MEF2C is required for *Ampkα2* myocardial enhancer activation, mice with the *Ampkα2*-HSP68 *lacZ* transgene from line 931 were crossed into the *Mef2c*^{+/-} background. Mice that were *Ampkα2*^{Tg/0}; *Mef2c*^{+/-} were then crossed with *Mef2c*^{+/-} mice to generate *Ampkα2*^{Tg/0}; *Mef2c*^{+/+} and *Ampkα2*^{Tg/0}; *Mef2c*^{-/-} embryos. *Mef2c*^{-/-} mice begin to die around E9.5 due to severe cardiovascular defects (Lin et al, 1997). Therefore, we isolated embryos at E8.5, prior to when the *Mef2c*-null mice start dying but after the cardiac precursor cells have been specified and the heart has begun to form (Buckingham et al, 2005). Wild-type embryos with the *Ampkα2* transgene have very robust *lacZ* expression in the linear heart tube at E8.5 (Fig. 2-11A). However, strikingly, *Mef2c*-null mice with the *Ampkα2* transgene have complete loss of *lacZ* expression (Fig. 2-11B). These data demonstrate that the MEF2C protein is required for activity of the *Ampkα2* enhancer *in vivo*.

We next wanted to know whether MEF2C is required for activation of the endogenous *Ampkα2* gene. We conducted *in situ* hybridization studies on wild-type and *Mef2c*-null embryos at E8.5 to examine *Ampkα2* expression levels (Fig. 2-11C, D). *Ampkα2* was expressed throughout the heart at E8.5 in wild-type embryos (Fig. 2-11C). Interestingly, *Ampkα2* was still expressed in the *Mef2c*-null heart at E8.5 (Fig. 2-11D), demonstrating that MEF2C is not required for endogenous *Ampkα2* expression.

Taken together, these data suggest that, although MEF2C is required for *Ampkα2* enhancer activity, it is not necessary for *Ampkα2* expression. It is possible that another element from the *Ampkα2* locus may also function to control endogenous *Ampkα2* in the heart.

MEF2C and Myocardin synergistically activate the *Ampkα2* myocardial enhancer and may form a ternary complex

The data presented thus far demonstrate that MEF2C is required both in *cis* and in *trans* for activation of the *Ampkα2* enhancer. However, the finding that the constitutively active form of MEF2C (Fig. 2-9D) robustly transactivated the *Ampkα2* enhancer compared to the non-constitutively active form (Fig. 2-9C) suggested that a co-factor might be interacting with MEF2C to activate the enhancer. Many co-factors for MEF2 proteins have been documented (Black and Cripps, 2010). In particular, one isoform of the SAP-domain, non-DNA binding protein Myocardin, Myocardin-935, has been identified as a potent co-activator of MEF2C specifically in cardiac muscle, and it directly interacts with MEF2C through its N-terminal domain (Creemers et al, 2006). Therefore, we hypothesized that Myocardin-935 may interact with MEF2C to synergistically transactivate the *Ampkα2* enhancer.

Initially, we wanted to determine if MEF2C and Myocardin-935 could form a complex on the *Ampkα2* sequence encompassing the MEF2 sites. To test this, we conducted an EMSA analysis in which increasing amounts of MEF2C protein were added to a constant amount of Myocardin-935 and incubated with a radioactively labeled probe that spanned both MEF2 sites in the *Ampkα2* myocardial enhancer (Fig. 2-12A). As expected, MEF2C bound to this probe in the absence of Myocardin-935 (lanes 2-5). Interestingly, when increasing amounts of MEF2C were in the presence of a constant amount of Myocardin-935, a slower mobility band became detectable, suggesting the formation of a ternary complex between MEF2C and Myocardin-935 (lanes 7-10). Addition of recombinant Myocardin protein alone did not result in the formation of a

complex (lane 6), consistent with published reports claiming that as Myocardin is not a DNA-binding protein (Pipes et al, 2006).

Since MEF2C and Myocardin formed a complex on the enhancer, we next tested whether MEF2C and Myocardin might activate the enhancer in combination with each other. Indeed, MEF2C and Myocardin-935 cooperatively activated the enhancer more than 60-fold in P19CL6 transactivations (Fig. 2-12B). Interestingly, this robust synergy was dependent on two intact MEF2 sites. When only a single MEF2 site was present, some cooperativity between the two factors occurred (Fig. 2-12B). However, cooperativity was dramatically reduced compared to the wild-type enhancer. Mutations of both MEF2 sites completely abolished activation and synergy. These data establish that robust synergistic activation of the *Ampkα2* myocardial enhancer by MEF2C and Myocardin-935 is dependent upon two intact MEF2 sites.

The synergistic activation of the *Ampkα2* myocardial enhancer and other MEF2-dependent enhancers by MEF2C and Myocardin requires dimerization between Myocardin molecules

In addition to the cardiac Myocardin-935, there is another isoform of Myocardin, Myocardin-856, which is a potent transcriptional coactivator for the transcription factor SRF and its regulation of smooth muscle genes (Creemers et al, 2006). It has also been well documented that many smooth muscle genes have two CArG boxes, which are consensus binding sequences for the transcription factor SRF (Shimizu et al, 1995; Li et al, 1997; Miano et al, 2000; Manabe and Owens, 2001; Lilly et al, 2001). Interestingly, Myocardin preferentially activates smooth muscle genes that have two CArG boxes near

each other that are bound by SRF proteins, thus allowing formation of a homodimer between each Myocardin molecule's leucine-zipper (LZ) domain (Wang et al, 2003). Therefore, we wanted to know whether Myocardin-935 functions in a similar mechanism when two MEF2 sites are near each other. We hypothesized that Myocardin molecules form a homodimer to preferentially interact with MEF2C proteins bound to the two MEF2 sites on the *Ampkα2* enhancer. To test this hypothesis, we mutated the LZ domain within Myocardin-935, which renders this protein incapable of dimerizing with another Myocardin molecule (Wang et al, 2003), and tested its ability to cooperate with MEF2C to synergistically activate the *Ampkα2* enhancer in transfection experiments. Indeed, the synergy between MEF2C and mut-LZ-Myocardin-935 was reduced by approximately one-half compared to the wild-type version of Myocardin-935 (Fig. 2-13A).

Based on the Myocardin dimerization model, we predicted that loss of a single MEF2 site would result in the same synergistic activation between mut-LZ-Myocardin-935 + MEF2C and WT-Myocardin-935 + MEF2C. However, we still observed some synergistic activation between the mutant form of Myocardin and MEF2C, suggesting that the mut-LZ-Myocardin-935 is still partially functional (Fig. 2-13A). Further experiments will need to be done to verify the stability of the mutant Myocardin-935 protein and its interaction with MEF2C.

We also tested the ability of Myocardin and MEF2C to activate other MEF2 target genes, including a region from the muscle creatine kinase (*CKM*) enhancer, which contains two MEF2 sites (Cserjesi et al, 1994) and a multimerized MEF2 consensus site reporter (4xMEF2-*lacZ*), both of which are active in the heart (Cserjesi et al, 1994). Interestingly, both the *CKM* enhancer and the 4xMEF2 reporter responded in a similar

way to Myocardin-935 + MEF2C as the myocardial enhancer from *Ampkα2* (Fig. 2-13B, C). Both constructs exhibited synergistic activation by MEF2C and Myocardin, and this cooperativity was reduced but not abolished by the mutation of the Myocardin leucine zipper. Furthermore, when both MEF2 sites in the *CKM* enhancer were mutated, the synergistic activation between MEF2C and either of the Myocardin constructs was lost (Fig. 2-13B), similar to the myocardial *Ampkα2* enhancer. MEF2C and Myocardin still synergistically activated the *CKM* mut MEF site #2 construct (Fig. 2-13B), albeit much weaker than the wild-type construct. There was no synergy between MEF2C and Myocardin on the *CKM* mut MEF site #1 construct (Fig. 2-13B).

The finding that the multimerized MEF2 reporter, the *CKM* cardiac promoter, and the *Ampkα2* myocardial enhancer all have two or more MEF2 sites and are synergistically activated by MEF2 and Myocardin-935 suggests that the observed two MEF2 site-Myocardin mechanism may be a more general regulation of cardiac gene expression.

Discussion

In this chapter, we identified a highly conserved enhancer from the mouse *Ampkα2* locus that is sufficient to direct expression to the myocardium and is active as early as E7.5, when the heart is beginning to form, and remains active into adulthood. The activity of the enhancer matches the pattern of endogenous *Ampkα2* expression at early stages of mouse embryogenesis. The *Ampkα2* myocardial enhancer contains two conserved MEF2 sites, both of which bind MEF2C and are required for enhancer activity in the myocardium of transgenic mouse embryos. Furthermore, we show that MEF2C and

Myocardin cooperatively regulate the *Ampkα2* enhancer, and that this cooperativity is dependent on the presence of two intact MEF2 sites. The data presented in this chapter are the first to demonstrate the transcriptional regulation of an AMPK gene in the heart, and also the first to show a MEF2C-Myocardin complex regulating cardiac metabolic gene transcription through two MEF2 sites. Importantly, this may be a more general mechanism for the transcriptional regulation of gene activation in the heart.

Identification of a transcriptional regulatory element for *Ampkα2* is important because of the critical role AMPK plays in metabolism. AMPK activates proteins that increase fatty acid oxidation, protein synthesis, glycolysis, and glucose oxidation, all in an effort to increase energy production in the cardiomyocyte (Dolinsky and Dyck, 2006). Much of the research on AMPK has focused on its role in adult cardiovascular function and disease. However, the findings in this chapter suggest that perhaps AMPK is also playing a role early in cardiac development. The fact that the *Ampkα2* enhancer is active as early as E7.5, when the heart is forming, and that expression of endogenous *Ampkα2* can be detected at such an early stage hints at a possible role for AMPK in early cardiac development. Exactly what role AMPK is playing in this stage of heart development remains to be determined. It is known that the early embryonic cardiomyocyte utilizes glycolysis for energy, and the transition to a mature cardiomyocyte requires a switch to mitochondrial oxidative phosphorylation for energy production (Chung et al, 2007; Chung et al, 2010; Lopaschuk and Jaswal, 2010). Precisely when this transition is occurring is not known, but AMPK could be playing a role in the energy switch. Another possibility is that cardiomyocyte precursors require a large amount of energy to undergo the rapid proliferation that occurs in the early stages of cardiogenesis (Lopaschuk and

Jaswal, 2010), and activation of *Ampkα2* may be important during this time period for providing that energy.

From the data presented in this chapter, it is evident that the *Ampkα2* myocardial enhancer identified here is under the transcriptional control of MEF2C during the early stages of cardiac development. However, one interesting finding was that the endogenous *Ampkα2* gene was still expressed in *Mef2c* null mice, even though the *Ampkα2* myocardial enhancer was completely inactive in these mice (Fig. 2-11). One explanation is that there are additional noncoding regions acting as myocardial enhancer elements. Several genes have multiple enhancers that can control their expression, either in different tissues or the same tissue. For example, *Mef2c*, *Myf5*, *MyoD*, *Nkx2-5*, *cardiac α-actin*, and *cardiac troponin C* all have multiple enhancers that either control expression of the gene in multiple tissues or in a single tissue (Dodou et al, 2003; Dodou et al, 2004; Latinkic et al, 2002; Christensen et al, 1993; Buchberger et al, 2003; Hadchouel et al, 2003; Asakura et al, 1995; Goldhamer et al, 1995; Searcy et al, 1998; Reecy et al, 1999). Another possibility is that the myocardial enhancer we have identified may be an early activator of *Ampkα2*, and that there may be another enhancer that is required for later maintenance of expression.

The work in this chapter not only reveals the transcriptional regulation of *Ampkα2* in the heart, but it also potentially identifies a more general mechanism for cardiac gene regulation, where MEF2C and Myocardin work together through a two-site mechanism to control cardiac gene expression. Synergy between MEF2C and Myocardin across two or more MEF2 sites was seen with the *Ampkα2* myocardial enhancer, as well as the *CKM* enhancer and a multimerized MEF2 reporter (Fig. 2-13). The possibility that this

mechanism is more general and not unique to the enhancers tested is likely. It is intriguing to speculate that Myocardin interacts with MEF2C bound to two sites to preferentially regulate a subset of cardiac genes. If this is a general method of cardiac gene regulation, one factor to consider is the precise spacing between the MEF2 sites. In the *Ampkα2* myocardial enhancer the sites are 54bp apart, whereas they are 126bp apart in the *CKM* enhancer. Further studies will need to be done to determine if there is a spacing requirement between the two MEF2 sites that dictates how Myocardin molecules interact with MEF2C proteins, and to determine how the sites need to be positioned in the context of chromatin.

From the data presented in this chapter, we propose a model (Fig. 2-14) in which a subset of cardiac genes is regulated by the presence of two MEF2 sites, each of which binds a dimer of MEF2C. Myocardin then interacts directly with each of the MEF2C dimers via its N-terminal domain. The close proximity of the two MEF2 sites allows for Myocardin molecules to dimerize through their leucine-zipper (LZ) domains, resulting in synergistic activation. Our model for the general regulation of cardiac enhancers by MEF2C and Myocardin through two MEF2 sites may be used to predict other regulatory elements from cardiac genes through a bioinformatics screen and further our understanding of the transcriptional control of genes during cardiac development.

Figure Legends

Figure 2-1: A highly conserved noncoding element resides within the intronic region of *Ampkα2*

(A) VISTA plot comparing the human and mouse sequences of *PRKAA2* (*Ampkα2*). The peaks in pink indicate regions of evolutionary conservation between human and mouse. The circled peak highlights a 930bp region that was identified as a putative regulatory element for *Ampkα2* based on the sequence conservation between human and mouse. (B) Schematic representation of the *Ampkα2* locus and the *Ampkα2-lacZ* transgene. The 930bp element from *Ampkα2* is located downstream of the transcriptional and translational start sites, between exons 1 and 2. To study its potential role as a regulatory element for *Ampkα2*, a reporter plasmid construct containing the 930bp conserved element fused to the transgenic reporter plasmid HSP68-*lacZ* was generated.

Figure 2-2: The *Ampkα2-lacZ* transgene is expressed in the myocardium throughout development and postnatally in line 931

Whole-mount (A-H), coronal (B', C', F'-H'), and transverse (D', E') sections of X-gal stained *Ampkα2-lacZ* transgenic embryos and postnatal hearts from line 931 are shown. Expression directed by the *Ampkα2-lacZ* transgene is exclusive to the heart as early as E7.5 (A), and continues throughout development (B-F) and postnatally (G, H). Sections of X-gal stained hearts demonstrate that the transgene is expressed in the myocardial cells of the heart from E7.75 throughout development (B'-E'). Expression is restricted to the myocardium and is absent from the pericardium/epicardium (E', arrow) and endocardium

(E', asterisk). Immunofluorescence for the expression of β gal was performed on coronal sections from E13.5, neonatal, and adult hearts (F'-H'). β gal protein was detected in the myocardium at each of these stages.

Figure 2-3: The *Ampk α 2-lacZ* transgene is expressed in the myocardium throughout development and postnatally in line 932

Whole-mount (A-D), transverse, (A', B'), and coronal (C', D') sections of X-gal stained *Ampk α 2-lacZ* transgenic embryos and postnatal hearts from line 932 are shown.

Expression directed by the *Ampk α 2-lacZ* transgene is exclusive to the heart as early as E9.5 (A), and this expression continues throughout development (B, C) and postnatally (D). Sections of X-gal stained hearts demonstrate that the transgene is expressed in the myocardial cells of the heart from E9.5 throughout development and postnatally (A'-D').

Figure 2-4: *Ampk α 2* is expressed in the heart during the earliest stages of cardiac development and maintains expression throughout development and postnatally

Whole-mount *in situ* hybridization for *Ampk α 2*. *Ampk α 2* is expressed in the cardiac precursor cells of the cardiac crescent at E7.75 (A). This expression is maintained throughout development during the linear heart tube stage at E8.5 (B), cardiac looping stage at E9.5 (C), and during cardiac growth and maturation at E11.5 and E13.5(D, E). *Ampk α 2* continues to be expressed postnatally in the heart (F).

Figure 2-5: Deletional analysis of the *Ampkα2* myocardial enhancer identifies a highly conserved element that is necessary and sufficient for enhancer function *in vivo*

Schematic diagram depicting the deletion constructs from the *Ampkα2* myocardial enhancer (A). The nucleotide positions of each deletion construct, relative to the full-length 930bp enhancer (Frag #1), are denoted on the left. Myocardium expression directed by each construct is depicted on the right, with a plus sign (+) indicating myocardial expression and a minus sign (-) indicating no detectable myocardial expression. The column on the far right indicates the number of independent transgenic F0 embryos that expressed *lacZ* in the myocardium as a fraction of the total number of transgene-positive F0 embryos examined. (B-E) Representative transgene-positive F0 embryos at E11.5 from each of the four fragments. Frag 2 and Frag 3 directed strong expression to the myocardium (C, D) and recapitulated the expression pattern of the full-length Frag 1 (A). Deletion of Frag 3 (Δ 443-642) from the full-length 930bp context to generate Frag 4 completely ablated transgene activity (E).

Figure 2-6: Sequence analysis of the *Ampkα2* myocardial enhancer reveals conserved binding sites for MEF2, NKX, and GATA transcription factors

ClustalW analysis comparing the mouse and human sequences from the necessary and sufficient region of the *Ampkα2* myocardial enhancer (443-642bp). The analysis identified two perfectly conserved, candidate binding sites for MEF2 transcription factors (green boxes), denoted as MEF2 #1 and MEF2 #2; one perfectly conserved, candidate binding site for NKX transcription factors (red box); and one conserved, candidate

binding site for GATA transcription factors (purple box). Asterisks denote nucleotides that have been perfectly conserved among species.

Figure 2-7: The *Ampkα2* myocardial enhancer contains a high-affinity GATA binding site that is not required for activity of the enhancer

(A) Recombinant GATA4 protein was used in EMSA with a radiolabeled double-stranded oligonucleotide encompassing either a control site (lanes 2-6) or the *Ampkα2* GATA site (lanes 8-12). Lanes 1 and 7 contain reticulocyte lysate without recombinant GATA4 (represented by a minus (-) sign). GATA4 efficiently bound to the *Ampkα2* GATA site (lane 8), and this binding was competed by an excess of unlabeled *Ampkα2* GATA probe (lane 11), but not by an excess of unlabeled mutant *Ampkα2* GATA probe (lane 12). The GATA control site (G) and mutant GATA control site (mG) come from the *Gata4* mesoderm enhancer (Rojas et al, 2005) (B, C) The *Ampkα2* myocardial enhancer is not dependent on a conserved GATA site for function *in vivo*. The wild-type *Ampkα2* enhancer transgene construct (B) and a transgene containing a mutation in the GATA site in the 930bp context (C) were used to generate transgenic embryos. Representative transgenic F0 embryos are shown at E11.5. Both the wild-type (B) and mGATA (C) constructs directed *lacZ* expression to the heart.

Figure 2-8: The *Ampkα2* myocardial enhancer contains a high-affinity NKE binding site that is not required for activity of the enhancer

(A) Recombinant NKX2-5 protein was used in EMSA with a radiolabeled double-stranded oligonucleotide encompassing either a control site (lanes 2-6) or the *Ampkα2*

NKE site (lanes 8-12). Lanes 1 and 7 contain reticulocyte lysate without recombinant NKX2-5 (represented by a minus (-) sign). NKX2-5 efficiently bound to the *Ampkα2* NKE site (lane 8), and this binding was competed by an excess of unlabeled *Ampkα2* NKE probe (lane 11), but not by an excess of unlabeled mutant *Ampkα2* NKE probe (lane 12). The NKE control site (N) and mutant NKE control site (mN) come from the *vnd-NKE* promoter (Wang et al, 2002). (B, C) The *Ampkα2* myocardial enhancer is not dependent on a conserved NKE site for function *in vivo*. The wild-type *Ampkα2* enhancer transgene construct (B) and a transgene containing a mutation in the NKE site in the 930bp context (C) were used to generate transgenic embryos. Representative transgenic F0 embryos are shown at E11.5. Both the wild-type (B) and mNKE (C) constructs directed *lacZ* expression to the heart.

Figure 2-9: The *Ampkα2* myocardial enhancer is dependent on two high-affinity MEF2 binding sites

(A) Recombinant MEF2C protein was used in EMSA with a radiolabeled double-stranded oligonucleotide encompassing either the *Ampkα2* MEF2 Site #1 (lanes 2-6) or the *Ampkα2* MEF2 Site #2 (lanes 8-12). Lanes 1 and 7 contain reticulocyte lysate without recombinant MEF2C (represented by a minus (-) sign). MEF2C efficiently bound to both of the *Ampkα2* MEF2 sites (lanes 2, 8), and this binding was competed by an excess of unlabeled *Ampkα2* MEF2 probe Site #1 (lane 5) or Site #2 (lane 11), but not by an excess of unlabeled mutant *Ampkα2* MEF2 probe Site #1 (lane 6) or Site #2 (lane 12). The MEF2C control site (M) and mutant MEF2C control site (mM) come from the *Myogenin* promoter (Yee and Rigby, 1993). (B) P19CL6 cardiomyocyte cells were transfected with

MEF2C expression plasmid and subjected to ChIP using either no antibody or anti-MEF2C antibody. Mock indicates no chromatin used in the pull-down and was used as an additional negative control. Following ChIP, the *Ampkα2* myocardial enhancer was detected using primers spanning the two MEF2 sites within the *Ampkα2* myocardial enhancer. (C) P19CL6 cells were co-transfected with MEF2C expression plasmid (black bars) or parental expression vector (white bars) and either parental reporter plasmid TK-βgal, wild-type *Ampkα2*-βgal reporter plasmid or mutant versions of this reporter construct containing disruptions in the MEF2 sites. Results are reported as fold activation of βgal reporter over the empty vectors (TK-βgal + vector). The data shown represent the mean values obtained in 14 independent transfections. Error bars represent the standard deviations. (D) P19CL6 cells were co-transfected with MEF2C-VP16 expression plasmid (black bars) or parental expression vector (white bars) and either parental reporter plasmid TK-βgal, wild-type *Ampkα2*-βgal reporter plasmid or mutant versions of this reporter construct containing disruptions in the MEF2 sites. Results are reported as fold activation of βgal reporter over the empty vectors (TK-βgal + vector). The data shown represent the mean values obtained in 8 independent transfections. Error bars represent the standard deviations. mMEF1 = mutant MEF2 site 1; mMEF2 = mutant MEF2 site 2; mMEF1&2 = mutant MEF2 sites 1&2.

Figure 2-10: The *Ampkα2* myocardial enhancer is dependent on both conserved MEF2 sites for function *in vivo*

The wild-type *Ampkα2* enhancer transgene construct (A) and transgenes containing mutations in MEF2 site #1 (B), MEF2 site #2 (C), or both MEF2 sites (D) in the 930bp

context were used to generate transgenic embryos. Representative transgenic F0 embryos are shown at E11.5. (E, F) Quantification of β gal activity in transgenic hearts. Transgenic embryos were generated from the wild-type *Ampk α 2* enhancer transgene construct (WT, n=10) or transgenes containing mutations in MEF2 site #1 (mut 1, n=12), MEF2 site #2 (mut 2, n=18), or both MEF2 sites (mut 1&2, n=6) in the 930bp context. Hearts were isolated from these embryos at E11.5 and cellular extracts were generated to quantify β gal activity by chemiluminescent β -galactosidase assay. (E) Graph depicting the β gal activity in 1 μ g of protein extract from each transgenic heart. (F) Log-scale graph depicting the β gal activity 1 μ g of protein extract from each transgenic heart. Each point represents a single, independent transgenic event. Statistical analysis done by one-way ANOVA, Newman-Keuls post-hoc test (*p<0.05; **p<0.005; ***p<0.001; NS=not significant). Error bars indicate standard deviation. (G, H) The MEF2 sites are required for activity of the *Ampk α 2* myocardial enhancer in the adult heart. The wild-type *Ampk α 2* enhancer transgene construct (G) and a transgene containing mutations in both MEF2 sites (H) in the 930bp context were used to generate transgenic mice. A representative adult heart from one of six independent transgenic lines with the double MEF2 mutation is shown (H).

Figure 2-11: MEF2C is required in *trans* for activation of the enhancer, but not for endogenous *Ampk α 2* expression

(A, B) The transgenic line 931 expressing the *Ampk α 2-lacZ* transgene was crossed into the *Mef2c*^{+/-} background to generate *Mef2c*^{+/-}; *Ampk α 2-lacZ*^{Tg/0} mice. These mice were then crossed to a *Mef2c*^{+/-} mouse to generate *Mef2c*^{+/+}; *Ampk α 2-lacZ*^{Tg/0} (A) or *Mef2c*^{-/-};

Ampkα2-lacZ^{Tg/0} (B) embryos. Whole-mount embryos collected at E8.5 and stained for X-gal are shown. Dotted line demarcates the linear heart tube characteristic of *Mef2c^{-/-}* embryos at this stage. Lack of MEF2C protein completely abolishes activity of the *Ampkα2* myocardial enhancer. (C, D) Whole-mount *in situ* hybridization for *Ampkα2* on wild-type and *Mef2c*-null embryos at E8.5. *Ampkα2* is expressed in the heart at E8.5 in both *Mef2c^{+/+}* (C) and *Mef2c^{-/-}* (D) embryos.

Figure 2-12: MEF2C and Myocardin may form a ternary complex and synergistically activate the *Ampkα2* myocardial enhancer

(A) MEF2C and Myocardin simultaneously bind the *Ampkα2* myocardial enhancer. A radiolabeled nucleotide probe encompassing both MEF2 sites was used in EMSA. Increasing amounts of recombinant MEF2C protein in the absence of Myocardin resulted in the formation of an increasing amount of MEF2C-DNA complex (lanes 2-5). However, increasing amounts of MEF2C in the presence of a constant amount of Myocardin resulted in the formation of the MEF2C-DNA complex, as well as a slower mobility band, suggesting the formation of a MEF2C-Myocardin-DNA ternary complex (lanes 7-10). In all samples, the total amount of total protein was held constant by the addition of the appropriate amount of unprogrammed reticulocyte lysate. (B) Maximal MEF2C and Myocardin synergistic activation of the *Ampkα2* myocardial enhancer depends on two intact MEF2 sites. P19CL6 cells were co-transfected with either parental expression vector (white bars), MEF2C expression plasmid (gray bars), Myocardin expression plasmid (black bars), or both MEF2C and Myocardin expression plasmids (slashed bars) and either parental reporter plasmid TK-βgal, wild-type *Ampkα2*-βgal

reporter plasmid or mutant versions of this reporter construct containing disruptions in the MEF2 sites. Results are reported as fold activation of β gal reporter over the empty vectors (TK- β gal + vector). The data shown represent the mean values obtained in 9 independent transfections. Error bars represent the standard deviations. mMEF1 = mutant MEF2 site 1; mMEF2 = mutant MEF2 site 2; mMEF1&2 = mutant MEF2 sites 1&2.

Figure 2-13: The synergistic activation of the *Ampk α 2* myocardial enhancer and other MEF2-dependent reporters by MEF2C and Myocardin requires the Myocardin leucine-zipper motif

(A) P19CL6 cells were co-transfected with either parental expression vector, MEF2C expression plasmid, Myocardin expression plasmid, Myocardin-mut LZ expression plasmid, both MEF2C and Myocardin expression plasmids, or both MEF2C and Myocardin-mut LZ expression plasmids, and either parental reporter plasmid TK- β gal, wild-type *Ampk α 2*-TK- β gal reporter plasmid, or mutant versions of this reporter construct containing disruptions in the MEF2 sites. Results are reported as fold activation of β gal reporter over the empty vectors (TK- β gal + vector). The data shown represent the mean values obtained in 5 independent transfections. Error bars represent the standard deviations. mMEF1 = mutant MEF2 site 1; mMEF2 = mutant MEF2 site 2; mMEF1&2 = mutant MEF2 sites 1&2. (B) P19CL6 cells were co-transfected with the same combination of expression plasmids as described above, and either parental reporter plasmid TK- β gal, wild-type CKM-TK- β gal reporter plasmid, or mutant versions of this reporter construct containing disruptions in the MEF2 sites. Results are reported as fold activation of β gal reporter over the empty vectors (TK- β gal + vector). The data shown

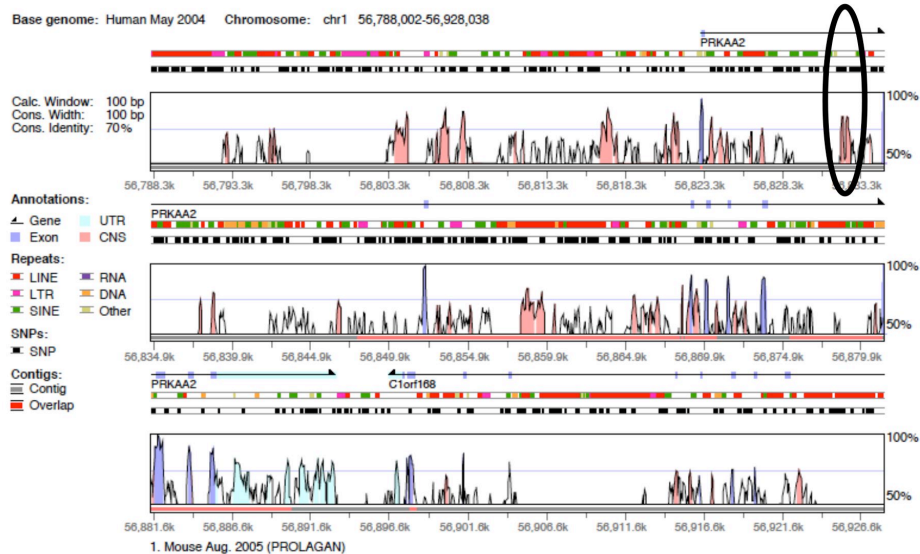
represent the mean values obtained in 4 independent transfections. Error bars represent the standard deviations. mMEF1 = mutant MEF2 site 1; mMEF2 = mutant MEF2 site 2; mMEF1&2 = mutant MEF2 sites 1&2. (C) P19CL6 cells were co-transfected with the same combination of expression plasmids as described above, and either parental reporter plasmid pE1B-*lacZ* or a multimerized MEF2 consensus site reporter (4xMEF2-*lacZ*). Results are reported as fold activation of *lacZ* reporter over the empty vectors (pE1B-*lacZ* + vector). The data shown represent the mean values obtained in 6 independent transfections. Error bars represent the standard deviations.

Figure 2-14: A model for the regulation of MEF2-dependent genes by MEF2C and Myocardin

Each MEF2 site binds a dimer of MEF2C. Myocardin interacts directly with each of the MEF2C dimers via its N-terminal domain. The close proximity of the two MEF2 sites allows for Myocardin molecules to dimerize through its leucine-zipper (LZ) domain, allowing for synergistic activation.

Figure 2-1

A



B

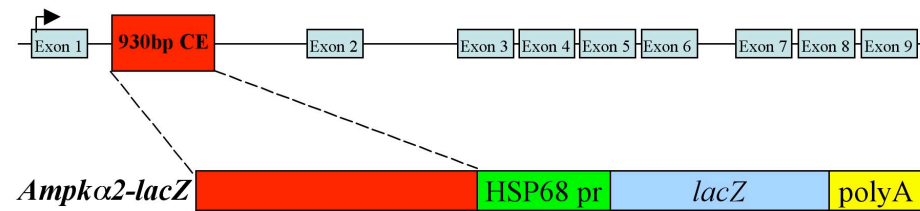


Figure 2-2

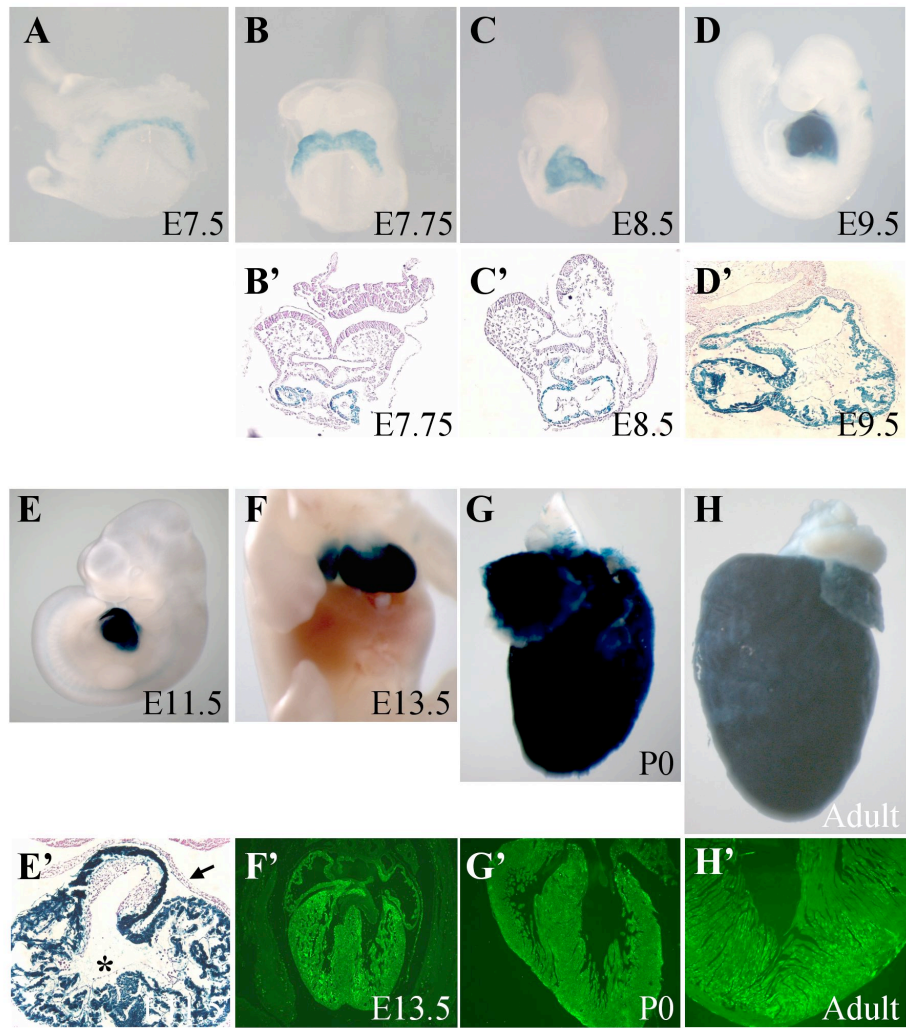


Figure 2-3

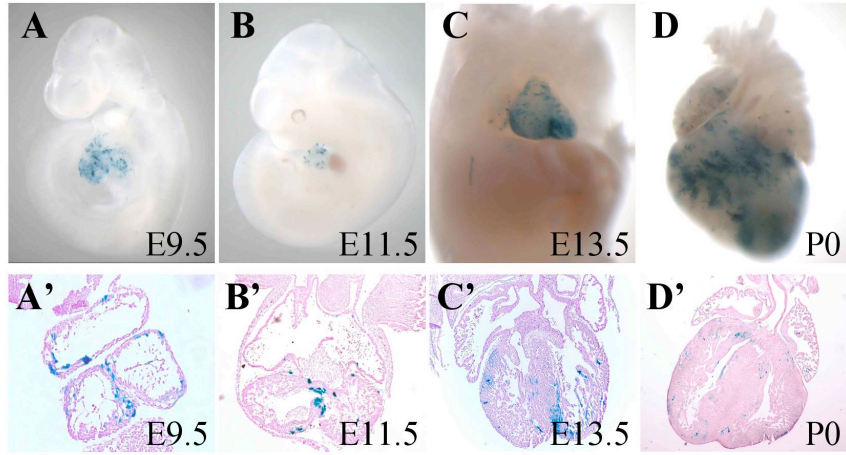


Figure 2-4

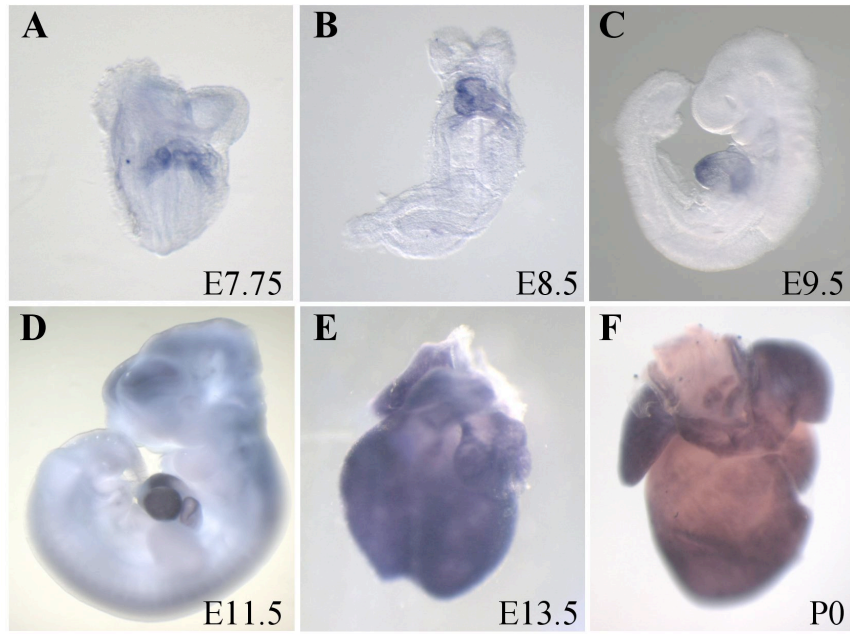


Figure 2-5

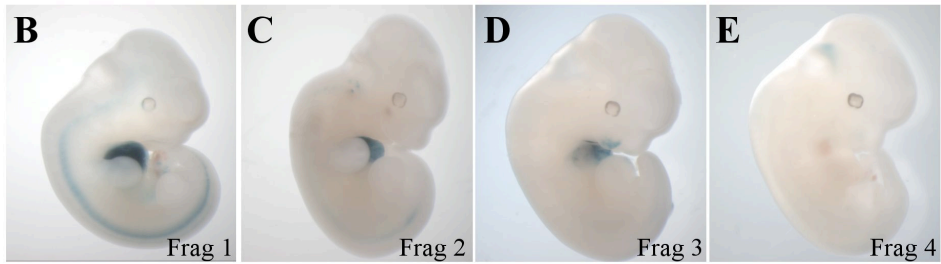
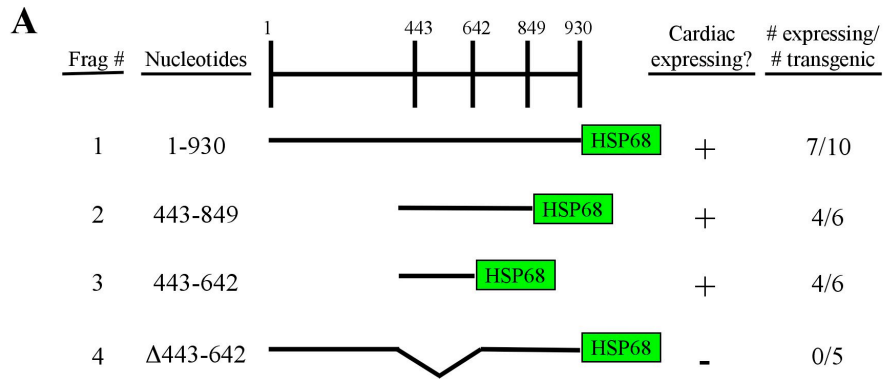


Figure 2-7

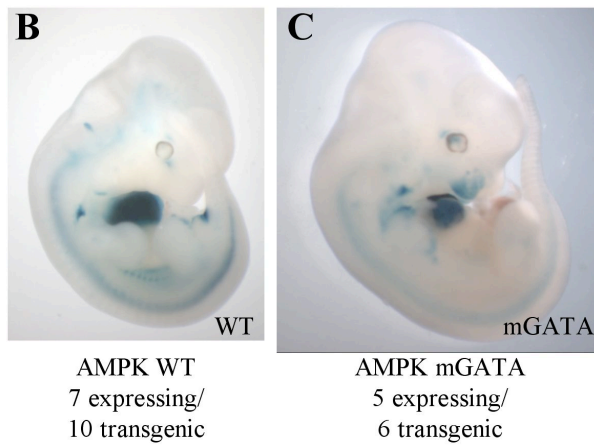
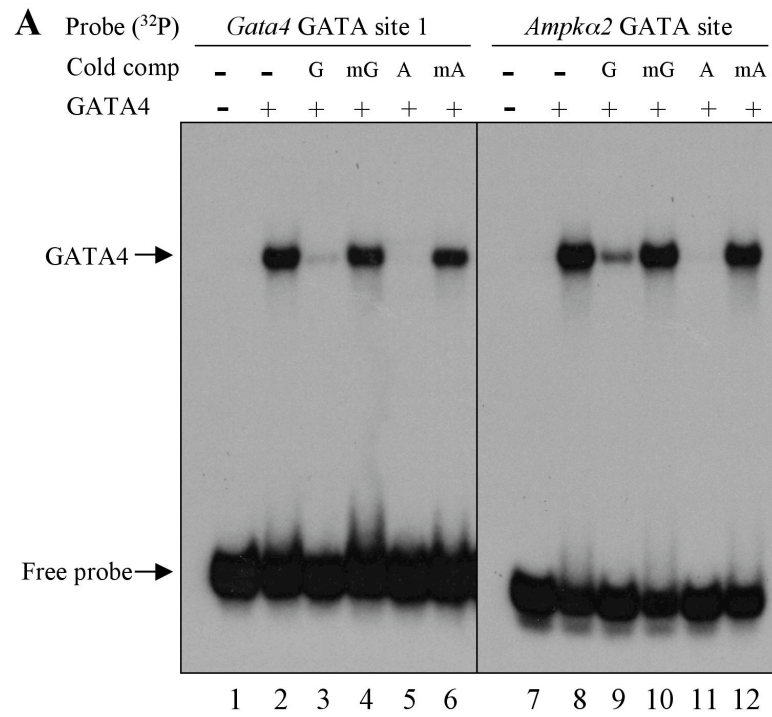
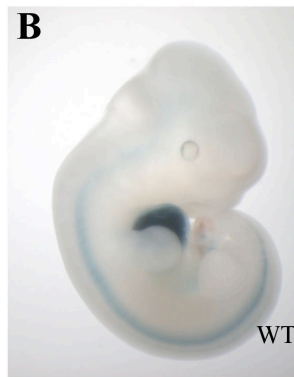
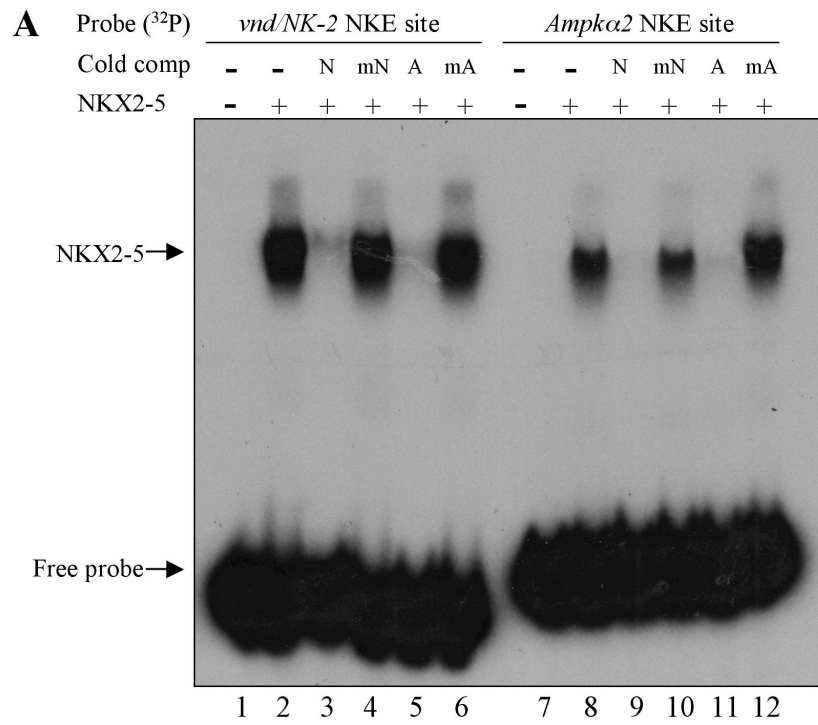


Figure 2-8



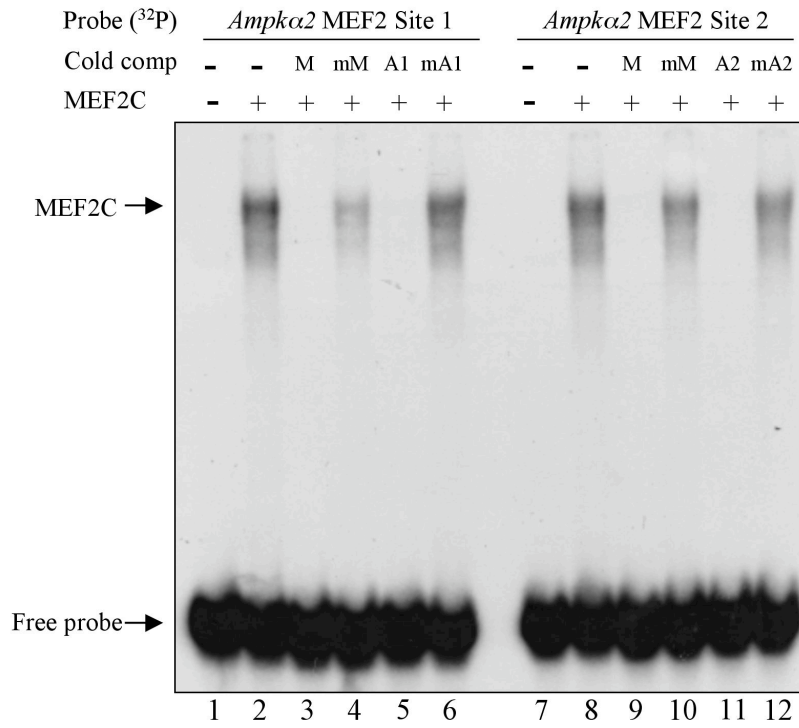
AMPK WT
7 expressing/
10 transgenic



AMPK mNKE
4 expressing/
6 transgenic

Figure 2-9

A



B

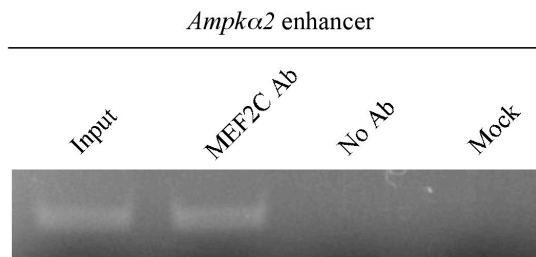
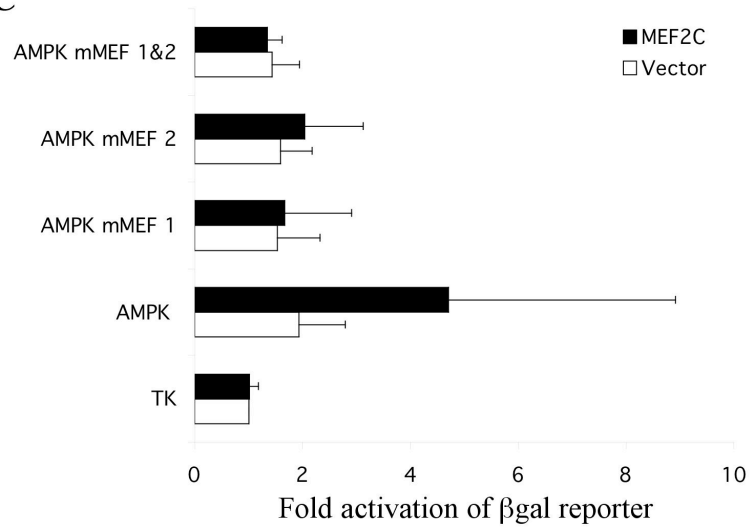


Figure 2-9 (cont'd)

C



D

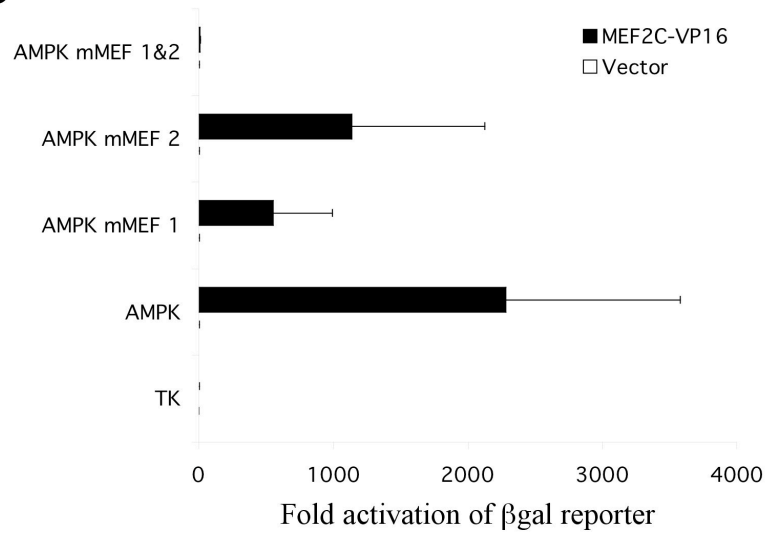


Figure 2-10

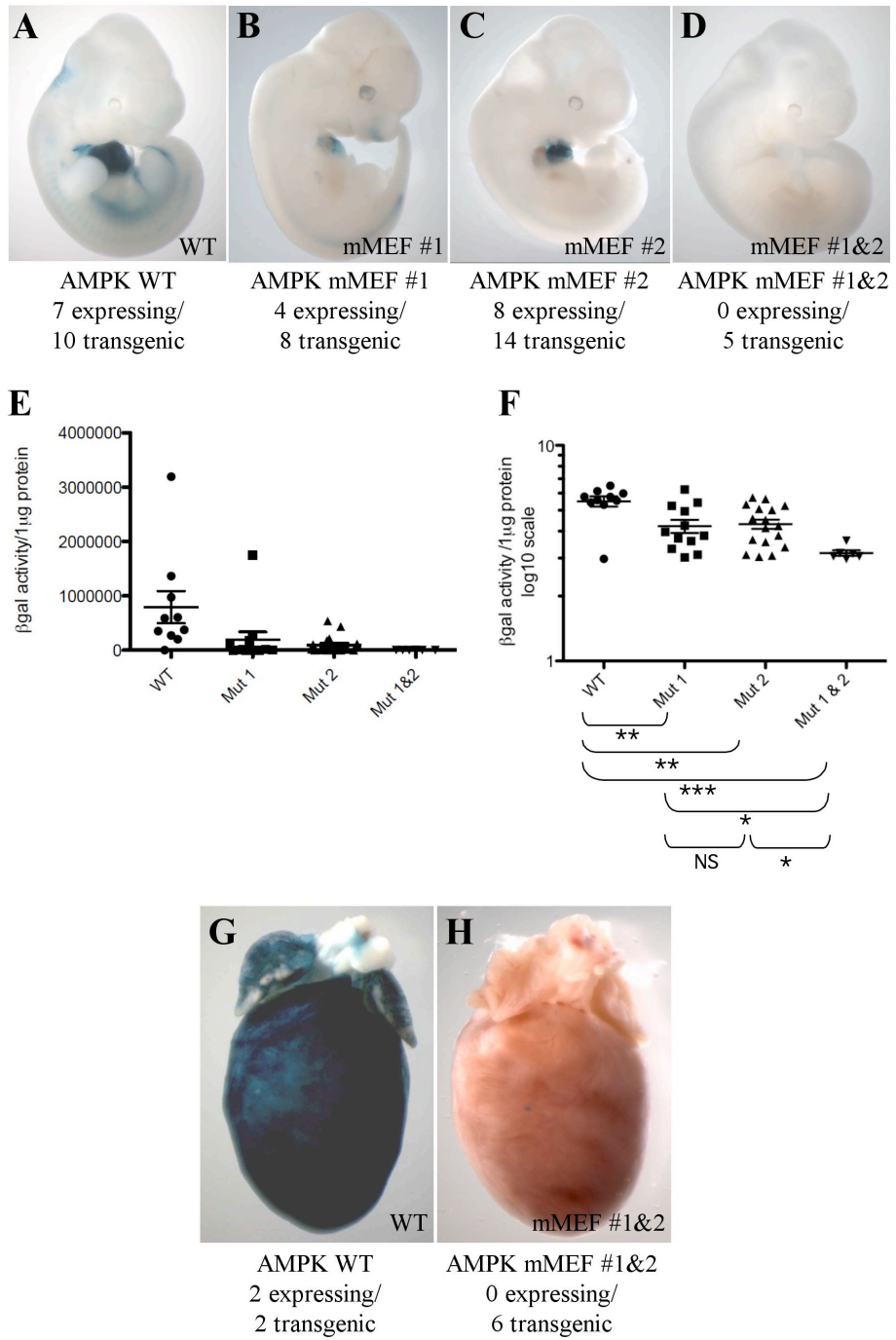


Figure 2-11

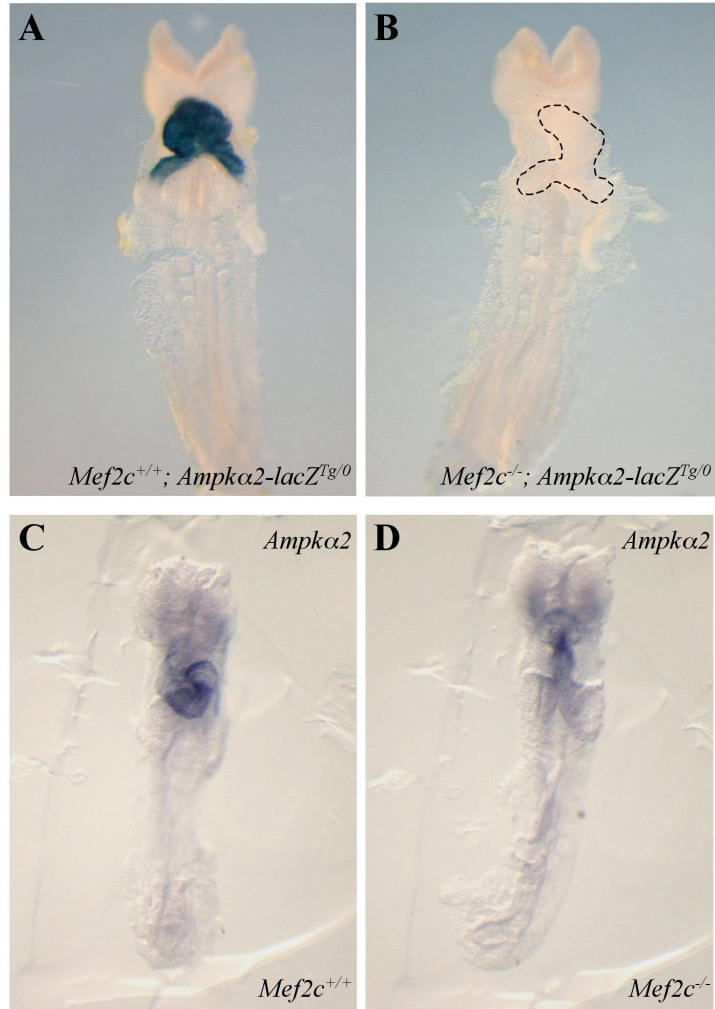


Figure 2-12

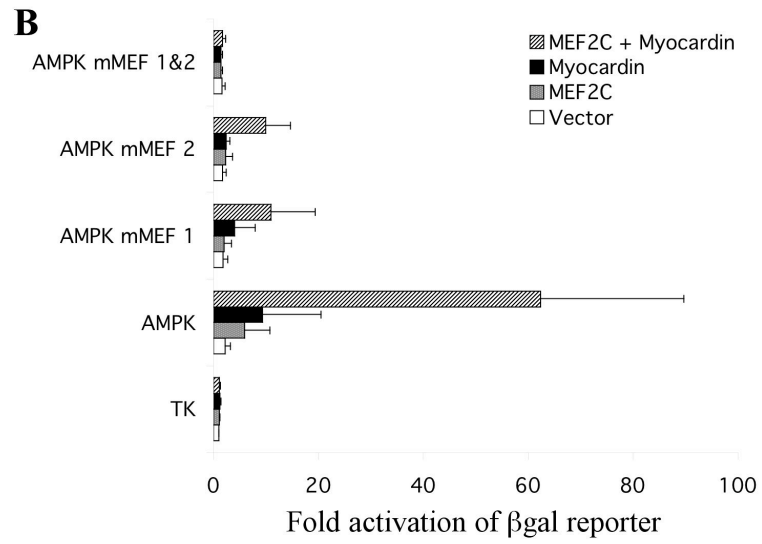
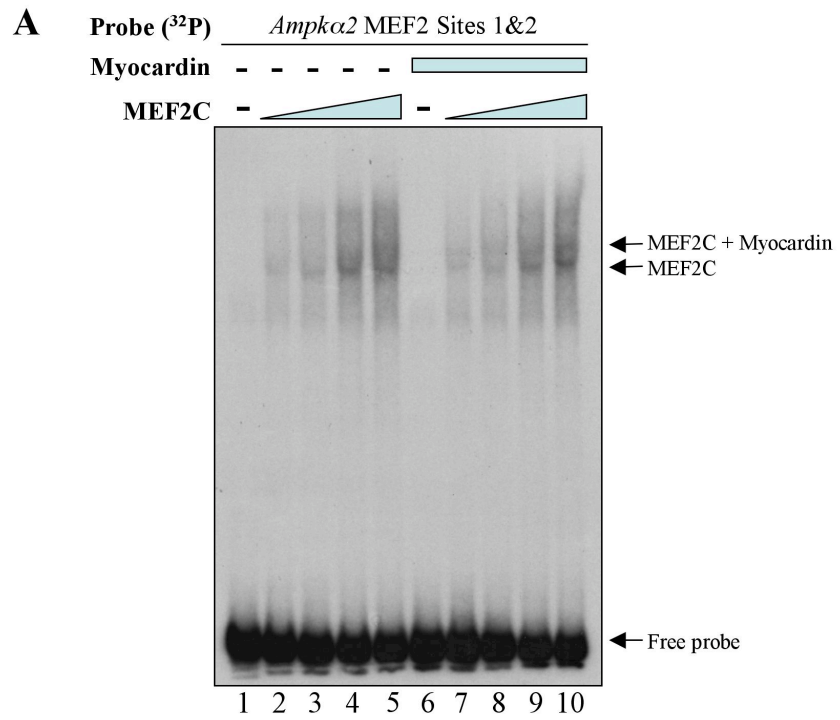


Figure 2-13

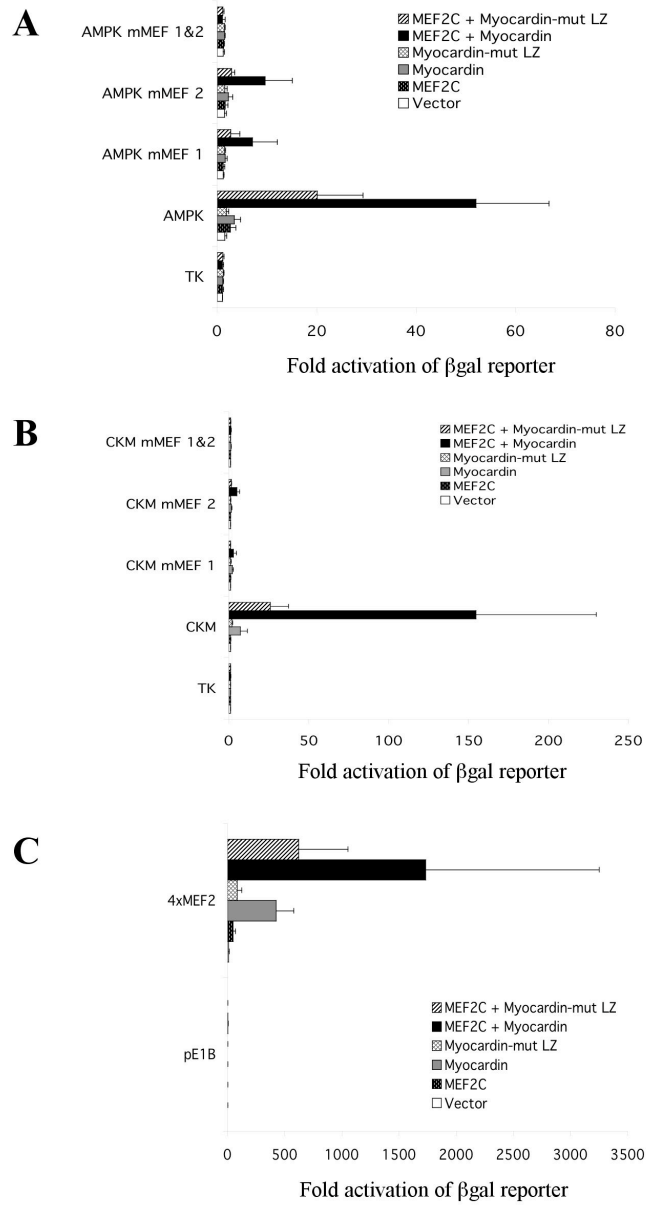
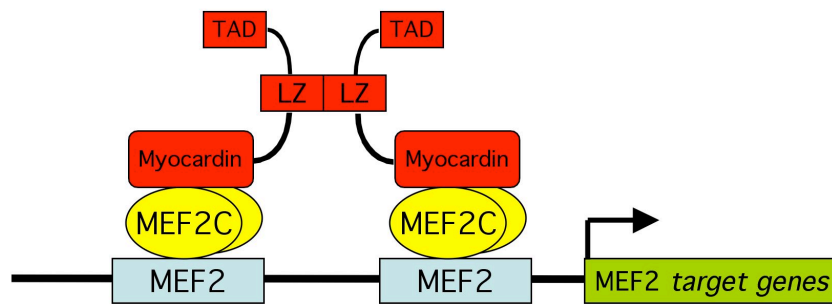


Figure 2-14



Chapter 3: MEF2C function in skeletal muscle is required for normal growth and glucose metabolism

Skeletal muscle plays an important role in whole-body energy homeostasis, making up approximately 40% of the total body mass and accounting for more than 30% of the energy expenditure in the mouse (Smith and Muscat, 2005; Stump et al, 2006). A number of bioenergetic adaptations occur in the muscle in order to maintain whole-body energy metabolism. Energy can be produced by the muscle in response to stimuli such as exercise, contraction, and insulin. During exercise, muscle can produce energy through glycogen metabolism into glucose, or glycogenolysis (Hargreaves, 2004). During exercise and insulin stimulation, skeletal muscle is the primary tissue for glucose uptake, disposal, and storage as glycogen for energy reserves (DeFronzo et al, 1981; Smith and Muscat, 2005). In turn, muscle can use glycogen to produce energy through glycogenolysis, or the breakdown of glycogen into glucose (Hargreaves, 2004). In addition, skeletal muscle can generate energy by contraction. Muscle fibers are comprised of sarcomeres containing repeating units of thick and thin myosin filaments (Russell et al, 2000). As the two filaments move past each other during contraction, energy in the form of ATP is produced (Russell et al, 2000). Depending on the type of myosin in the muscle fiber, contraction can be slow or fast (Pette and Spamer, 1986).

Heterogeneous muscle fibers comprise skeletal muscle and display a variety of metabolic profiles and contractile properties (Bassel-Duby and Olson, 2006). There are four isoforms of fibers: Type I, Type IIa, Type IIc, and Type IIx. Type I fibers are high in mitochondrial content, utilize oxidative metabolism for energy, are slow to fatigue, and

are suited for endurance activities (Pette and Spamer, 1986). Type II fibers, on the other hand, use glycolysis for energy, are quick to fatigue, and are best suited for strength and speed activities (Pette and Spamer, 1986). The proportion of fiber types plays a pivotal role in whole-body metabolism: a predominance of Type I fibers leads to resistance to diet-induced obesity (Wang et al, 2004), and an increase in Type IIb fibers leads to reduced body weight and fat mass due to increased fatty acid metabolism in the liver (Izumiya et al, 2008).

The MADS domain transcription factor family MEF2 is known to play a critical role in skeletal muscle differentiation, growth, and fiber type (Zetser et al, 1999; Wu et al, 2000; Potthoff et al, 2007b), and several skeletal muscle genes have been shown to be targets of MEF2 (Black and Olson, 1998). MEF2C in particular is important in skeletal muscle development and metabolism, as it is expressed at the onset of skeletal muscle differentiation (Edmondson et al, 1994). However, mice that are lacking MEF2C die between E9.5 and E10.5 (Lin et al, 1997), before skeletal muscle has fully developed, thereby precluding any studies on the requirement of *Mef2c* in skeletal muscle in the germline knockout. Therefore, in this chapter, we sought to determine the role of MEF2C in postnatal skeletal muscle by inactivating *Mef2c* specifically in skeletal muscle using a conditional knockout approach.

The *Mef2c*-73K-Cre transgene and the *Myogenin*-1565-Cre transgene both direct Cre expression exclusively in skeletal muscle

To generate a conditional knockout of *Mef2c* in skeletal muscle, we utilized the Cre-lox system (Sauer and Henderson, 1988), in which the enzyme Cre recombinase

catalyzes recombination between two loxP sites that flank a gene of interest, thereby deleting the gene. Tissue specific deletion of a gene can be achieved by putting the Cre recombinase under the control of a tissue specific enhancer or promoter. We utilized two different transgenic mouse lines that expressed Cre recombinase under the control of two skeletal muscle specific promoters, *Mef2c-73K* and *Myogenin-1565*. *Mef2c-73K* is a highly conserved promoter from the mouse *Mef2c* gene and directs expression exclusively to skeletal muscle (Dodou et al, 2003). The *Mef2c-73K-Cre* transgene has been previously described, and is highly specific for skeletal muscle (Heidt and Black, 2005). ROSA26R Cre-dependent *lacZ* reporter mice (Soriano, 1999) show expression of Cre as early as E9.5 in the somites, when skeletal muscle is first being specified, and continuing into the postnatal muscle (Heidt and Black, 2005). This expression is specific for the skeletal muscle, as Cre is detected in every skeletal muscle fiber and *lacZ* staining is undetectable in the postnatal heart (Heidt and Black, 2005). The *Mef2c-73K-Cre* expression pattern also follows the pattern of the *Mef2c-73K* promoter (Dodou et al, 2003).

The *Myogenin-1565-Cre* transgene was generated using a highly conserved promoter from the mouse *Myogenin* gene that is also highly specific for skeletal muscle (Cheng et al, 1992). The *Myogenin-1565-Cre* plasmid was generated by Analeah Heidt and Dustin Khiem. ROSA26R Cre-dependent *lacZ* reporter mice (Soriano, 1999) showed expression of Cre as early as E9.5 in the somites (Fig. 3-1A) and continuing into the postnatal muscle (Fig. 3-1D, E). This expression was specific for skeletal muscle, with the exception that there was some *lacZ* staining detectable in the brain during development and in the postnatal heart, albeit much weaker than in the skeletal muscle

(Fig. 3-1A-G). The *Myogenin*-1565-Cre expression pattern also followed the pattern of the *Myogenin*-1565 promoter, as the staining detected in the brain by ROSA26R analyses correlated with the weak detection of *lacZ* staining in the brain from the *Myogenin*-1565 promoter analysis (Cheng et al, 1992).

We used both skeletal muscle specific Cre transgenic lines to delete *Mef2c* from skeletal muscle. *Myogenin* is active in skeletal muscle precursor cells slightly earlier in development than *Mef2c* (Wright et al, 1989; Edmondson et al, 1994). *Myogenin* can be detected in the somites as early as E8.5 (Wright et al, 1989), whereas *Mef2c* is detected by E9.0 (Edmondson et al, 1994). Even though the *Mef2c*-73K-Cre transgenic line is very specific to muscle and has no expression in the brain, unlike the *Myogenin*-1565-Cre transgenic line, using the *Myogenin*-1565-Cre line would ensure that *Mef2c* is excised prior to activation of the endogenous *Mef2c* gene. Furthermore, we did not know the precise excision capabilities of the Cre constructs, and therefore used both to see if there was a difference in the ability of *Mef2c*-73K-Cre and *Myogenin*-1565-Cre to excise *Mef2c* in skeletal muscle.

Generation of skeletal-muscle specific *Mef2c* conditional knockout mice

To generate skeletal muscle specific mouse knockouts of *Mef2c*, *Mef2c*-73K-Cre or *Myogenin*-1565-Cre transgenic mice were crossed into a heterozygous *Mef2c* background (Lin et al, 1997) to generate mice expressing either *Mef2c*-73K-Cre or *Myogenin*-1565-Cre and heterozygous for *Mef2c* (*Mef2c*-73K-Cre^{Tg/0}; *Mef2c*^{+/-} or *Myogenin*-1565-Cre^{Tg/0}; *Mef2c*^{+/-}). Male mice of this genotype were then crossed to female mice that were homozygous for a Cre-dependent conditional allele of *Mef2c*

(*Mef2c*^{flox/flox}). The *Mef2c*^{flox/flox} mice have been previously described and have no obvious phenotype (Vong et al, 2005). Skeletal muscle-specific knockout mice generated using the *Mef2c*-73K-Cre transgenic line were present at normal Mendelian frequency at birth and all survived through the weaning period (Fig. 3-2B). However, all mice harboring the *Myogenin*-1565-Cre transgenic line were present at significantly less than expected Mendelian frequency at birth (Fig. 3-2C). Mice of all genotypes that were born survived through the weaning period (Fig. 3-2C). The fact that approximately 25% of the *Myogenin*-1565-Cre transgenic mice die prior to birth suggests that the *Myogenin*-1565-Cre transgene is partially lethal. The reduced viability associated with the *Myogenin*-1565-Cre transgene did not appear to be attributable to defects in skeletal muscle and there was no gender bias in surviving mice. It is likely that the transgene insertion created in *Myogenin*-1565-Cre transgenic mice had a deleterious effect on embryo survival, although we have not pursued the lethality due to the *Myogenin*-1565-Cre transgene, as 75% of *Myogenin*-1565-Cre transgenic mice were still viable and lived to adulthood.

The *Mef2c*-73K-Cre transgene and the *Myogenin*-1565-Cre transgene both efficiently delete *Mef2c* from skeletal muscle

To determine the efficiency of *Mef2c* gene inactivation in skeletal muscle, we examined the expression of *Mef2c* within the skeletal muscle of control (referred to herein as control and consist of mice with the genotype *Mef2c*^{flox/+}) and knockout (referred to herein as KO and consist of mice with the genotype *Mef2c*^{flox/-}; Cre^{Tg/0}) mice by *in situ* hybridization and semi-quantitative RT-PCR (Fig. 3-3). Embryos, neonatal (P0) limbs, and adult quadriceps muscle were isolated from crosses using both the *Mef2c*-

73K-Cre (Fig. 3-3A-I) and *Myogenin*-1565-Cre (Fig. 3-3J-R) transgenes. At E9.5, control embryos showed strong expression of *Mef2c* in the myotomal compartment of the somites (Fig. 3-3A, J). *Mef2c* expression in the skeletal muscle of the limbs and in intercostal muscles was also readily apparent in control embryos at E11.5 and E13.5 and in postnatal muscle (Fig. 3-3A-D, J-M). By contrast, *Mef2c* expression was disrupted in KO mice such that it was not detectable in skeletal muscle by *in situ* hybridization at any stage examined, including E9.5, E11.5, E13.5, and P0 (Fig. 3-3E-H, N-Q). *Mef2c* transcripts were not detectable in the quadriceps muscle in adult *Mef2c*^{SKM-KO} mice by RT-PCR under conditions where *Mef2c* expression was readily detectable in control mice (Fig. 3-3I, R).

Mice lacking *Mef2c* in skeletal muscle are viable, but significantly smaller during the weaning period

KO mice resulting from the *Mef2c*-73K-Cre transgene appeared overtly normal and showed no decrease in viability compared to littermate controls. However, these KO mice weighed significantly less than age- and sex-matched controls, beginning at birth and continuing throughout the weaning period (28 days post-birth) (Fig. 3-4A, B). KO mice resulting from the *Myogenin*-1565-Cre transgene also showed no decrease in viability compared to littermate controls and appeared overtly normal in the first few days of birth, but by postnatal day 10 they appeared to be smaller in size. Indeed, when measured, these KO mice weighed significantly less than age- and sex-matched controls, beginning at birth and continuing throughout the weaning period (Fig. 3-4C, D). Interestingly, even though KO mice resulting from both Cre transgenes were smaller in

size, the KO mice from the *Myogenin*-1565-Cre transgene had a 21% (female)-26% (male) reduction in body weight compared to control mice at P28, whereas the KO mice from the *Mef2c*-73K-Cre transgene had a 6% (female)-13% (male) reduction in body weight. These results suggest that, not only are mice lacking *Mef2c* in skeletal muscle smaller in size, but that there is a more severe phenotype in KO mice using the *Myogenin*-1565-Cre transgene. The difference in body weight was maintained even in adult KO male and female mice resulting from the *Myogenin*-1565-Cre transgene (Fig. 3-5B). However, using the *Mef2c*-73K-Cre transgene, there was no change in the body weights of control and KO female mice, and only male KO mice were significantly smaller.

To determine if this weight difference affected all organs and tissues equally, we measured heart, kidney, and spleen weights from adult control and KO mice. In mice resulting from the *Mef2c*-73K-Cre transgene, heart, kidney, and spleen weights remained unchanged in the KO mice compared to age- and sex-matched controls (Fig. 3-5C). However, in mice resulting from the *Myogenin*-1565-Cre transgene, the spleen weight was significantly less in male KO mice compared to male control mice, the kidney weight was significantly less in female KO mice compared to female control mice, and the heart weight was significantly less in all KO mice compared to control mice (Fig. 3-5D). These data correlate with the body weight data in that the KO mice from the *Myogenin*-1565-Cre transgene have a more severe size difference in organ size and are overall smaller in size compared to KO mice from the *Mef2c*-73K-Cre transgene, in which body size is smaller but organ size is not. To further determine if overall body size is affected by the absence of *Mef2c* in skeletal muscle, we measured the tibia length of

control and KO mice. Male and female KO mice from both transgenic lines had significantly shorter tibia length compared to age- and sex-matched controls (Fig. 3-6).

It is important to note that these mice are from an outbred mouse background, so the subtle variations in phenotype may be due to the inherent variability from such a background. However, taken together, these data suggest that overall body size and growth is limited when *Mef2c* is absent from skeletal muscle.

Deletion of *Mef2c* in skeletal muscle by the *Myogenin-1565-Cre* transgene, but not by the *Mef2c-73K-Cre* transgene, results in smaller muscle and fiber size

Because mice lacking *Mef2c* in skeletal muscle had a defect in overall body size, we wanted to determine the size of the muscles and fibers of KO mice compared to control mice. Therefore, we measured gastrocnemius (gastroc) muscle weight from control and KO male and female mice resulting from crosses with the *Mef2c-73K-Cre* transgene (Fig. 3-7A) or the *Myogenin-1565-Cre* transgene (Fig. 3-7E). Gastroc weights from mice resulting from the *Mef2c-73K-Cre* transgene remained unchanged in KO mice compared to age- and sex-matched controls (Fig. 3-7A). However, in mice resulting from the *Myogenin-1565-Cre* transgene, gastroc weights were significantly less in both male and female KO mice compared to age- and sex-matched controls (Fig. 3-7E).

To further define the muscle size, we measured the cross-sectional area of the muscle fibers. Immunohistochemistry (IHC) for laminin, which outlines the membranes of muscle fibers, was performed on sections from the soleus muscle of control and KO mice from both the *Mef2c-73K-Cre* transgene (Fig. 3-7B, C) and *Myogenin-1565-Cre* transgene (Fig. 3-7F, G). Quantification of the cross-sectional area of each individual

muscle fiber revealed that KO mice resulting from the *Myogenin*-1565-Cre transgene had significantly smaller muscle fibers compared to control mice (Fig. 3-7H). However, KO mice resulting from the *Mef2c*-73K-Cre transgene had no difference in their muscle fiber size (Fig. 3-7D). These results correlate with the gastroc weight data and demonstrate that skeletal muscle weight and size is smaller in mice lacking *Mef2c* generated by the *Myogenin*-1565-Cre transgene.

Mice lacking *Mef2c* in skeletal muscle have fewer slow-twitch skeletal muscle fibers

Skeletal muscle is composed of two major fiber types: Type I fibers, which are slow contracting, high in mitochondrial content, and exhibit oxidative metabolism, and Type II fibers, which are fast contracting, exhibit glycolytic metabolism and fatigue easily (Schiaffino and Reggiani, 1996). Type II fibers can further be divided into 3 subtypes (IIa, IIb, and IIx), each with a varying degree of oxidative capacity and mitochondrial content (Schiaffino and Reggiani, 1996). Specification of fiber type is highly plastic and dynamic – exercise, increased calcium, contraction, and other processes can cause a fiber to switch from Type II to Type I, and conversely, lack of neuromuscular activity can lead to a switch from Type I to Type II (Potthoff et al, 2007a). It has been previously shown that MEF2C plays an important role in fiber type establishment and maintenance (Chin et al, 1998; Wu et al, 2000), and overexpression of MEF2C in skeletal muscle *in vivo* results in an increased number of Type I/slow-twitch fibers (Potthoff et al, 2007b).

Therefore, to determine if mice lacking *Mef2c* in skeletal muscle had a defect in fiber type composition, we measured the percentage of Type I muscle fibers in the soleus

muscle, which has a large proportion of Type I fibers (Gollnick et al, 1974) (Fig. 3-8). The antibody MY32 recognizes all fast type fibers, and IHC revealed that KO mice from both transgenic Cre lines showed a significantly higher number of MY32-positive/ Type II fibers compared to control mice (Fig. 3-8). Quantification of these IHCs demonstrated that mice lacking *Mef2c* in skeletal muscle had significantly fewer Type I fibers in the soleus muscle compared to control mice (Fig. 3-8C, F). These data correlate with previous findings in the literature implicating the role of MEF2C in fiber type switching (Chin et al, 1998; Wu et al, 2000; Potthoff et al, 2007b) and suggest that *Mef2c* is required in skeletal muscle for the formation of Type I/slow-twitch fibers.

Mice lacking *Mef2c* in skeletal muscle do not have impairments in voluntary running ability

Fiber type composition is important for skeletal muscle function. For aerobic exercises such as endurance running, Type I/slow-twitch fibers function well because of their high mitochondrial content and oxidative capacity (Schiaffino and Reggiani, 1996). However, anaerobic activities selectively utilize Type II/fast-twitch fibers, which use glycogen and glycolysis as an energy source (Schiaffino and Reggiani, 1996). Mice overexpressing *Mef2c* have an increase in Type I/slow-twitch fibers and excel at running in a forced treadmill exercise compared to controls (Potthoff et al, 2007b). Based on our observation that *Mef2c* skeletal muscle KO mice had a reduction in the percentage of Type I fibers, we wanted to see if they also had impairments in exercise capabilities. To test this hypothesis, control and KO mice ran in a voluntary exercise assay for 7 days after an initial 3-day training period. Control and KO male and female mice generated

from both the *Mef2c*-73K-Cre transgene (Fig. 3-9A-C) or the *Myogenin*-1565-Cre transgene (Fig. 3-9D-F) had no difference in the time run, distance run, or the average speed run. These data demonstrate that, despite a reduction in Type I/slow-twitch fibers, mice lacking *Mef2c* in skeletal muscle do not have impairments in voluntary exercise capability.

Deletion of *Mef2c* in skeletal muscle by the *Mef2c*-73K-Cre transgene, but not by the *Myogenin*-1565-Cre transgene, results in increased glycogen accumulation in the muscle fibers post-exercise

Although mice lacking MEF2C in skeletal muscle do not have impaired running ability in a voluntary assay, we considered the possibility that MEF2C might be important for normal muscle sarcomere architecture either prior to or after exercise, as has been previously reported (Potthoff et al, 2007b). To determine if KO mice had sarcomeric structural defects prior to or after running, we analyzed the cellular architecture of the soleus muscle in control and KO mice generated by the *Mef2c*-73K-Cre transgene pre- and post-exercise by electron microscopy (Fig. 3-10). Electron micrographs from non-exercised mice demonstrated that both control and KO mice had well-organized sarcomeres and essentially no difference in the ultrastructure of the muscle (Fig. 3-10C, D). Analyses of post-exercise skeletal muscle demonstrated an increased number of mitochondria in both control and *Mef2c*^{SKM-KO} mice compared to mice that had not been subjected to voluntary exercise (Fig. 3-10E, F). This was an expected result since increased mitochondrial biogenesis is a normal response seen in

post-exercise animals as energy demand and oxidative metabolism increase (Holloszy and Coyle 1984).

Importantly, we observed the presence of large vacuolar inclusion bodies in the soleus muscle of KO mice following 7 days of voluntary exercise (Fig. 3-10E, F). These vacuoles were present throughout the muscle and contained a granular material (Fig. 3-10E, F). Toluidine blue staining of thin sections, which was used to check the quality of the sections for electron microscopy, also revealed the presence of several inclusions, as well as centrally-located nuclei, in the muscle fibers of exercised KO mice (Fig. 3-10B). By contrast, vacuoles were not present in control mice after 7 days of voluntary wheel running (Fig. 3-10A).

The granular vacuoles in KO mice superficially resembled glycogen deposits. To test the notion that glycogen was abnormally accumulated in the exercised muscle of KO mice, we used periodic acid/Schiff's base (PAS) to stain frozen sections from the soleus muscle of control and KO non-run and run mice (Fig. 3-11). Control and KO mice generated using the *Mef2c-73K-Cre* transgene had similar glycogen levels under no exercise conditions (Fig. 3-11A, B). However, control mice had a slight drop in glycogen levels post-exercise, while KO mice had an increase in glycogen content post-exercise compared to controls (Fig. 3-11C, D). Quantification of the glycogen in the muscles of these mice, as determined by glycogen precipitation and glucose release from glycogen, demonstrated a significant increase in glycogen in KO mice in response to exercise compared to control run mice (Fig. 3-11E). Taken together, these results demonstrate that MEF2C is necessary for appropriate glycogen metabolism in skeletal muscle in mice in response to the demand of an exercise challenge.

However, in mice generated from the *Myogenin*-1565-Cre transgene, we observed different results. In no run animals, both control and KO mice had comparable glycogen levels (Fig. 3-11F, G). Upon exercise, control and KO mice had increased glycogen in their muscles compared to their no run counterparts, however there was no significant difference in glycogen content between control and KO run mice (Fig. 3-11H, I). Quantification of muscle glycogen content confirmed these observations and demonstrated that while there was a significant increase in glycogen content between control no run and run mice, and KO no run and run mice, there was no significant difference between control and KO run mice.

Deletion of *Mef2c* in skeletal muscle by the *Mef2c*-73K-Cre transgene results in better tolerance of glucose, but has no effect on insulin resistance

The abnormal synthesis or metabolism of glycogen and the overall smaller body size in KO mice suggested that MEF2C function in skeletal muscle might be important for normal glucose homeostasis. To test this hypothesis, we measured blood glucose in control and KO mice after 16 hours of fasting (Fig. 3-12A). We observed that KO mice had significantly lower blood glucose levels compared to control mice at time point 0 minutes (Fig. 3-12A). Furthermore, when mice were given a bolus injection of glucose after 16 hours of fasting, KO mice cleared the glucose from their bloodstream more quickly than control mice (Fig. 3-12A). Taken together, these data suggest that MEF2C is required in skeletal muscle for normal glucose homeostasis and whole body glucose metabolism.

For the insulin resistance test, mice were treated with a bolus of insulin and their blood glucose levels were measured at the indicated time points (Fig. 3-12B). While the control mice responded appropriately, with a decrease in blood glucose levels in response to insulin, there was no significant difference in the response of KO mice to insulin compared to control mice. These data suggest that while mice lacking *Mef2c* in skeletal muscle may have slightly better clearance of glucose from the bloodstream, they are not insulin resistant and therefore do not display the basic attributes of Type 2 diabetes, nor do they have an improved metabolic profile.

Activation of MEF2C by insulin receptor stimulation through p38 phosphorylation

From the data presented thus far, we have clear evidence supporting a role for MEF2C in controlling overall body growth, muscle growth, and fiber type composition. To understand the molecular mechanisms underlying this role for MEF2C in metabolism, we wanted to know which downstream targets were affected in mice lacking *Mef2c* in skeletal muscle. To address this, we conducted a microarray on E11.5 control and KO embryos, as well as on newborn muscle from control and KO P0 mice, generated from the *Myogenin-1565-Cre* transgene. To our surprise, the microarray was not able to detect significant differences in any genes (data not shown). These results could be due to the fact that other MEF2 isoforms, MEF2A and MEF2D, are present in skeletal muscle at these time points (Edmondson et al, 1994), and they could be compensating for the lack of MEF2C in muscle.

However, we do observe a strong phenotype of small body size and muscle size, which suggests that MEF2C is playing some role in skeletal muscle metabolism. Since

we could not identify any downstream targets of MEF2C, we then addressed which upstream signaling pathways might affect the ability of MEF2C to function in skeletal muscle. MEF2 proteins function as transcriptional switches and can be repressed or activated depending on post-translational modifications (Black and Cripps, 2010). MEF2C is phosphorylated by the MAP kinase p38 (Yang et al, 1999; Zetser et al, 1999; Zhao et al, 1999), and can induce skeletal muscle differentiation upon activation by p38 (Zetser et al, 1999). In skeletal muscle, numerous upstream pathways can activate the MAPK cascade, in particular the insulin receptor signaling pathway (Sweeney et al, 1999). Furthermore, it has been well documented that insulin signaling plays a crucial role in regulating body and muscle size (reviewed in Plum et al, 2005). Lastly, it has been shown *in vitro* that insulin stimulation increases the DNA binding capabilities of MEF2C, and this can be blocked by the p38 inhibitor SB203580 (Al-Khalili et al, 2004; Khiem et al, 2008). Based on the literature, MEF2C has been implicated in insulin receptor signaling, however the direct link between MEF2C, p38, and insulin has not been investigated. We hypothesized that the insulin receptor, upon stimulation, promotes activation of the p38 MAPK cascade, which then phosphorylates and activates MEF2C, allowing MEF2C to carry out its functions in skeletal muscle.

To test our hypothesis, we took advantage of a multimerized MEF2 consensus site reporter, 4xMEF2-*lacZ*. We treated transfected C2C12 myoblasts with insulin and measured MEF2-dependent reporter activity (Fig. 3-13). Treatment with insulin led to a significant increase in activity of the reporter (Fig. 3-13A), suggesting that insulin stimulates the activation of endogenous MEF2. However, this activation of endogenous

MEF2 is not through a p38 pathway, as addition of SB203580 does not reduce insulin-stimulated activation of the reporter (Fig. 3-13A).

Interestingly, cotransfection of C2C12 myoblasts with the 4xMEF2-*lacZ* reporter and the MEF2C expression plasmid followed by treatment with insulin led to an even greater activation of the reporter, and this activity was significantly reduced with the addition of SB203580 (Fig. 3-13B). These data suggest that insulin stimulates activation of overexpressed MEF2C through a p38 MAPK pathway.

Finally, C2C12 myoblasts were co-transfected with the 4xMEF2-*lacZ* reporter and a phospho-mutant form of MEF2C (p-mut MEF2C), in which the three p38 phosphorylation sites of MEF2C (T293, T300, and S387) were mutated to alanines (Khiem et al, 2008) (Fig. 3-13C). The phospho-mutant form of MEF2C reduced the insulin receptor stimulation of the 4xMEF2-*lacZ* reporter (Fig. 3-13C). These results demonstrate that p38 phosphorylation is required for insulin activation of MEF2C.

To demonstrate that insulin receptor stimulation of MEF2C is working through the p38 MAPK pathway *in vivo*, we differentiated C2C12 myoblasts into myofibers and then treated with PBS, insulin, SB203580, or a combination of insulin and SB203580 (Fig. 3-14). Insulin led to a robust increase in myofiber diameter size (Fig. 3-14C), and this increase in hypertrophy was blocked by SB203580 (Fig. 3-14D). Myofiber diameters were quantified, and while more experiments need to be done to determine significance, it appears that inhibition of p38 blocked insulin-induced hypertrophy of the myofibers (Fig. 3-14E). Taken together with the transfection results, these data suggest a pathway in which MEF2C acts downstream of insulin receptor signaling via the p38 MAPK cascade,

and that insulin-stimulated myofiber hypertrophy occurs through the p38 MAPK pathway.

Discussion

MEF2C plays a crucial role in skeletal muscle differentiation *in vitro* and has been implicated in skeletal muscle metabolism. In this chapter, using two independent, transgenic Cre lines, we determined that *Mef2c* is required in skeletal muscle not only for muscle growth, but also for overall body size. Mice lacking *Mef2c* have defects in fiber type composition and mild glycogen accumulation, but these impairments do not have an effect on exercise abilities. Lastly, we show that MEF2C may function downstream of insulin receptor signaling through a p38 MAPK signaling pathway in skeletal muscle.

Table 1: *Mef2c* skeletal muscle conditional knockout phenotypes

	<i>Mef2c</i> -73K-Cre KOs	<i>Myogenin</i> -1565-Cre KOs
Mendelian frequencies	Normal	25% of all Cre transgenic mice are not present at birth
<i>Mef2c</i> muscle expression	Reduced, but not completely absent	Absent
Weights through weaning	Males are smaller from P10 to P28; Females are smaller from P7 to P21	Males are smaller from P10 to P28; Females are smaller from P1 to P28
Weights in adults	Males are smaller; no change in females	Males and females are smaller
Organ weights	No change in males or females	Male spleens and hearts are smaller; Female hearts and kidneys are smaller
Tibia length	Males and females are smaller	Males and females are smaller
Gastroc weight	No change in males or females	Males and females are smaller
Fiber size	No change	Fibers are smaller in cross-sectional area
Fiber type	Reduced slow twitch fibers	Reduced slow twitch fibers

Running ability	No change in males or females	No change in males or females
Glycogen accumulation	Run mice abnormally accumulate glycogen	No change
Glucose/Insulin response	Clear glucose more quickly, but no change in insulin response	<i>*not tested</i>

The similarities and differences observed between the *Mef2c* skeletal muscle conditional knockout mice generated by the two Cre lines are highlighted in Table 1. The common phenotypes observed between the two lines were small overall body size, small tibia length, and reduced slow twitch fibers. KO mice generated from the *Mef2c*-73K-Cre transgene also had abnormal glycogen accumulation post-exercise and better glucose tolerance compared to controls, however these phenotypes were not observed in KO mice generated from the *Myogenin*-1565-Cre transgene. The observed phenotypes may be due to the fact that all experiments were done on an outbred mouse background, which have more genetic variation than an inbred mouse background (Linder and Davisson, 2004). The lack of genetic homogeneity in outbred mice may also confound some of the results observed in our mice.

It is important to acknowledge that a previous report of mice lacking *Mef2c* in skeletal muscle has been published (Potthoff et al, 2007b; Potthoff et al, 2007c). In these studies, mice lacking *Mef2c* in skeletal muscle die by postnatal day 2 due to abnormally formed sarcomeres and weakened M lines, and the authors show that *Mef2c* directly regulates the M-line-specific genes *Myomesin 1* and *2*. Interestingly, the authors did not report any metabolic or growth defects. However, there were several differences in their experimental design that may account for the different phenotypes between our *Mef2c* skeletal muscle conditional knockout mice and theirs. First, in these previous studies,

mice were generated from an inbred strain, and the authors note that using other backgrounds such as 129/SvEv resulted in a less severe phenotype (Potthoff et al, 2007c), suggesting that *Mef2c* is sensitive to genetic modifiers. Furthermore, the authors used a skeletal muscle specific Cre transgene containing both the *Myogenin* promoter and the *Mef2c* skeletal muscle enhancer. The authors acknowledge that the use of another Cre transgene that deletes *Mef2c* at E18.5, *MCK-Cre*, resulted in viable KO mice and no disruption of the myofiber organization, however these mice do have reduced Type I/slow-twitch fibers, similar to the results seen with our KO mice. These studies demonstrate a role for MEF2C in the maintenance of sarcomeric integrity and postnatal muscle function, whereas our studies suggest an additional role for MEF2C in skeletal muscle metabolism and whole body growth.

The phenotypes of the *Mef2c* skeletal muscle conditional knockout mice identified in this chapter raise an interesting question: how does deletion of *Mef2c* in skeletal muscle affect whole body size? Skeletal muscle responds to external factors such as glucose, IGF, and insulin to control growth of muscle fibers, and calcium to control fiber type (Bassel-Duby and Olson, 2006). In turn, skeletal muscle generates energy in the form of ATP from fatty acid oxidation and glycolysis, which helps control whole body size (Smith and Muscat, 2005). It has been shown that insulin stimulates glucose uptake and protein synthesis in the muscle by activating two pathways: the AKT/mTOR pathway (reviewed in Bolster et al, 2004) and the p38 MAPK pathway (Sweeney et al, 1999). Another study has demonstrated that MEF2 DNA binding increases in response to insulin, and this binding is blocked by a p38 inhibitor (Al-Khalili et al, 2004). Our work suggests a connection between these two points and indicates that MEF2C may be in a

direct pathway downstream of insulin signaling and p38 MAPK phosphorylation in the control of skeletal muscle hypertrophy (Fig. 3-14). Given the impact of diabetes and obesity on our society's health, defining a role for MEF2C in skeletal muscle and whole body metabolism will be of great help to further understand these diseases and identify cures and therapies.

Figure Legends

Figure 3-1: The *Mef2c*-73K-Cre transgene and the *Myogenin*-1565-Cre transgene both direct Cre expression exclusively in skeletal muscle

Whole-mount X-gal stained embryos and neonatal tissues resulting from crossing Cre-positive transgenic mice to ROSA26R Cre-dependent *lacZ* reporter mice. (A) The *Mef2c*-73K-Cre transgene, published by Heidt AB and Black BL, 2005. (B-G) The *Myogenin*-1565-Cre transgene.

Figure 3-2: Generation of skeletal-muscle specific *Mef2c* conditional knockout mice

(A) Schematic depicting the strategy for deleting *Mef2c* from skeletal muscle. Male mice that were *Mef2c*^{+/-}; Cre^{Tg/0} were crossed to female mice that were *Mef2c*^{Flox/Flox}. Control mice have the genotype *Mef2c*^{+/floX}, and conditional knockout mice (KO) have the genotype *Mef2c*^{-/floX}; Cre^{Tg/0}. (B) Using the 73K-Cre transgene, all mice, including KO mice, were born at expected Mendelian ratios (control vs. KO, p>0.5). (C) Using the 1565-Cre transgene, all mice harboring the 1565-Cre transgene were born at significantly lower frequency than expected (control vs. KO, p<0.0001; control vs. *Mef2c*^{+/floX}; 1565-Cre^{Tg/0}, p<0.0001).

Figure 3-3: Both the *Mef2c*-73K-Cre transgene and the *Myogenin*-1565-Cre transgene efficiently delete *Mef2c* from skeletal muscle

Whole-mount *in situ* hybridization for *Mef2c* (A-H, J-Q) and semi-quantitative RT-PCR for *Mef2c* and the loading control *L7* (I, R). (A-I) Deletion of *Mef2c* by the *Mef2c*-73K-

Cre transgene during embryonic development was detected by *in situ* hybridization for *Mef2c* in control and KO embryos (A-C, E-G) and neonatal limbs (D, H). Deletion of *Mef2c* by the *Mef2c-73K-Cre* transgene in control and KO adult quadriceps muscle was detected by semi-quantitative RT-PCR (I). (J-R) Deletion of *Mef2c* by the *Myogenin-1565-Cre* transgene during embryonic development was detected by *in situ* hybridization for *Mef2c* in control and KO embryos (J-L, N-P) and neonatal limbs (M, Q). Deletion of *Mef2c* by the *Myogenin-1565-Cre* transgene in control and KO adult quadriceps muscle was detected by semi-quantitative RT-PCR (R).

Figure 3-4: Mice lacking *Mef2c* in skeletal muscle are viable but are significantly smaller during the weaning period

Whole body weights for male (A, C) and female (B, D) mice. Body weights were taken for mice of each genotype noted at postnatal day 1, 4, 7, 10, 14, 21, and 28. (A, B) Body weights for mice resulting from crosses with the *Mef2c-73K-Cre* transgene. Error bars represent standard deviations. Male control vs. KO: P10 p=0.0031, P14 p=0.0191, P21 p<0.0001, P28 p<0.0001. Female control vs. KO: P7 p=0.0419, P10 p=0.0369, P14 p=0.0224, P21 p=0.0021. (C, D) Body weights for mice resulting from crosses with the *Myogenin-1565-Cre* transgene. Error bars represent standard deviations. Male control vs. KO: P10 p=0.0370, P14 p=0.0029, P21 p=0.0051, P28 p=0.0006. Female control vs. KO: P1 p=0.0015, P4 p=0.036, P7 p=0.035, P14 p=0.0063, P21 p=0.0033, P28 p=0.0039.

Figure 3-5: Mice lacking *Mef2c* in skeletal muscle remain smaller in size during adulthood and have smaller organ size

(A, B) Whole body weights for male (blue bars) and female (pink bars) mice. Body weights were taken for control and KO mice at 52 days of age. (A) Body weights for mice resulting from crosses with the *Mef2c*-73K-Cre transgene. Error bars represent standard deviations. Male control vs. KO $p=0.0247$. (B) Body weights for mice resulting from crosses with the *Myogenin*-1565-Cre transgene. Error bars represent standard deviations. Male control vs. KO $p=0.049$. Female control vs. KO $p=0.0025$. (C, D) Weights of spleen, heart, and kidney from male (blue bars) and female (pink bars) control and KO mice at 52 days of age. (C) Organ weights from mice resulting from crosses with the *Mef2c*-73K-Cre transgene. Error bars represent standard deviations. (D) Organ weights from mice resulting from crosses with the *Myogenin*-1565-Cre transgene. Error bars represent standard deviations. Male spleen control vs. KO $p=0.0440$. Male heart control vs. KO $p=0.0004$. Female heart control vs. KO $p=0.0012$. Female kidney control vs. KO $p=0.0314$.

Figure 3-6: Deletion of *Mef2c* in skeletal muscle results in shorter tibia length

Tibia length measurements from male (blue bars) and female (pink bars) mice. Tibia length was measured in control and KO mice at 52 days of age. (A) Tibia length for mice resulting from crosses with the *Mef2c*-73K-Cre transgene. Error bars represent standard deviations. Male control vs. KO $p=0.034$. Female control vs. KO $p=0.0013$. (B) Tibia length for mice resulting from crosses with the *Myogenin*-1565-Cre transgene. Error bars represent standard deviations. Male control vs. KO $p<0.0001$. Female control vs. KO $p<0.0001$.

Figure 3-7: Deletion of *Mef2c* in skeletal muscle by the *Myogenin-1565-Cre* transgene, but not by the *Mef2c-73K-Cre* transgene, results in smaller muscle and fiber size

(A, E) Weights of gastrocnemius (gastroc) muscle from male (blue bars) and female (pink bars) control and KO mice at 52 days of age. (A) Gastroc weight from mice resulting from crosses with the *Mef2c-73K-Cre* transgene. Error bars represent standard deviations. (E) Gastroc weight from mice resulting from crosses with the *Myogenin-1565-Cre* transgene. Error bars represent standard deviations. Male control vs. KO $p=0.0002$. Female control vs. KO $p=0.0008$. (B, C, F, G) Laminin immunofluorescent staining on sections from the soleus muscle of males at 52 days of age outlining each individual muscle fiber at 10x magnification. (B, C) Soleus muscle sections from mice resulting from crosses with the *Mef2c-73K-Cre* transgene. (F, G) Soleus muscle sections from mice resulting from crosses with the *Myogenin-1565-Cre* transgene. (D, H) Quantification of cross-sectional area of soleus muscle fibers from control and KO male mice at 52 days of age. Each muscle fiber in a 10x field outlined by laminin immunofluorescent staining was measured using Image J software. Measurements were taken from 5 sections from throughout the length of the muscle from one animal and averaged to generate a mean value for $n=1$, and this was done for 4 animals for each genotype. (D) Cross-sectional area of soleus muscle from mice resulting from crosses with the *Mef2c-73K-Cre* transgene. Error bars represent standard deviations. (H) Cross-sectional area of soleus muscle from mice resulting from crosses with the *Myogenin-1565-Cre* transgene. Error bars represent standard deviations. Control vs. KO $p<0.0001$.

Figure 3-8: Mice lacking *Mef2c* in skeletal muscle have fewer slow-twitch skeletal muscle fibers

(A, B, D, E) Myosin-32 (MY32) immunofluorescent staining for fiber type identification from soleus muscle sections of males at 52 days of age at 10x magnification. Red fibers indicate fast twitch/Type II fibers and black fibers indicated slow-twitch/Type I fibers.

(A, B) Soleus muscle sections from mice resulting from crosses with the *Mef2c*-73K-Cre transgene. (D, E) Soleus muscle sections from mice resulting from crosses with the *Myogenin*-1565-Cre transgene. (C, F) Quantification of slow-twitch/Type I muscle fibers in the soleus muscle of 52-day old male mice. The number of black and red fibers in a 10x field was counted. Measurements were taken from 2 sections from throughout the length of the muscle from one animal and averaged to generate a mean value for n=1, and this was done for 5-9 animals for each genotype. The data is presented as the percent of slow-twitch/Type I fibers out of the total number of fibers counted. (C) The percent of slow-twitch/Type I fibers in the soleus muscle from mice resulting from crosses with the *Mef2c*-73K-Cre transgene. Error bars represent standard deviations. Control vs. KO p<0.0001. (H) The percent of slow-twitch/Type I fibers in the soleus muscle from mice resulting from crosses with the *Myogenin*-1565-Cre transgene. Error bars represent standard deviations. Control vs. KO p=0.0157.

Figure 3-9: Mice lacking *Mef2c* in skeletal muscle do not have impairments in voluntary running ability

Adult mice (6 weeks of age) were tested for their ability to voluntarily run on a running wheel for one week. Mice underwent a 3-day training period to become acclimated to the

wheel, then were allowed to voluntarily run for 7 days. Measurements for distance run (A, D) and time run (B, E) were taken each day and then averaged. Speed (C, F) was determined by dividing the distance run over the time run. Measurements were taken for male (blue bars) and female (pink bars) mice. (A-C) Running data from mice resulting from crosses with the *Mef2c*-73K-Cre transgene. Error bars represent standard deviations. (D-F) Running data from mice resulting from crosses with the *Myogenin*-1565-Cre transgene. Error bars represent standard deviations.

Figure 3-10: Deletion of *Mef2c* in skeletal muscle by the *Mef2c*-73K-Cre transgene results in accumulation of glycogen in vacuoles in muscle fibers post-exercise

Control or KO mice resulting from crosses with the *Mef2c*-73K-Cre transgene underwent either 7 days of voluntary running or no running, and then the soleus muscle was examined by electron microscopy (EM) for ultrastructure analysis. (A, B) Sections from control and KO mice that ran were stained with toluidine blue to examine the quality of the sections for EM analysis at 20x magnification. Toluidine blue stain reveals inclusions (solid arrows) within the muscle fibers of KO run mice, as well as the presence of centrally-located nuclei (dashed arrow) (B). (C-F) Ultrastructural analysis of the soleus muscle from no run (C, D) and run (E, F) mice was determined by electron microscopy at 8000x magnification. Control (C) and KO (D) no run mice both have very well organized sarcomeres. After exercise both control (E) and KO (F) mice have an increase in mitochondria. Run KO mice (F) also have increased accumulation of glycogen vacuoles (arrows) in between the sarcomeres.

Figure 3-11: Deletion of *Mef2c* in skeletal muscle by the *Mef2c*-73K-Cre transgene, but not by the *Myogenin*-1565-Cre transgene, results in increased glycogen accumulation in the muscle fibers post-exercise

Glycogen content was qualitatively analyzed in the soleus muscle from no run and run adult mice by periodic acid Schiff's (PAS) stain at 10x magnification (A-D, F-I). Control and KO mice underwent either 7 days of voluntary running or no running, and the quadriceps muscle was isolated for PAS stain. (E, J) Glycogen content was quantified by measuring the amount of glucose resulting from the breakdown of glycogen in the gastrocnemius muscle from no run and run adult mice. Each point represents an individual animal's glycogen content, and n=4-9 mice per genotype and treatment group. Data is presented as milligrams of glucose per gram of muscle tissue used in the assay. (A-E) Control or KO mice resulting from crosses with the *Mef2c*-73K-Cre transgene. Control run vs. KO run p=0.032. (F-J) Control or KO mice resulting from crosses with the *Myogenin*-1565-Cre transgene. Control no run vs. control run p=0.0035. KO no run vs. KO run p=0.0128.

Figure 3-12: Deletion of *Mef2c* in skeletal muscle by the *Mef2c*-73K-Cre transgene results in better tolerance of glucose but has no effect on insulin resistance

10-week old control or KO mice resulting from crosses with the *Mef2c*-73K-Cre transgene were tested for glucose tolerance (A) or insulin resistance (B). (A) For the glucose tolerance test, mice were fasted for 16 hours, then treated with glucose (1g glucose/kg body weight) for 2 hours. Blood glucose readings were taken at 0, 15, 30, 60 and 120 minutes. Error bars represent standard deviations. Control vs. KO: 0 min

p=0.0005, 30 min p=0.016, 60 min p=0.0064, 120 min p=0.0073 (B) For the insulin resistance test, mice were treated with insulin (0.75 units/kg body weight) for 45 minutes. Blood glucose readings were taken at 0, 15, and 45 minutes. Error bars represent standard deviations.

Figure 3-13: Activation of MEF2C by insulin receptor stimulation

(A) C2C12 myoblasts were co-transfected with either the parental reporter plasmid pE1B-*lacZ* (white bars) or a multimerized MEF2 consensus site reporter (4xMEF2-*lacZ*; black bars), and then treated four hours later with either PBS, 25nM insulin, 10 μ m SB203580, or insulin + SB203580. Results are reported as fold activation of *lacZ* reporter over the empty vector treated with PBS (pE1B-*lacZ* + PBS). The data shown represent the mean values obtained in 6 independent transfections. Error bars represent standard deviations. 4xMEF2-*lacZ* PBS vs. insulin p=0.0075. (B) C2C12 myoblasts were co-transfected with either pE1B-*lacZ* or 4xMEF2-*lacZ*, and either the parental expression vector pRK5 or MEF2C expression plasmid. Cells were then treated four hours later with either PBS, 25nM insulin, 10 μ m SB203580, or insulin + SB203580. Results are reported as fold activation of *lacZ* reporter over the empty vectors treated with PBS (pE1B-*lacZ* + pRK5 + PBS). The data shown represent the mean values obtained in 6 independent transfections. Error bars represent standard deviations. 4xMEF2-*lacZ* PBS vs. insulin p=0.0075. 4xMEF2-*lacZ* + MEF2C PBS vs. insulin p=0.002. 4xMEF2-*lacZ* + MEF2C insulin vs. insulin + SB203580 p=0.0431. (C) C2C12 myoblasts were co-transfected with either pE1B-*lacZ* or 4xMEF2-*lacZ*, and either the parental expression vector pRK5, the wild-type MEF2C expression plasmid, or a phospho-mutant form of MEF2C (p-mut

MEF2C). Cells were then treated four hours later with either PBS, 25nM insulin, 10 μ m SB203580, or insulin + SB203580. Results are reported as fold activation of *lacZ* reporter over the empty vectors treated with PBS (pE1B-*lacZ* + pRK5 + PBS). The data shown represent the mean values obtained in 5 independent transfections. Error bars represent standard deviations. 4xMEF2-*lacZ* + MEF2C PBS vs. insulin p=0.002. 4xMEF2-*lacZ* + insulin MEF2C vs. p-mut MEF2C p=0.0177.

Figure 3-14: Insulin-stimulated myofiber hypertrophy requires p38-MAPK phosphorylation

(A-D) MF20 immunofluorescent staining in differentiated C2C12 myofibers. C2C12 myoblasts were plated on collagen-coated coverslips in 3cm plates in high-serum media on day 1. The myoblasts were switched to low-serum media on day 2, and allowed to differentiate for 2 days. On day 4, the differentiated myofibers were treated with PBS (A), 10 μ m SB203580 (B), 100nM insulin (C), and insulin + SB203580 (D) for 48 hours. (E) Fiber diameter measurement was determined using Image J software. Ten 10x magnification fields were randomly chosen from a 3cm plate of the C2C12 differentiated myofibers described in (A-D). Within each field, ten myofibers were measured three times along the length of the myofiber. The data represent the mean values obtained in 2 independent differentiation assays.

Figure 3-1 **1565 Cre**

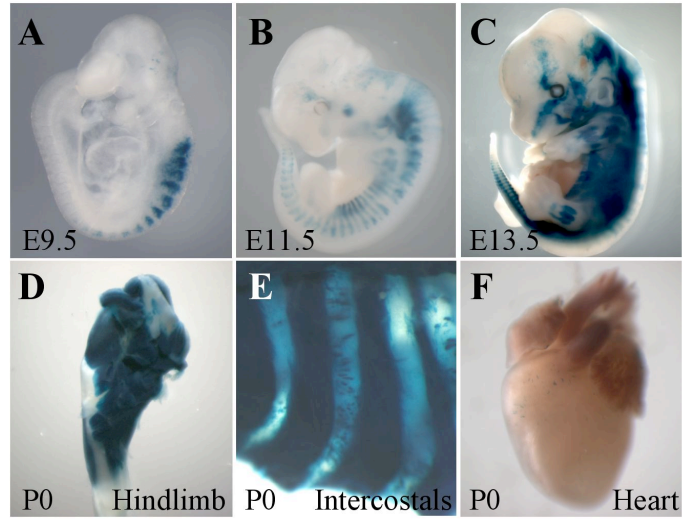
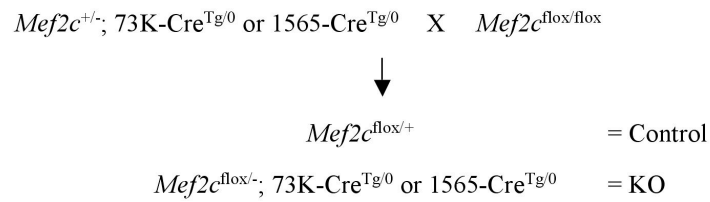


Figure 3-2

A



B

73K Cre	Expected	Observed
$Mef2c^{flox/+}$	81.5	82
$Mef2c^{flox/-}$	81.5	75
$Mef2c^{flox/+}; 73K-Cre^{Tg/0}$	81.5	95
$Mef2c^{flox/-}; 73K-Cre^{Tg/0}$	81.5	74

C

1565 Cre	Expected	Observed	
$Mef2c^{flox/+}$	108.75	131	
$Mef2c^{flox/-}$	108.75	139	
$Mef2c^{flox/+}; 1565-Cre^{Tg/0}$	108.75	90	***
$Mef2c^{flox/-}; 1565-Cre^{Tg/0}$	108.75	75	***

Figure 3-3

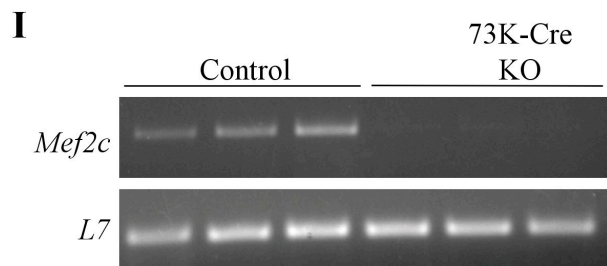
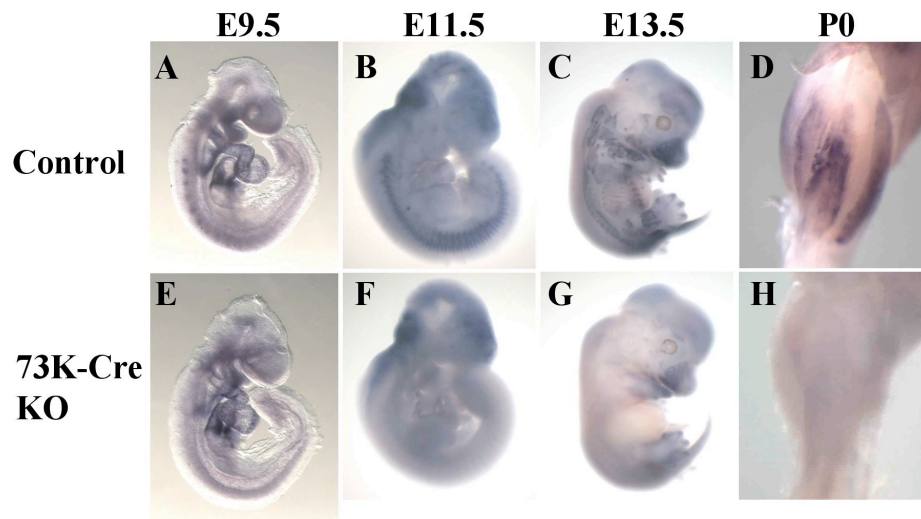


Figure 3-3 (cont'd)

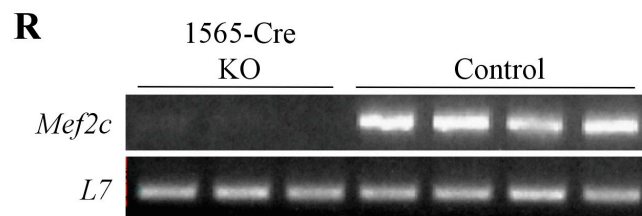
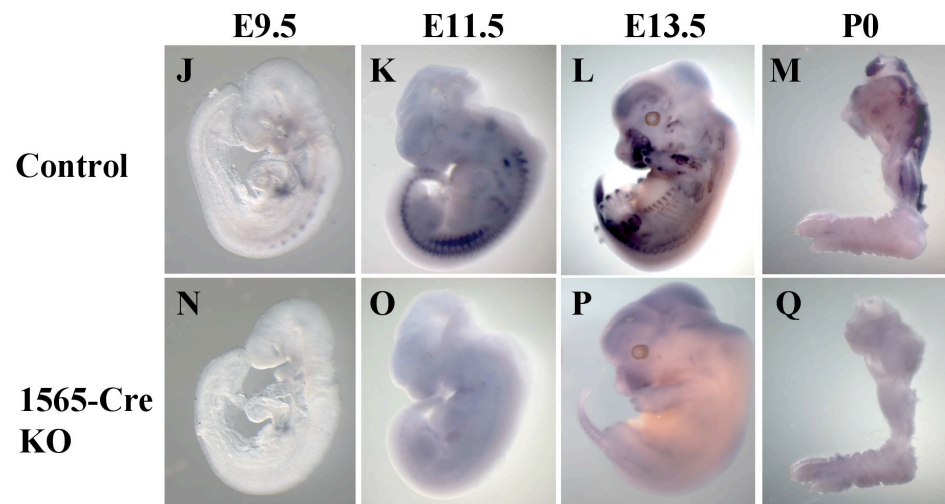


Figure 3-4

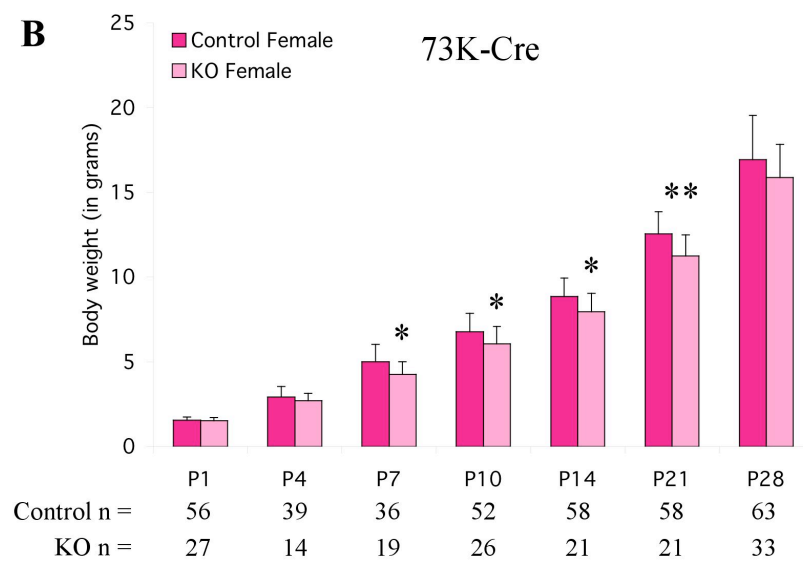
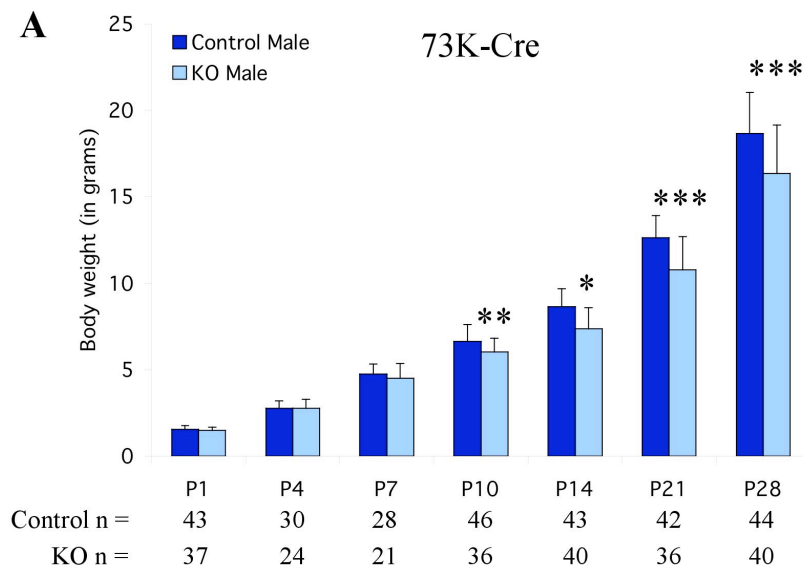


Figure 3-4 (cont'd)

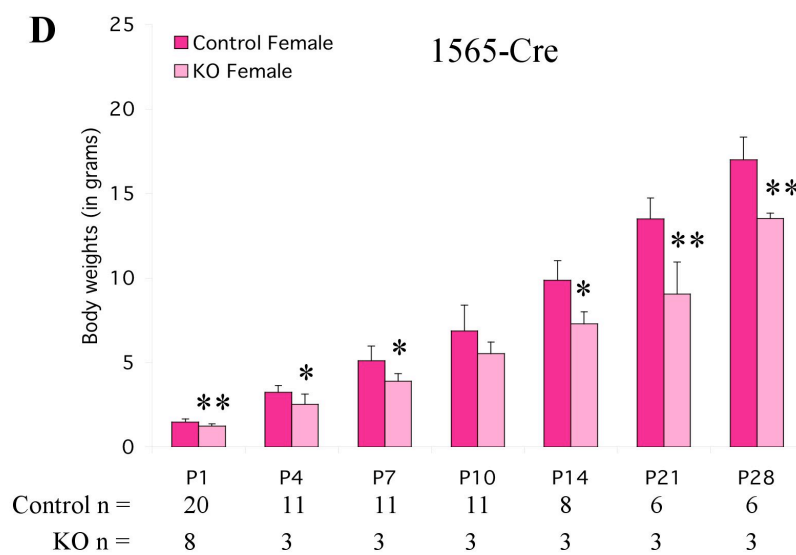
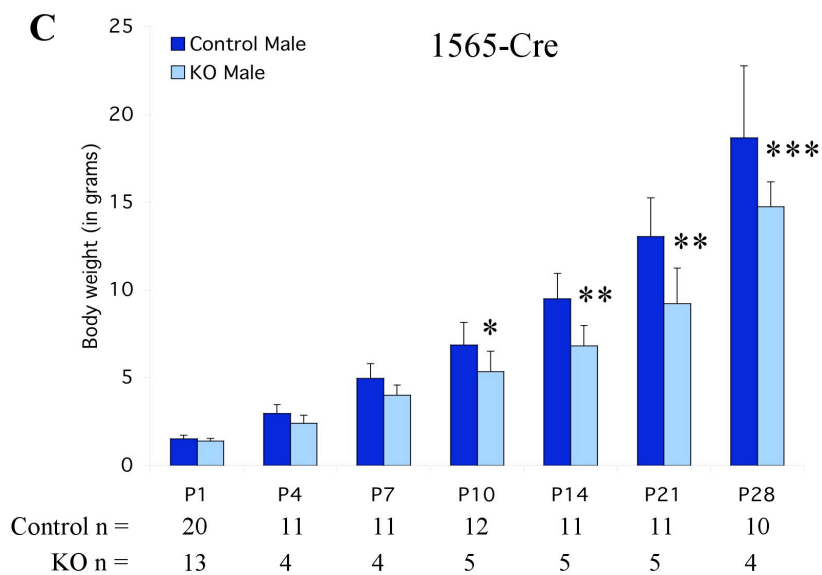


Figure 3-5

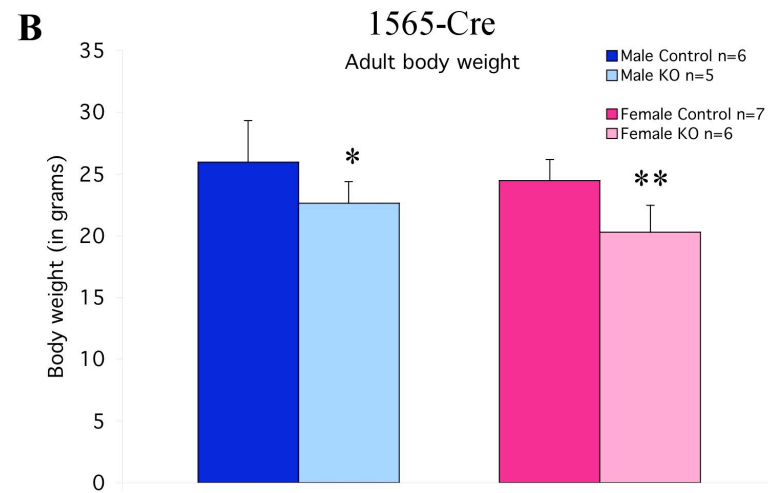
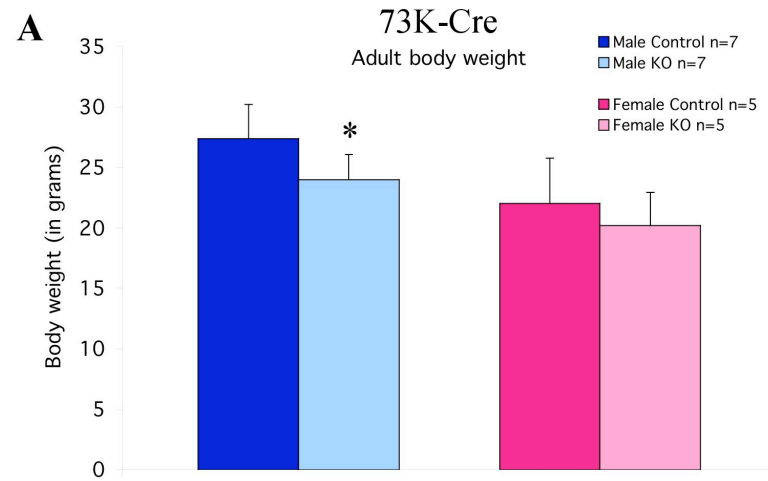


Figure 3-5 (cont'd)

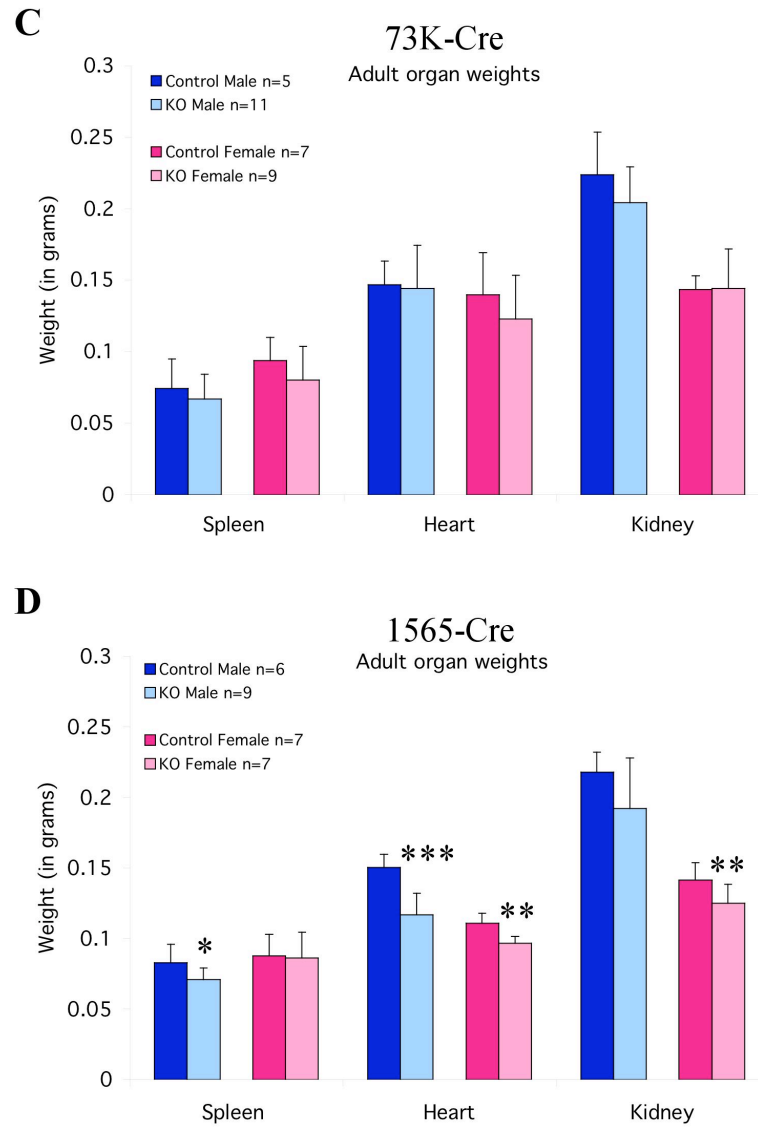


Figure 3-6

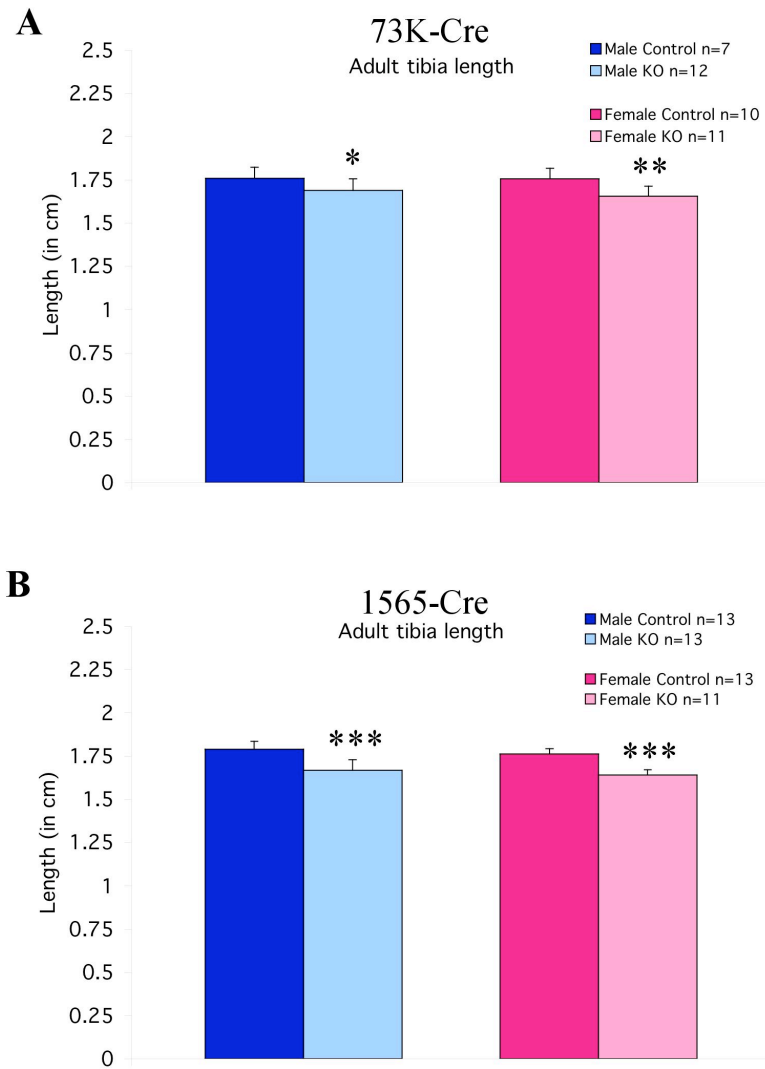


Figure 3-7

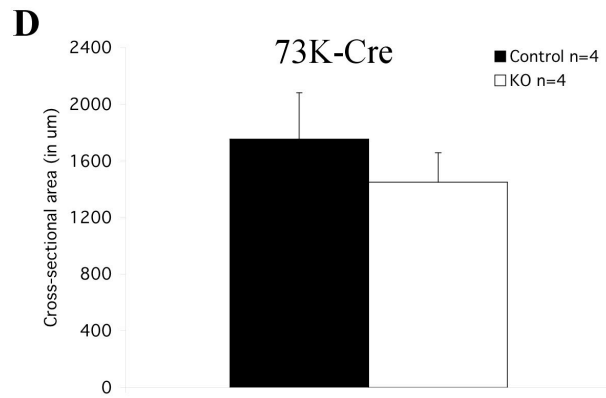
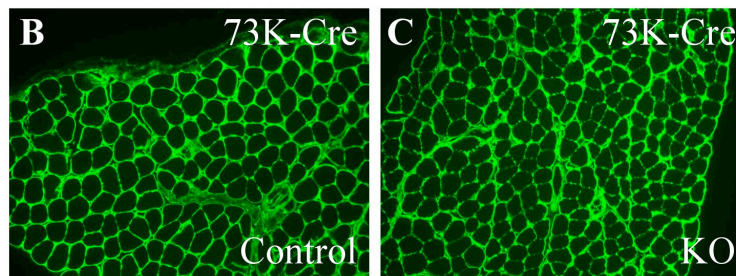
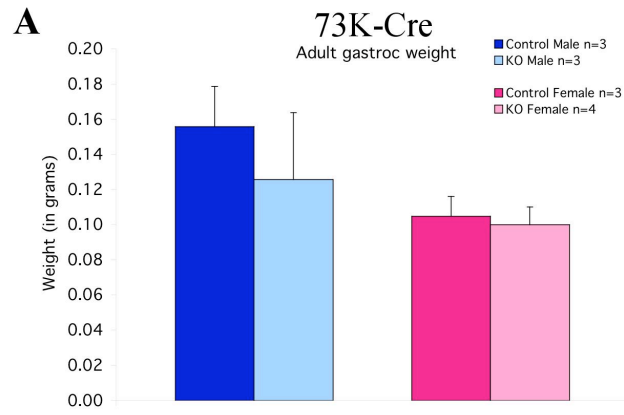


Figure 3-7 (cont'd)

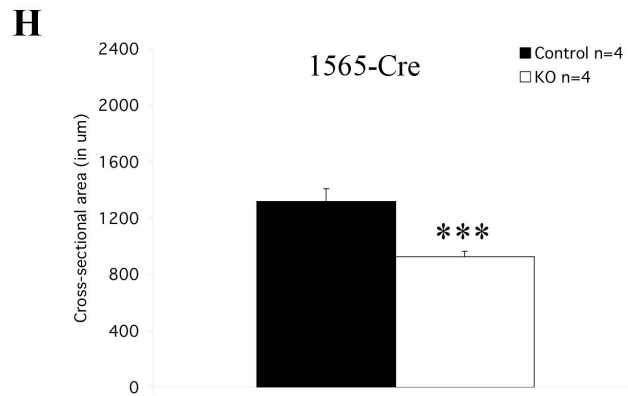
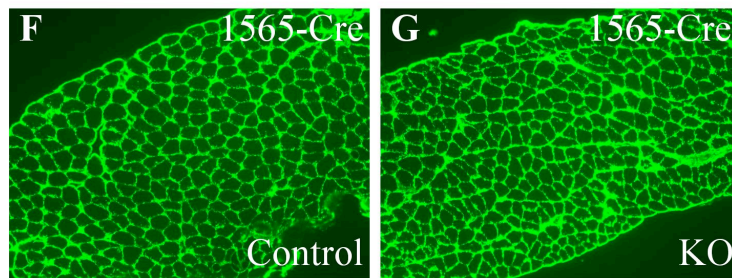
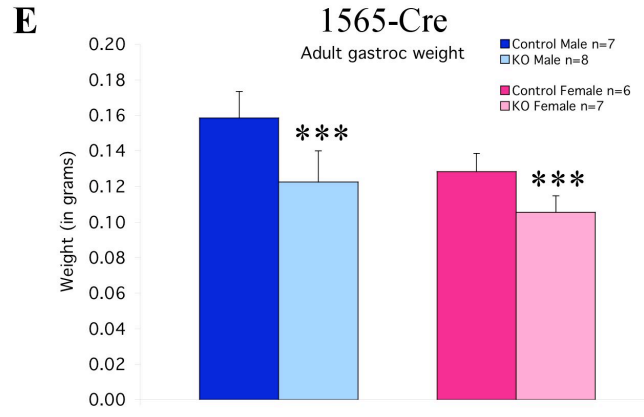


Figure 3-8

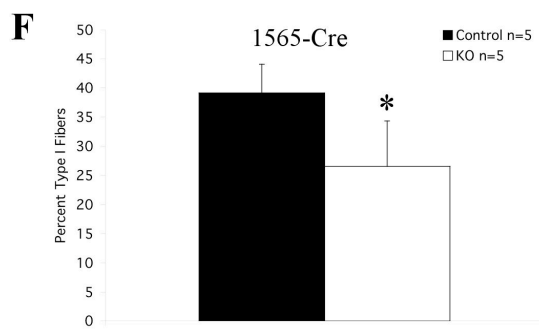
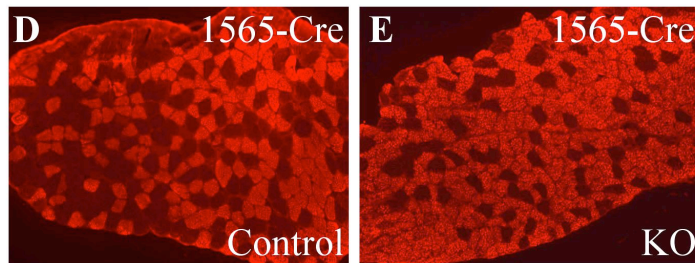
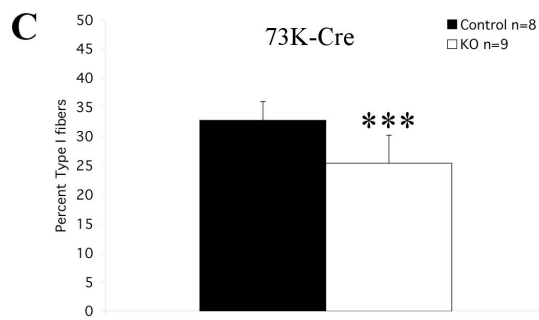
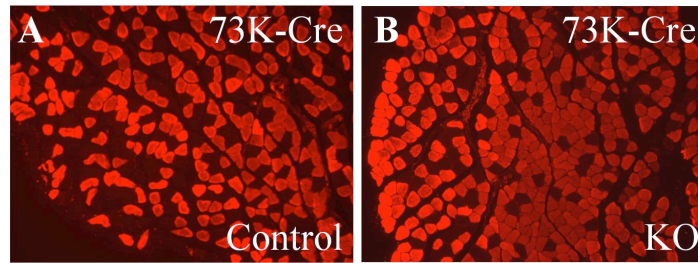


Figure 3-9 73K-Cre

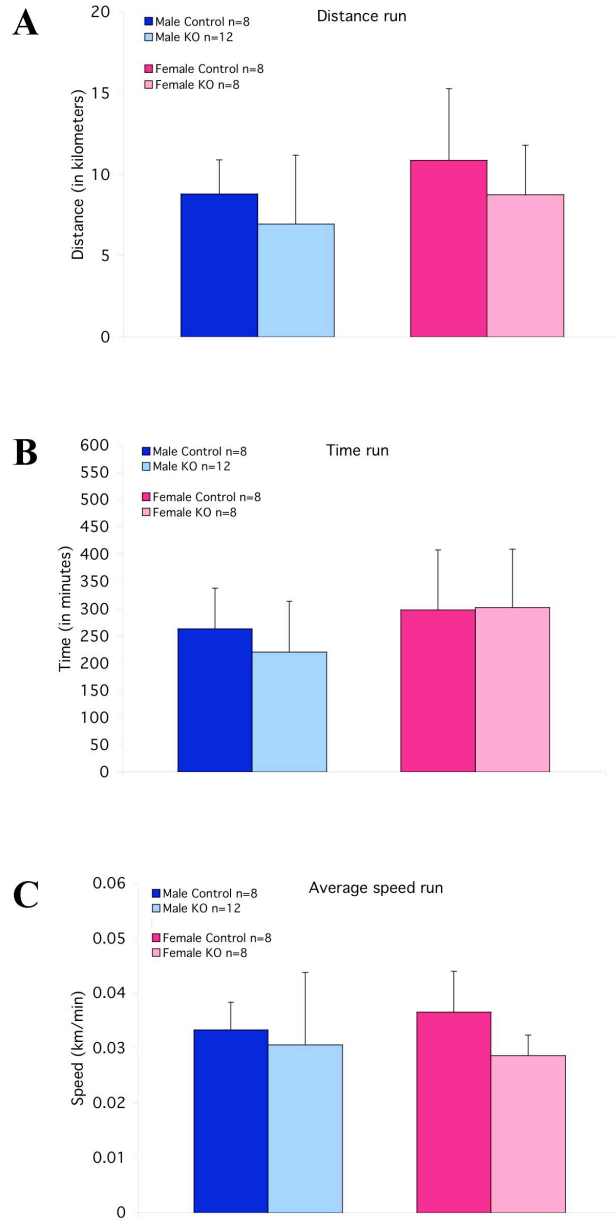


Figure 3-9 (cont'd) 1565-Cre

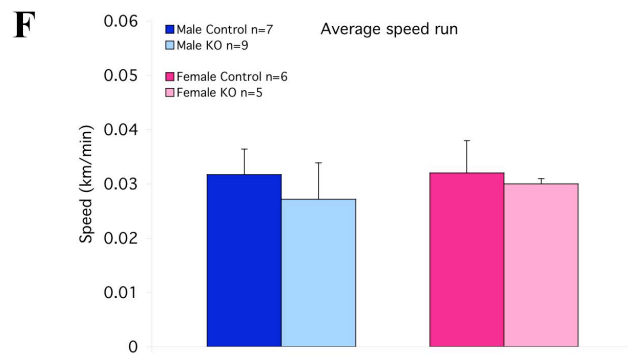
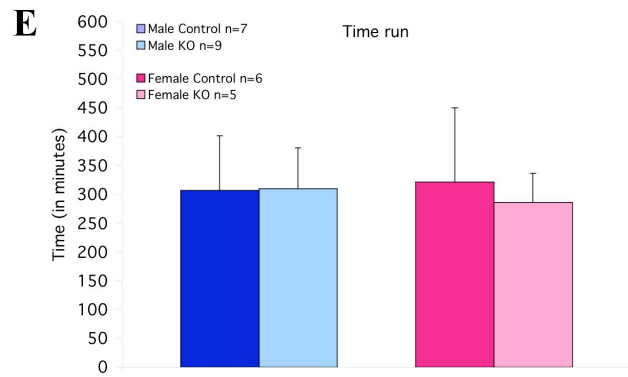
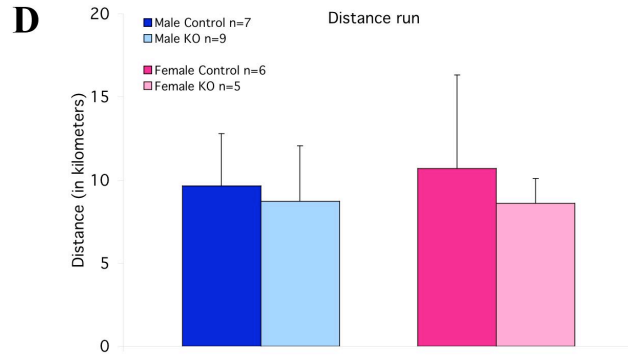


Figure 3-10

73K-Cre

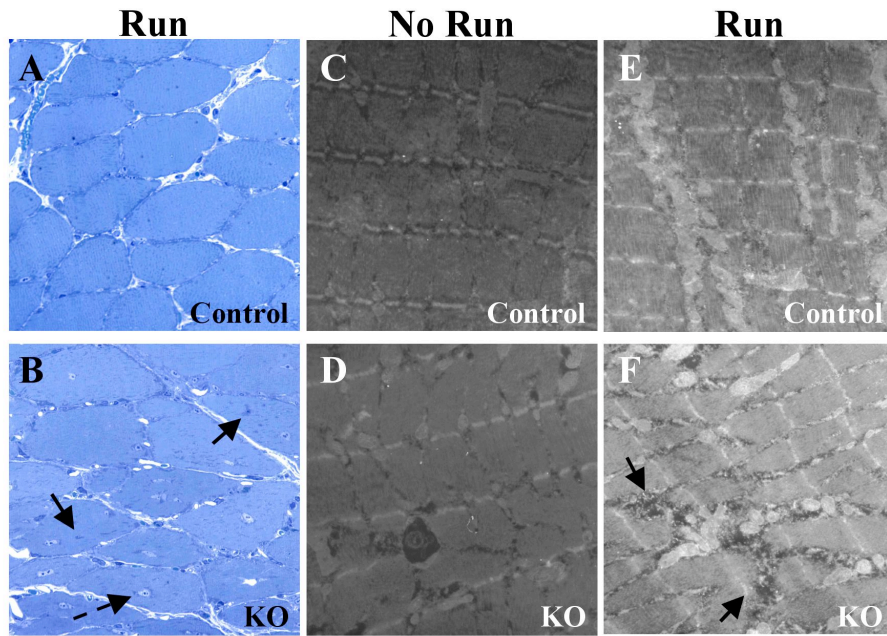


Figure 3-11 **73K-Cre**

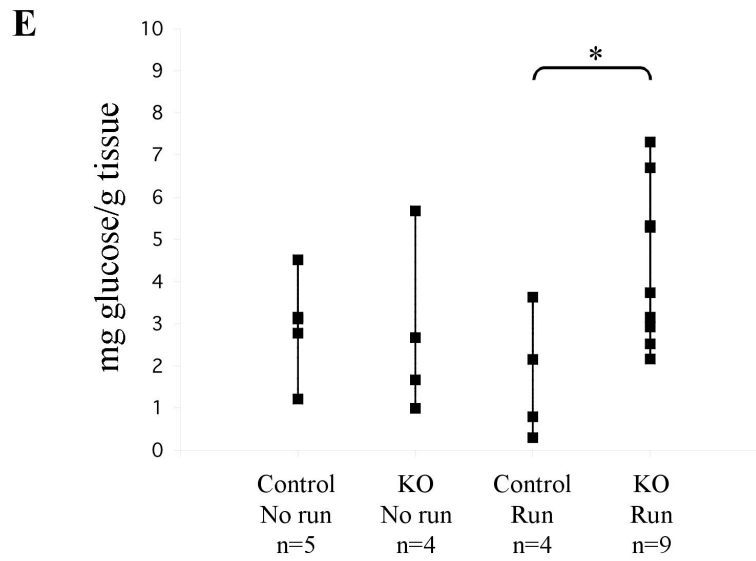
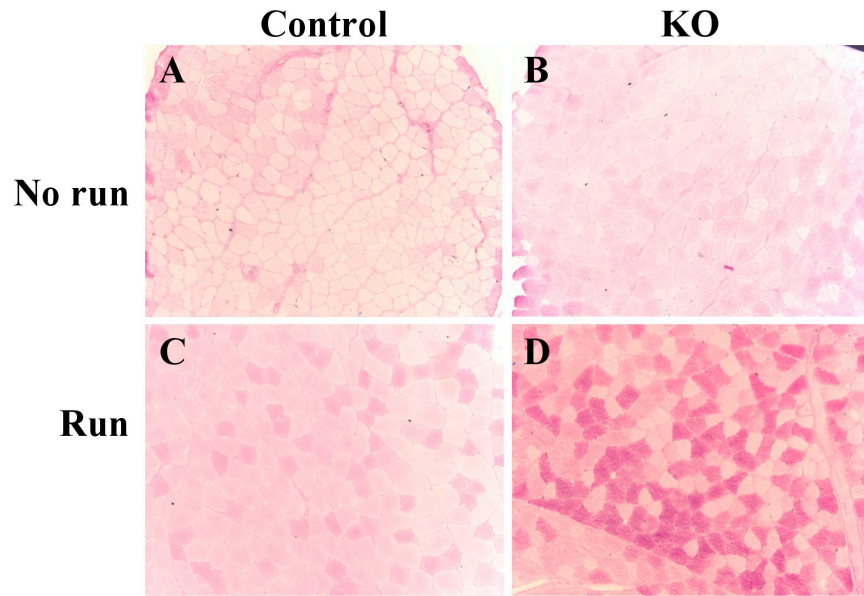


Figure 3-11 (cont'd) 1565-Cre

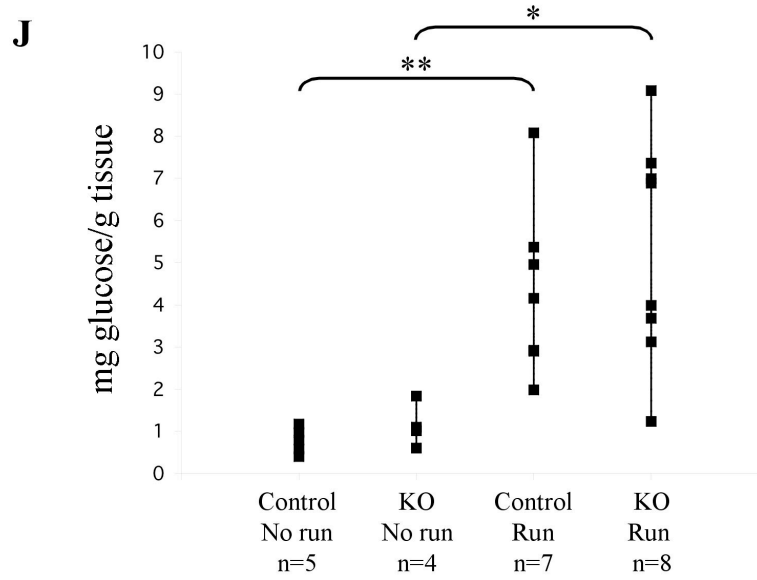
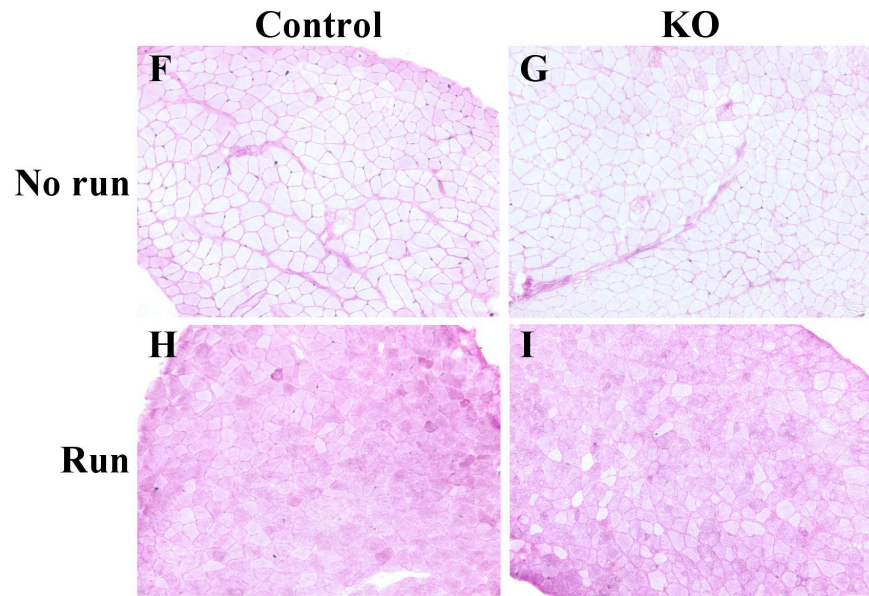


Figure 3-12

73K-Cre

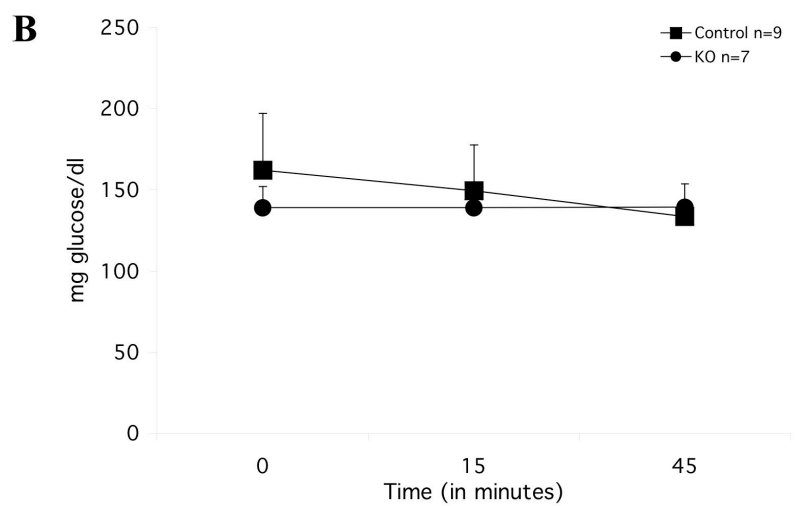
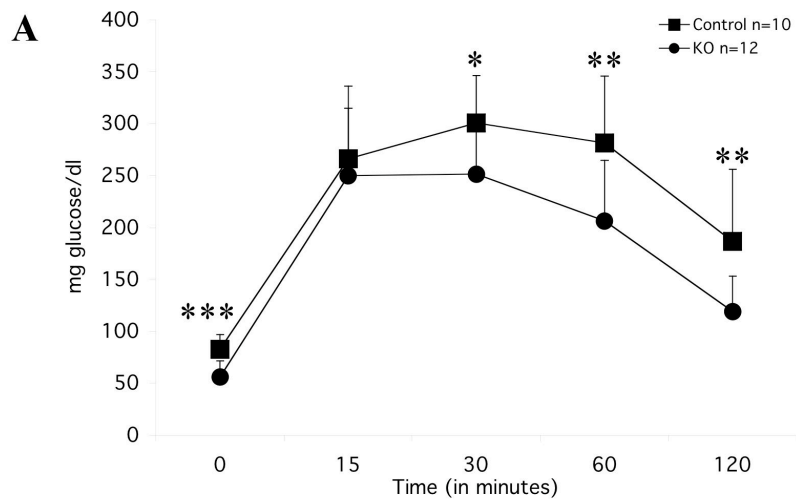


Figure 3-13

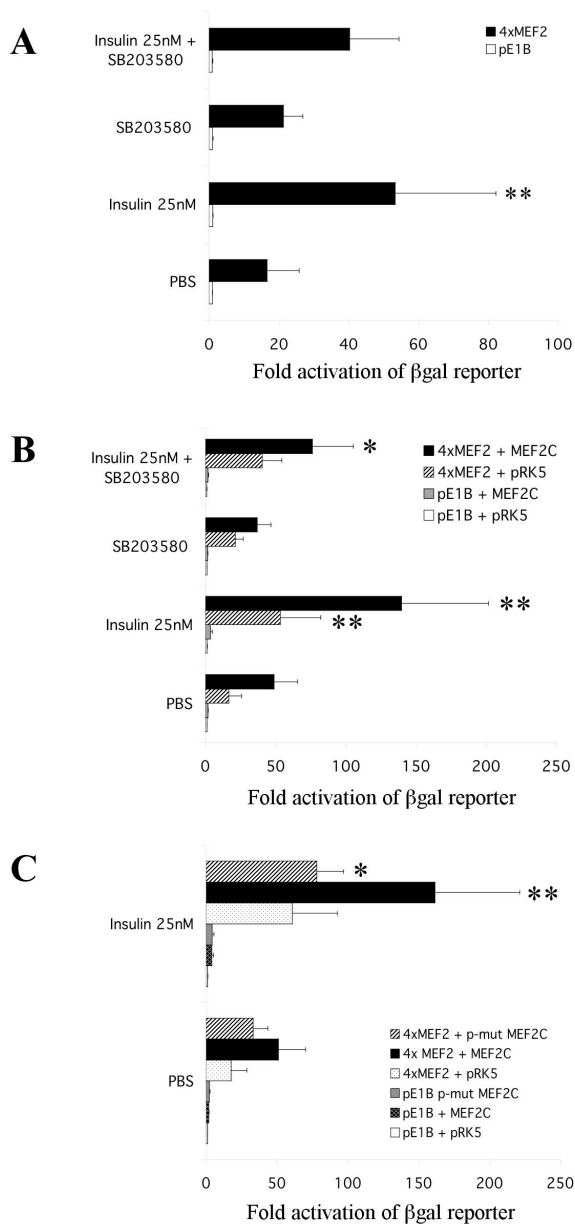
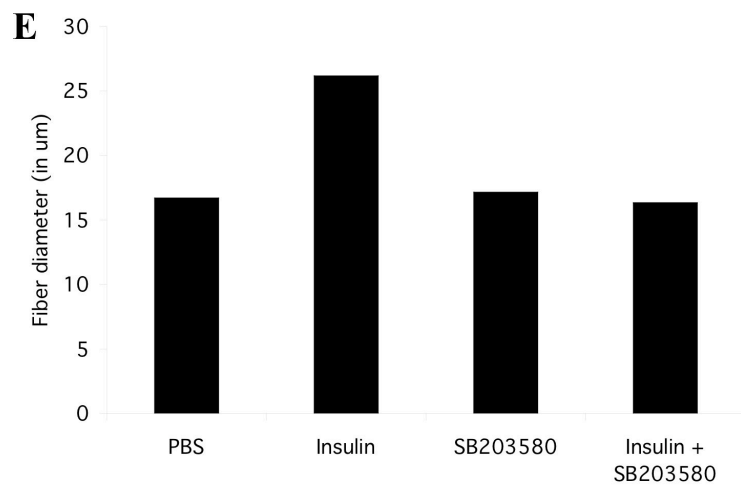
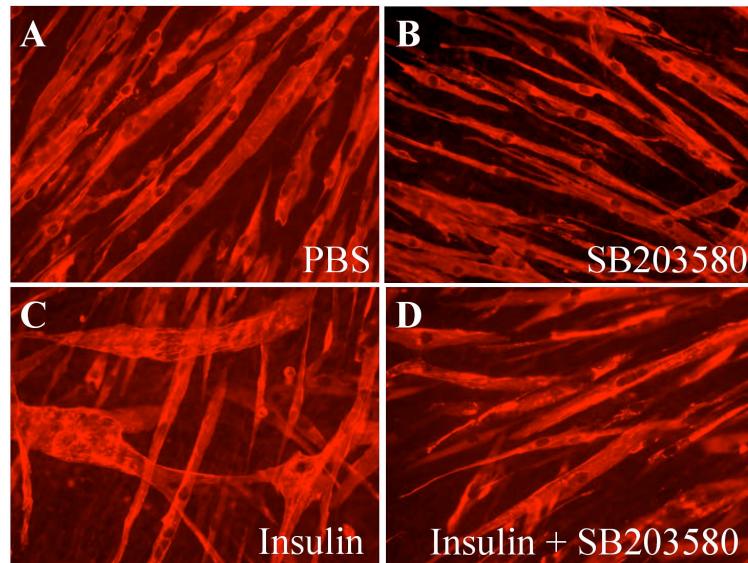


Figure 3-14



Chapter 4: General Conclusions

The MEF2 family of transcription factors plays an important role in cardiac and skeletal muscle development and metabolism. MEF2C, in particular, is crucial for cardiac development, as mice that lack *Mef2c* die by E9.5 due to cardiac looping defects (Lin et al, 1997). MEF2C is also important for the transcriptional regulation of several cardiac and skeletal muscle metabolism genes, including PGC1 α and GLUT4 (Lin et al, 2002; Czubryt et al, 2003; Thai et al, 1998). The work presented in this thesis examines the role of the MADS domain transcription factor MEF2C in cardiac and skeletal muscle metabolism.

Heart disease is a serious health crisis in the United States. It is the leading cause of death, accounting for 26% of the deaths in the United States in 2006, and heart attacks are the most common type of heart disease (source: Centers for Disease Control). However, heart disease is not limited to adults only – congenital heart defects are the leading birth defect, with 1 out of 125 births resulting in a congenital heart defect (source: March of Dimes). Identifying the molecular mechanisms underlying cardiac development and function can lead to therapies for such illnesses.

AMPK plays a crucial role in cardiac function and metabolism – it activates proteins that increase fatty acid oxidation, protein synthesis, glycolysis, and glucose oxidation, all in an effort to increase energy production in the cardiomyocyte (Dolinsky and Dyck, 2006). Furthermore, humans with a mutation in the γ subunit of AMPK display cardiac hypertrophy, ventricular preexcitation, and glycogen deposition (Arad et al, 2003). Lastly, several studies have shown that the catalytic α subunit of AMPK is

necessary for maintaining energy homeostasis during cardiac ischemia, and it is protective against cardiac hypertrophy (Zarrinpashneh et al, 2006; Carvajal et al, 2007). Despite its important role in the heart, the transcriptional regulation of AMPK has not been studied.

In chapter 1, I identified a highly conserved enhancer from the mouse *Ampkα2* locus that is regulated by MEF2C and Myocardin in the heart. This enhancer is sufficient to direct expression to the myocardium, is active early in development when the heart is beginning to form, and remains active into adulthood. Much of the research on AMPK has focused on its role in adult cardiovascular function and disease. However, the findings in this chapter suggest that perhaps AMPK is also playing a role earlier in cardiac development. It is possible that AMPK is required for cardiomyocyte proliferation and providing the necessary energy to undergo such an energy-demanding process. Identifying the role of AMPK in early cardiac development will be a useful addition to the cardiac metabolic and developmental fields.

In addition, we show that MEF2C and Myocardin cooperatively regulate the *Ampkα2* enhancer and other MEF2 target genes, and that this cooperativity is dependent on the presence of two MEF2 sites. These data suggest that there may be a more general mechanism for the transcriptional regulation of gene activation in the heart. In smooth muscle many genes have two CArG boxes, and are synergistically activated by SRF and Myocardin (Wang et al, 2003). Furthermore, it was recently shown by our lab that endothelial enhancers can be predicted based on the identification of a FOX:ETS motif in the genome (DeVal et al, 2008). Therefore, it is possible that cardiac enhancers regulated by a MEF2C-Myocardin complex can be determined based on the presence of two MEF2

sites. Such a model would be useful in identifying novel genes that are involved in cardiac development and/or metabolism.

In addition to its role in metabolic gene regulation in the heart, MEF2C is also important in skeletal muscle differentiation and function. The work presented in chapter 2 suggests a metabolic role for MEF2C in skeletal muscle in that it is required for maintaining whole body energy homeostasis and glucose metabolism. In chapter 2, using two independent, transgenic Cre lines, we determined that *Mef2c* is required in skeletal muscle not only for muscle growth, but also for overall body size. Mice lacking *Mef2c* in skeletal muscle also have defects in fiber type switching and mild glycogen accumulation, but these impairments do not have an effect on exercise abilities. Lastly, we show that MEF2C may function downstream of insulin receptor signaling through a p38 MAPK signaling pathway in skeletal muscle.

These findings are particularly interesting because they support an ever-growing role for skeletal muscle in regulating whole body size and in the development of the metabolic syndrome. The metabolic syndrome is characterized by obesity, high blood pressure, high triglyceride levels, low high-density lipoprotein (HDL) cholesterol levels, and resistance to insulin (Stump et al, 2006). Decreased tissue response to insulin is a key component of the syndrome. Given that skeletal muscle is the most abundant insulin-sensitive tissue in the body and it is responsible for almost all insulin-mediated glucose disposal (Baron et al, 1988), skeletal muscle is a critical contributor to the development of obesity and the metabolic syndrome, which affects approximately 35% of the US population (source: American Heart Association). Our results demonstrate that MEF2C is required in skeletal muscle for normal whole body growth and glucose metabolism, and

highlight a possible role for MEF2C in skeletal muscle metabolism and possibly the metabolic syndrome.

Chapter 5: Materials and Methods

Plasmids

1. AMPK α 2 930bp – TOPO, TK- β gal, and HSP68-*lacZ*

The full-length enhancer element was initially cloned into the pCR2.1-TOPO vector (Invitrogen) from the PCR product generated using mouse genomic DNA with the following primers:

Forward primer: 5'-ACCCTGTAAAGAGGGAAAACCAAAC-3'

Reverse primer: 5'-GCCAAAGCCTCGTGGTTCCTGCCAGC-3'

TOPO constructs of the enhancer were generated in the forward and reverse orientation. Because the forward construct was inactive in cell culture, we focused solely on the reverse orientation of the enhancer. All subsequent constructs for AMPK α 2 were constructed using the reverse orientation of the enhancer.

TK- β gal-AMPK α 2 930bp was subcloned from pCR2.1-TOPO by digesting the reverse orientation TOPO construct with KpnI/XhoI and ligating into TK- β gal cut with KpnI/XhoI. HSP68-*lacZ*-AMPK α 2 930bp was subcloned from pCR2.1-TOPO by digesting the forward orientation TOPO construct with HindIII/XhoI and ligating into the HSP68-*lacZ* transgenic reporter plasmid cut with HindIII/XhoI (Kothary et al, 1989).

2. AMPK α 2 407bp – TOPO, TK- β gal, and HSP68-*lacZ*

This deletion construct (443-849bp) was initially cloned into the pCRII-TOPO dual promoter vector (Invitrogen) from the PCR product generated using mouse genomic DNA with the following primers:

Forward primer: 5'-AGAGGCCAGCACCCACCTAAC-3'

Reverse primer: 5'-GGGAAAATATTTTGCAGAAA-3'

TK- β gal-AMPK α 2 407bp was subcloned from pCRII-TOPO by digesting the TOPO construct with KpnI/XhoI and ligating into TK- β gal cut with KpnI/XhoI. HSP68-*lacZ*-AMPK α 2 407bp was subcloned from TK- β gal by digesting the construct with SmaI/XhoI, then blunting with Klenow fragment, and ligating into HSP68-*lacZ* cut with SmaI.

3. AMPK α 2 200bp – TOPO, TK- β gal, and HSP68-*lacZ*

This deletion construct (443-642bp) was initially cloned into the pCRII-TOPO dual promoter vector (Invitrogen) from the PCR product generated using mouse genomic DNA with the following primers:

Forward primer: 5'-AGAGGCCAGCACCCACCTAAC-3'

Reverse primer: 5'-GTCTAAGCAAATGAGATGAA-3'

TK- β gal-AMPK α 2 200bp was subcloned from pCRII-TOPO by digesting the TOPO construct with KpnI/XhoI and ligating into TK- β gal cut with KpnI/XhoI. HSP68-*lacZ*-AMPK α 2 200bp was subcloned from TK- β gal by digesting the construct with SmaI/XhoI, then blunting with Klenow fragment, and ligating into HSP68-*lacZ* cut with SmaI.

4. AMPK α 2 Δ 200bp – TK- β gal and HSP68-*lacZ*

This deletion construct (Δ 443-649bp) was initially cloned using the gene SOEing technique (Horton et al, 1997). The following primers were used with the AMPK α 2 930bp – TOPO construct and T7/M13 reverse primers:

Forward primer: 5'-AAAGTGGAAATCCATCAGAAAAGGT-3'

Reverse primer: 5'-GGTTTGTACCTTTTCTGATGGATTT-3'

The resulting SOEing product was digested with KpnI/XhoI and ligated into TK- β gal cut with KpnI/XhoI.

HSP68-*lacZ*-AMPK α 2 Δ 200bp was subcloned from TK- β gal by digesting the construct with SmaI/XhoI, then blunting with Klenow fragment, and ligating into HSP68-*lacZ* cut with SmaI.

5. AMPK α 2 930bp mut MEF2 Site 1 – TK- β gal and HSP68-*lacZ*

This mutational construct was initially cloned using the gene SOEing technique (Horton et al, 1997). The following primers were used with the AMPK α 2 930bp – TOPO construct and T7/M13 reverse primers (MEF2 site underlined, mutation introduced in lowercase):

Forward primer: 5'-GCACCATGCTAAAAaccAAAATGGTTTAC-3'

Reverse primer: 5'-TGTGGTAAACCATTTTgggTTTAGC-3'

The resulting SOEing product was digested with KpnI/XhoI and ligated into TK- β gal cut with KpnI/XhoI.

HSP68-*lacZ*-AMPK α 2 930bp mut MEF2 Site 1 was subcloned from TK- β gal by digesting the construct with SmaI/XhoI, then blunting with Klenow fragment, and ligating into HSP68-*lacZ* cut with SmaI.

6. AMPK α 2 930bp mut MEF2 Site 2 – TK- β gal and HSP68-*lacZ*

This mutational construct was initially cloned using the gene SOEing technique (Horton et al, 1997). The following primers were used with the AMPK α 2 930bp – TOPO construct and T7/M13 reverse primers (MEF2 site underlined, mutation introduced in lowercase):

Forward primer: 5'-GAAAGTTTCTATTcccAGCAGAGATAAA-3'

Reverse primer: 5'-CAGTTTTTATCTCTGCTgggAATAG-3'

The resulting SOEing product was digested with KpnI/XhoI and ligated into TK- β gal cut with KpnI/XhoI.

HSP68-*lacZ*-AMPK α 2 930bp mut MEF2 Site 2 was subcloned from TK- β gal by digesting the construct with SmaI/XhoI, then blunting with Klenow fragment, and ligating into HSP68-*lacZ* cut with SmaI.

7. AMPK α 2 930bp mut MEF2 Sites 1&2 – TK- β gal and HSP68-*lacZ*

To create the double MEF2 mutant, the mutant MEF2 site 2 sequence was introduced into a form of the AMPK α 2 fragment that already contained the mutant MEF2 site 1 sequence through cloning using the gene SOEing technique (Horton et al, 1997). The resulting SOEing product was digested with KpnI/XhoI and ligated into TK- β gal cut with KpnI/XhoI.

HSP68-*lacZ*-AMPK α 2 930bp mut MEF2 Sites 1&2 was subcloned from TK- β gal by digesting the construct with SmaI/XhoI, then blunting with Klenow fragment, and ligating into HSP68-*lacZ* cut with SmaI.

8. AMPK α 2 407bp mut MEF2 Site 1, Site 2, and Sites 1&2 – TK- β gal and HSP68-*lacZ*

These constructs were cloned from the corresponding TK- β gal-AMPK α 2 930bp mutant plasmid using the following primers:

Forward primer: 5'-AGAGGCCAGCACCACTAAC-3'

Reverse primer: 5'-GGGAAAATATTTTGCAGAAA-3'

The resulting PCR product was digested with KpnI/XhoI and ligated into TK- β gal cut with KpnI/XhoI.

HSP68-*lacZ*-AMPK α 2 407bp mut MEF2 Site 1, Site 2, and Sites 1&2 were subcloned from TK- β gal by digesting the constructs with SmaI/XhoI, then blunting with Klenow fragment, and ligating into HSP68-*lacZ* cut with SmaI.

9. AMPK α 2 200bp mut MEF2 Site 1, Site 2 and Sites 1&2 – TK- β gal and HSP68-*lacZ*

These constructs were cloned from the corresponding TK- β gal-AMPK α 2 930bp mutant plasmid using the following primers:

Forward primer: 5'-AGAGGCCAGCACCACTAAC-3'

Reverse primer: 5'-GTCTAAGCAAATGAGATGAA-3'

The resulting PCR product was digested with KpnI/XhoI and ligated into TK- β gal cut with KpnI/XhoI.

HSP68-*lacZ*-AMPK α 2 200bp mut MEF2 Site 1, Site 2, and Sites 1&2 were subcloned from TK- β gal by digesting the constructs with SmaI/XhoI, then blunting with Klenow fragment, and ligating into HSP68-*lacZ* cut with SmaI.

10. AMPK α 2 930bp mut NKE – TK- β gal and HSP68-*lacZ*

This mutational construct was initially cloned using the gene SOEing technique (Horton et al, 1997). The following primers were used with the AMPK α 2 930bp – TOPO construct and T7/M13 reverse primers (NKE site underlined, mutation introduced in lowercase):

Forward primer: 5'-TAACAAGTCCCCgtcTAAGCAAGG-3'

Reverse primer: 5'-AGTCTCCTTGCTTagacGGGGACT-3'

The resulting SOEing product was digested with KpnI/XhoI and ligated into TK- β gal cut with KpnI/XhoI.

HSP68-*lacZ*-AMPK α 2 930bp mut NKE was subcloned from TK- β gal by digesting the construct with SmaI/XhoI, then blunting with Klenow fragment, and ligating into HSP68-*lacZ* cut with SmaI.

11. AMPK α 2 200bp mut NKE – TK- β gal and HSP68-*lacZ*

These constructs were cloned from the TK- β gal-AMPK α 2 930bp mut NKE plasmid using the following primers:

Forward primer: 5'-AGAGGCCAGCACCACTAAC-3'

Reverse primer: 5'-GTCTAAGCAAATGAGATGAA-3'

The resulting PCR product was digested with KpnI/XhoI and ligated into TK-βgal cut with KpnI/XhoI.

HSP68-*lacZ*-AMPKα2 200bp mut NKE was subcloned from TK-βgal by digesting the construct with SmaI/XhoI, then blunting with Klenow fragment, and ligating into HSP68-*lacZ* cut with SmaI.

12. AMPKα2 930bp mut GATA – TK-βgal and HSP68-*lacZ*

This mutational construct was initially cloned using the gene SOEing technique (Horton et al, 1997). The following primers were used with the AMPKα2 930bp – TOPO construct and T7/M13 reverse primers (GATA site underlined, mutation introduced in lowercase):

Forward primer: 5'-CTATTATTAGCAGAtgcAAAAACT-3'

Reverse primer: 5'-TTTCAGGCAGTTTTTgcaTCTGCT-3'

The resulting SOEing product was digested with KpnI/XhoI and ligated into TK-βgal cut with KpnI/XhoI.

HSP68-*lacZ*-AMPKα2 930bp mut GATA was subcloned from TK-βgal by digesting the construct with SmaI/XhoI, then blunting with Klenow fragment, and ligating into HSP68-*lacZ* cut with SmaI.

13. AMPKα2 200bp mut GATA – TK-βgal and HSP68-*lacZ*

These constructs were cloned from the TK-βgal-AMPKα2 930bp mut GATA plasmid using the following primers:

Forward primer: 5'-AGAGGCCAGCACCACCTAAC-3'

Reverse primer: 5'-GTCTAAGCAAATGAGATGAA-3'

The resulting PCR product was digested with KpnI/XhoI and ligated into TK- β gal cut with KpnI/XhoI.

HSP68-*lacZ*-AMPK α 2 200bp mut GATA was subcloned from TK- β gal by digesting the construct with SmaI/XhoI, then blunting with Klenow fragment, and ligating into HSP68-*lacZ* cut with SmaI.

14. CKM 429bp – TOPO and TK- β gal

This enhancer element has been previously described (Cserjesi et al, 1994). It was cloned into the pCRII-TOPO vector (Invitrogen) from the PCR product generated using the plasmid -4800 MCK-CAT (mouse sequence) with the following primers:

Forward primer: 5'-CCATTCTTGGGAAAACAAACC-3'

Reverse primer: 5'-CCACAGTGCATCTCACTTCC-3'

TOPO constructs of the enhancer were generated in the forward and reverse orientation. Because the reverse construct had very robust activity in cell culture, we focused solely on the reverse orientation of the enhancer. All subsequent constructs for CKM were constructed using the reverse orientation of the enhancer.

TK- β gal-CKM 429bp was subcloned from pCRII-TOPO by digesting the reverse orientation TOPO construct with KpnI/XhoI and ligating into TK- β gal cut with KpnI/XhoI.

15. CKM 429bp mut MEF2 Site 1 – TK- β gal

This mutational construct was initially cloned using the gene SOEing technique (Horton et al, 1997). The following primers were used with the CKM 429bp – TOPO construct and T7/Sp6 reverse primers (MEF2 site underlined, mutation introduced in lowercase):

Forward primer: 5'-CATGTCTGGGTTgggTATAACCAGG-3'

Reverse primer: 5'-AGATGCCTGGTTATAccAACCCAG-3'

The resulting SOEing product was digested with KpnI/XhoI and ligated into TK-βgal cut with KpnI/XhoI.

16. CKM 429bp mut MEF2 Site 2 – TK-βgal

This mutational construct was initially cloned using the gene SOEing technique (Horton et al, 1997). The following primers were used with the CKM 429bp – TOPO construct and T7/Sp6 reverse primers (MEF2 site underlined, mutation introduced in lowercase):

Forward primer: 5'-AGGGACAGGGTgggTTTAGAGCGA-3'

Reverse primer: 5'-GAAGCTCGCTCTAAAccAACCCTG-3'

The resulting SOEing product was digested with KpnI/XhoI and ligated into TK-βgal cut with KpnI/XhoI.

17. CKM 429bp mut MEF2 Sites 1&2 – TK-βgal

To create the double MEF2 mutant, the mutant MEF2 site 2 sequence was introduced into a form of the CKM fragment that already contained the mutant MEF2 site 1 sequence through cloning using the gene SOEing technique (Horton et al, 1997). The

resulting SOEing product was digested with KpnI/XhoI and ligated into TK-βgal cut with KpnI/XhoI.

18. pCDNA3-Myocardin-mut LZ

This plasmid was made using the same mutations as described in Wang et al 2003. This mutational construct was initially cloned using the gene SOEing technique (Horton et al, 1997). The following primers were used with the wild-type pCDNA3-Myocardin expression plasmid and T7/Bgh rev primers (mutations introduced are in lowercase):

Forward: 5'-GCAGAAAGTGaccAACCAGaccACCTGGAAGaccCGGCAA-3'

Reverse: 5'-GCTCTTGCCGggtCTTCCAGGTggtCTGGTTggtCACTTT-3'

The plasmids pCDNA1-MEF2C and pCDNA1-MEF2C-VP16 have been previously described (Black et al, 1996). The plasmid pCDNA3-Myocardin 935 was a gift from Eric Olson (UT Southwestern) (Creemers et al, 2006). The plasmid pCITE-2B-MEF2C has been previously described (Heidt, 2006). The plasmid pCDNA3-NKX2.5 was a gift from Benoit Bruneau (UCSF). The plasmid pRK5-GATA4 was generated by Anabel Rojas. The plasmid pE1B-4xMEF2-βgal was generated by Jae Yeon Jeong.

The *Myogenin*-1565-Cre and *Mef2c*-73K-Cre plasmids have been previously described (Heidt, 2006; Heidt and Black, 2005). The plasmids pRK5-MEF2C and pRK5-p-mut MEF2C have been previously described (Khiem et al, 2008).

Genotyping

DNA was extracted from the yolk sac of embryos or from tail biopsies from mice by digestion in tail lysis buffer (100mM NaCl, 25mM EDTA pH8.0, 1% sodium dodecyl sulfate, 10mM Tris-HCl pH8.0, 5µg proteinase K) at 56°C overnight. Digested samples were extracted once with phenol:chloroform and ethanol precipitated. DNA pellets were resuspended in TE buffer (10mM Tris, 0.1mM EDTA; pH7.4) for 1 hr at 55°C and stored at -20°C.

For *lacZ* transgene detection by PCR, the following primers and program were used:

LacZ For: 5'-CGGTGAATGGTGCTGCGTTGGA-3'

LacZ Rev: 5'-ACCACCGCACGATAGAGATTC-3'

94°C 5', {94°C 30", 52°C 30", 72°C 45"} 10 cycles, {94°C 30", 57°C 30", 72°C 45"} 18 cycles, 72°C 7'

Product size: 385bp

For *lacZ* transgene detection by Southern, the plasmid pCR2.1-TOPO-*lacZ*, which contains the *lacZ* cDNA, was digested with EcoRI to generate a 352bp Southern probe. Genomic DNA was digested with PstI, run on a 0.5x TBE agarose gel, and hybridized with the *lacZ* Southern probe overnight at 65°C. Blots were washed two times in blot wash 1 (0.2x SSC, 0.1% SDS) at 65°C, and exposed to film.

For Cre transgene detection by PCR, the following primers and program were used:

Cre For: 5'-TGCCACGACCAAGTGACAGC-3'

Cre Rev: 5'-CCAGGTTACGGATATAGTTCATG-3'

94°C 5', {94°C 30", 52°C 30", 72°C 45"} 33 cycles, 72°C 7'

Product size: 700bp

For Cre transgene detection by Southern, the plasmid pBS-Cre (obtained from Hiroshi Kataoka in the laboratory of Shaun Coughlin (UCSF)), which contains the Cre cDNA, was digested with NcoI and BamHI to generate a 387bp Southern probe. Genomic DNA was digested with EcoRV, run on a 0.5x TBE agarose gel, and hybridized with the Cre Southern probe overnight at 65°C. Blots were washed two times in blot wash 1 (0.2x SSC, 0.1% SDS) at 65°C, and exposed to film.

Genotyping for the *Mef2c* allele was detected by Southern blot using a probe known as Tm1. The plasmid pCR2.1-TOPO-Tm1 5' was digested with BglIII and XmaI sequentially to generate 4 fragments, of which the 600bp fragment was isolated as the Southern probe. Genomic DNA was digested with PstI, run on a 0.5x TBE agarose gel, and hybridized with the Tm1 Southern probe overnight at 65°C. Blots were washed two times in blot wash 1 (0.2x SSC, 0.1% SDS) at 65°C, and exposed to film.

Generation of *Mef2c* total knockout and conditional knockout mice

The *Mef2c* heterozygous and null mice have been previously described (Lin et al, 1997). Generation of the *Mef2c* skeletal muscle conditional knockout mice was previously described by Analeah Heidt (Heidt, 2006). In brief, mice expressing *Mef2c*-73K-Cre or *Myogenin*-1565-Cre were crossed into a heterozygous *Mef2c* background (*Mef2c*^{+/-}). Male mice that were Cre^{Tg/0}; *Mef2c*^{+/-} were crossed with female mice that were homozygous for the conditional allele of *Mef2c* (*Mef2c*^{flox/flox}), obtained from John

Schwarz (Albany Medical College) (Vong et al, 2005). Genotypes were determined by Southern blot using genomic tail or embryonic yolk sac DNA as described above.

Generation and analysis of transgenic mice

Transgenic reporter constructs were digested away from the HSP68-*lacZ* plasmid backbone with NotI/XhoI, gel purified, and suspended in 5mM Tris-HCl, 0.2mM EDTA (pH 7.4) at a concentration of 2ng/μl for pronuclear injection as described previously (Hogan et al, 2004). Injected embryos were implanted into pseudopregnant CD-1 females, and embryos were either collected at various stages of development or allowed to grow to adulthood to generate stable transgenic lines. The presence of the *lacZ* transgene was detected by Southern blot or PCR as described above.

For analysis of Cre expression and recombination in *Myogenin*-1565-Cre transgenic mice, transgenic males were crossed to female ROSA26R *lacZ* reporter mice (Soriano, 1999). Genotyping for Cre and *lacZ* was performed as described above. Embryos and tissues were collected at various stages of development and were analyzed for β-galactosidase expression.

β-galactosidase expression from *lacZ* transgenic embryos or tissues was detected by X-gal staining. In brief, embryos or tissues were fixed in 2% paraformaldehyde, 0.2% glutaraldehyde in 1x phosphate buffered saline (PBS) at 4°C for 30 min to 2 hours, depending on the age of the embryo or tissue. Embryos were rinsed twice in PBS and stained for β-galactosidase overnight in the dark at room temperature in PBS containing 5mM K₄Fe(CN)₆, 5mM K₃Fe(CN)₆, 2mM MgCl₂, 1mg/ml 5-bromo-4-chloro-3-indolyl β-D-galactopyranoside (X-gal). Following staining, embryos or tissues were rinsed twice in

PBS and post-fixed in 4% paraformaldehyde overnight at 4°C. For sections, X-gal stained embryos were embedded in paraffin, and transverse and sagittal sections were cut at a thickness of 7µm and counterstained with Nuclear Fast Red.

Cell culture, transfections, and β-galactosidase assays

C2C12 cells were maintained in DMEM supplemented with 15% fetal bovine serum (FBS), 1% L-glutamine, and 1% penicillin-streptomycin (P/S). Cells were seeded at 2×10^4 cells/well in a 24-well plate and were transfected using the Fugene 6 protocol (Roche). In each transfection, 375ng of the indicated reporter plasmid was cotransfected with 375ng of each indicated transactivator (for a total of 750ng DNA per reaction) by mixing the DNA with 2.25µl of Fugene 6 and up to 37.5µl serum-free DMEM. In samples where a cDNA expression plasmid was not transfected, an equal amount of the parental expression vector was transfected. In transfections where there was more than one transactivator, equal amounts of expression plasmid and reporter plasmid DNA was used so that the total amount of DNA was 750ng per reaction. The reaction was incubated for 30 min at room temperature, during which time cells were washed with PBS and 250µl of DMEM with FBS was added to each well. Each reaction was then added to the appropriate well and incubated at 37°C. After 4 hours, the cells were treated with the appropriate drug (PBS, 25nM insulin + PBS, 10µM SB203580 + PBS, or 25nM insulin + 10µM SB203580) and allowed to incubate for 48 hours. Transfected cells were harvested and cellular extracts were prepared by resuspending the cells in 37.5µl 0.1M NaPO₄ buffer and freeze/thawing three times. Chemiluminescent β-galactosidase assays were performed using the Luminescent β-gal kit (Clontech) according to the manufacturer's

directions, and relative light units were detected using a GloMax MultiDetection microplate luminometer (Promega). Protein concentration was performed using the Bradford assay with protein assay dye reagent (Bio-Rad).

P19CL6 cells were maintained in α MEM with nucleosides supplemented with 10% FBS and 1% P/S. Cells were seeded at 1.25×10^4 cells/well in a 24-well plate and were transfected using the Fugene 6 protocol (Roche). In each transfection, 250ng of the indicated reporter plasmid was cotransfected with 250ng of each indicated transactivator (for a total of 750ng DNA per reaction) by mixing the DNA with 2.25 μ l of Fugene 6 and up to 37.5 μ l serum-free α MEM. In samples where a cDNA expression plasmid was not transfected, an equal amount of the parental expression vector was transfected. The reaction was incubated for 30 min at room temperature, during which time cells were washed with PBS and 250 μ l of α MEM with FBS was added to each well. Each reaction was then added to the appropriate well and allowed to incubate for 48 hours. Cells were harvested and β -galactosidase assays were performed as described above.

For quantification of *lacZ* expression in transgenic embryonic hearts, hearts were harvested at E11.5, snap-frozen in liquid nitrogen, and stored at -80°C until genotyping was confirmed. Cellular extracts from transgenic hearts were prepared by resuspending the hearts in 30 μ l 0.1M NaPO₄ buffer and freeze/thawing three times. β -galactosidase and Bradford assays were performed as described above, except that 1 μ g of lysate was used for the β -galactosidase assay. These embryo quantification experiments were done with the assistance of Mansu Kim.

Electrophoretic mobility shift assays

2µg of double-stranded oligonucleotides for use in binding reactions were labeled with [³²P]-dCTP using Klenow to fill in overhanging 5' ends and purified on a nondenaturing polyacrylamide-TBE gel. Binding reactions were preincubated at room temperature for 10 min prior to probe addition in 1x binding buffer (40mM KCl, 15mM HEPES pH7.9, 1mM EDTA, 0.5mM DTT, 5% glycerol) containing recombinant protein or unprogrammed lysate, 1µg of poly-dI-dC, and competitor DNA (100 fold excess where indicated). Reactions were incubated an additional 20 min at room temperature after probe addition and then were electrophoresed on a 6% nondenaturing polyacrylamide gel at 150V for 2.5 hours at room temperature. Gels were then vacuum-dried and exposed to film.

For the MEF2C-Myocardin ternary complex EMSA, binding reactions containing 1x Ptashne buffer (45mM KCl, 10mM HEPES pH7.9, 6mM β-mercaptoethanol, 1mM EDTA, 5% glycerol, 1mg/ml BSA), 1µg of poly-dI-dC, and 8µl of recombinant protein or unprogrammed lysate was incubated with probe for 30 min at room temperature. 2µl of Myocardin IVT protein was mixed with increasing amounts of MEF2C protein (0, 1, 2, 4 or 6µl) and the total volume was brought to 8µl with unprogrammed lysate. After incubation, reactions were electrophoresed on a 6% nondenaturing polyacrylamide gel at 150V for 3.5-4 hours at room temperature. Gels were vacuum-dried and exposed to film.

The *Mef2c*, *Myocardin*, *Nkx2.5*, and *Gata4* cDNAs were transcribed and translated using the TNT QuickCoupled Transcription/Translation System (Promega), according to the manufacturer's directions. MEF2C protein was generated using T7 polymerase from the plasmid pCITE-2B-MEF2C. Myocardin protein was generated

using T7 polymerase from the plasmid pCDNA3-Myocardin-935. NKX2.5 protein was generated using T7 polymerase from the plasmid pCDNA3-NKX2.5. GATA4 protein was generated using Sp6 polymerase from the plasmid pRK5-GATA4.

The MEF2 control site and mutated forms are from the *Myogenin* promoter, which has been previously described (Yee and Rigby, 1993). The NKE control site and mutated forms are from the *vnd/NK-2* promoter, which has been previously described (Wang et al, 2002). The GATA control site and mutated forms are from the *GATA4* mesoderm enhancer (site 1), which has been previously described (Rojas et al, 2005). The sense strand sequences of the remaining oligonucleotides used for EMSA were as follows, with transcription factor sites underlined and mutations in lower-case:

Table 2: List of EMSA probes

Name of oligo	Sequence of sense strand
AMPK MEF2 #1	5'-GGGCACCATG <u>GCTAAAAATAAAATGGTTT</u> -3'
AMPK MEF2 #2	5'-GGGAAAGTTT <u>CTATTATTAGCAGAGATA</u> -3'
AMPK mMEF2 #1	5'- GGGCACCATG <u>GCTAAA</u> <u>ccc</u> <u>AAAATGGTTT</u> -3'
AMPK mMEF2 #2	5'- GGGAAAGTTT <u>CTATT</u> <u>ccc</u> <u>AGCAGAGATA</u> -3'
AMPK MEF2 #1&2	5'-GGAAAGAAAGTTT <u>CTATTATTAGCAGAGATA</u> AAAACTGCC TGAAATTCCTTCCTCACTAGCACCATG <u>GCTAAAAATAAAATGG</u> TTTAC-3'
AMPK NKE	5'-GGACAAGT <u>CCCCACTTAAGCAAGGAGA</u> -3'
AMPK mNKE	5'-GGACAAGT <u>CCCC</u> <u>gtc</u> <u>TAAGCAAGGAGA</u> -3'
AMPK GATA	5'-GGTTATTAGCAG <u>AGATA</u> AAAACTGCCT-3'
AMPK mGATA	5'-GGTTATTAGCAG <u>Atgc</u> AAAACTGCCT-3'

Chromatin immunoprecipitation

Chromatin immunoprecipitation (ChIP) assays were performed using the ChIP assay kit from Millipore/Upstate Pharmaceuticals (catalog #17-295), following the recommendations of the manufacturer. A 10-cm plate, previously transfected with either pCDNA1-MEF2C (as described above) and containing approximately 1×10^6 P19CL6 cells, was treated with 1% paraformaldehyde at 37°C for 10 min to cross-link protein-DNA complexes. Cells were then lysed and sonicated (4x10 sec sonication with a 30 sec rest in between each cycle on ice) to shear the DNA into fragments between 300 and 500bp. The cleared supernatant was incubated with 4ug of anti-MEF2C antibody E17 (Santa Cruz) at 4°C overnight. A sample incubated without antibody was included as a negative control. The next day, the samples were incubated with protein A-agarose beads for 1h at 4°C. The beads were then washed in a series of buffered solutions for 10 min each at room temperature. Protein/DNA complexes were then eluted from the beads with elution buffer (1% SDS, 0.1M NaHCO₃) and then incubated with 5M NaCl at 65°C for 4h to reverse the cross-links. DNA was recovered by phenol-chloroform extraction and ethanol precipitation overnight at -20°C. The following primers and program were used to amplify the region from the *Ampk α 2* enhancer that contains two MEF2 sites:

AMPK ChIP For: 5'-GACACCAGCAAAGA-3'

AMPK ChIP Rev: 5'-GGCACCAGTGGTGAA-3'

94°C 5', {94°C 30", 56°C 30", 72°C 45"} 33 cycles, 72°C 7'

Product size: 330bp

In situ hybridization

Whole-mount *in situ* hybridization was performed as previously described (Wilkinson and Nieto, 1993). Embryos and tissues were fixed overnight in 4% paraformaldehyde at 4°C, washed twice with PBS, and dehydrated with one wash in 50% methanol/PBT (1x PBS, 0.1% Tween-20) and two washes in 100% methanol. Embryos and tissues were then rehydrated in a series of PBT-methanol washes (75%, 50%, 25%), and washed twice in PBT. Embryos and tissues were then bleached in 6% hydrogen peroxide for 1h at room temperature and washed three times with PBT. Following bleaching, embryos and tissues were treated at room temperature for 30 min with varying amounts of proteinase K depending on the age of the embryo/tissue: E7.5 and E9.5 embryos were incubated at 2ug/ml, E11.5 and E13.5 embryos, and P0 hearts and limbs were incubated at 20ug/ml. Following proteinase K treatment, embryos and tissues were rinsed with 2 mg/ml glycine in PBT and washed two times in PBT. Embryos and tissues were fixed in 4% paraformaldehyde and 0.2% glutaraldehyde for 20 min at room temperature, and then washed three times in PBT. Embryos and tissues were allowed to pre-hybridize for 1h at 70°C in hybridization solution (50% formamide, 5x SSC pH 4.5, 50ug/ml yeast tRNA, 1% SDS, 50ug/ml heparin), then the labeled RNA probes were added and allowed to hybridize over night at 70°C. *In situ* hybridization was performed with digoxigenin-labeled antisense or sense RNA probes at a concentration of 0.5mg/ml in 100µl of hybridization buffer. Following hybridization, embryos and tissues were washed three times 30 min each at 70°C in wash solution #1 (50% formamide, 5xSSC pH 4.5, 1% SDS), three times 30 min each at 65°C in wash solution #2 (50% formamide, 2xSSC pH 4.5), and then three times 5 min at room temperature in TBST (1x tris-

buffered saline, 1% Tween-20). Embryos and tissues were blocked for 2.5 hours at room temperature in 10% sheep serum, then incubated with an alkaline phosphatase-conjugated anti-digoxigenin antibody (Roche) at a dilution of 1:5000 in 1% sheep serum overnight at 4°C. Following antibody incubation, embryos and tissues were washed six times 30 min each at room temperature with TBST, then rinsed three times 10 min each at room temperature with NTMT (100mM NaCl, 100mM Tris pH 9.5, 50mM MgCl₂, 0.1% Tween-20, 2mM levimasole). Signal was detected using BM Purple alkaline phosphatase substrate (Roche).

To generate the *Ampkα2* antisense and sense probe, a region of the mRNA and 3' UTR from *Ampkα2* (nucleotides 899 to 1952) was cloned into pCRII-TOPO (Invitrogen) by PCR using the following primers: 5'- ATTCCTGAAGACCCCTCCTACGAT-3' and 5'- CCTGTGCCTGTGACAAGTTTGCATG-3'. The *Ampkα2* antisense probe was generated by linearizing the plasmid with BamHI and transcribing it with T7 polymerase. The sense probe was generated by linearizing the plasmid with XhoI and transcribing it with Sp6 polymerase.

The *Mef2c* antisense and sense probes were generated from the plasmid pBS-SK+ MEF2C, made by Pooja Agarwal and previously described (Agarwal, 2009). A 208bp fragment from the *Mef2c* cDNA from nucleotides 630 to 836 was cloned into pBS-SK+. The *Mef2c* antisense probe was generated by linearizing the plasmid with HindIII and transcribing it with T3 polymerase. The sense probe was generated by linearizing the plasmid with BamHI and transcribing it with T7 polymerase.

β-galactosidase immunohistochemistry

For β-galactosidase immunohistochemistry (IHC) on embryos and hearts, 7μm thick paraffin-embedded sections were dewaxed and rehydrated, incubated in PBS for 5 min, and post-fixed in ice cold 100% acetone for 10 min on ice. The sections were then washed with PBS for 5 min and blocked in 5% milk, 5% normal goat serum, and 0.1% Triton X-100 in PBS for 1 hr at room temperature. Incubation with the primary antibody, rabbit anti β-galactosidase (ICN), was done overnight at 4°C in a humid chamber at a 1:200 dilution. Following incubation with the primary antibody, sections were washed three times with PBS for 20 min each at room temperature. The sections were then incubated with the secondary antibody, Oregon Green 488 goat anti-rabbit (Invitrogen), at a 1:500 dilution for 2 hr at room temperature. Sections were then washed three times with PBS for 20 min each at room temperature and mounted using Slow-Fade Gold antifade reagent with DAPI (Invitrogen) and photographed on a fluorescence microscope.

Body and organ weights and tibia length measurement

All mice from litters intended to generate conditional knockout mice were weighed on the evening of the day of birth and this was designated as P1. Overall body weight was also measured on P4, P7, P10, P14, P21, P28 and P52. Organ weights were measured at 52 days of age by dissecting the spleen, kidney, heart, and gastrocnemius muscle and weighing each tissue. Tibia length was measured at 52 days of age by dissecting the tibia and measuring length using a vernier caliper (Fine Science Tools, Item #30087-20).

Exercise assays

Voluntary exercise assays were conducted as described previously (Allen et al, 2001). 6-week old control and KO mice were housed individually in microisolator rodent cages covered on the sides with paper so that competition between each mouse was eliminated. Each cage contained standard metal rodent wheels (11.5 cm in diameter) suspended from two wire arms that hung over the edge of the cage and that had a magnet super-glued to its outer edge. A bicycle computer (Sigma Sport model BC600 or BC800) was mounted on each wheel such that the magnet passed the sensor with each revolution of the wheel. The computers were calibrated for the diameter of the running wheel prior to use according to the manufacturer's instructions. The distance and time run on the wheels was recorded from 6pm to 10am each night for seven consecutive nights, after an initial training period lasting 3 nights. The exercise assays were performed under standard light/dark conditions, and mice were provided unlimited access to food and water throughout the course of the experiment. Control (no run) mice were housed in a cage containing no wheel for the duration of the experiment. After the 7-day exercise period, the mice were weighed and sacrificed, and the muscles were removed and prepared for various uses as described.

Skeletal muscle histology

For skeletal muscle histology, muscles were freshly frozen (not fixed or embedded in paraffin wax). Muscles were isolated from mice and immediately placed on a cork round sliced from a wine cork. The muscle was either placed flat for longitudinal sections or cut in half using two razor blades in a slicing motion and placed cut-side

down for transverse sections. The muscle was coated in OCT embedding medium (Tissue Tek) and then lowered into a liquid nitrogen-cooled beaker of isopentane. It is crucial that the isopentane be at the correct temperature, and this was determined by the formation of a few ice crystals in the isopentane. The cork was lowered into the isopentane, swirled around for 15 sec, and then allowed to sit in the isopentane for 2 min. After this time, the embedded tissue was placed on dry ice to allow the alcohol to dry and then stored at -80°C .

For cryosectioning of freshly frozen embedded muscles, the cryostat was first cooled to a chamber temperature of -22°C , and the arm was cooled to -18°C . Embedded muscles were then placed in the cooled cryostat chamber and allowed to come up to temperature (approximately 30 minutes). A cryostat metal “chuck” was coated with OCT medium and the corks with embedded muscle were immediately placed on the chuck to secure it in place. Once the medium solidified, the chuck was secured in place and sections were cut at a thickness of $10\mu\text{m}$. Sections were then stored at -80°C until ready for use.

Skeletal muscle cross-sectional area and fiber type measurement

For cross-sectional area measurement, laminin IHC was performed. Freshly frozen soleus muscle sections from male control and KO mice at 52 days of age were allowed to air-dry at room temperature for 30 min. Sections were fixed in 4% paraformaldehyde for 10 minutes, rinsed in 1x PBS, and blocked in 3% normal goat serum in PBS for 1h at room temperature in a humid chamber. Sections were then incubated in mouse monoclonal anti-laminin (Sigma L9393) diluted 1:50 in 3% normal

goat serum in PBS for 1h at room temperature in a humid chamber. Following incubation, the primary antibody was removed and sections were washed three times for 10 min in PBS. The secondary antibody, Oregon Green 488 goat anti-rabbit (Invitrogen), was diluted 1:300 in 3% normal goat serum, and sections were incubated for 1h at room temperature in a humid chamber in the dark. Sections were then washed three times with PBS for 20 min each at room temperature and mounted using Slow-Fade Gold antifade reagent with DAPI (Invitrogen) and photographed on a fluorescence microscope. For quantification of the cross-sectional area of soleus muscle fibers, each muscle fiber in a 10x field outlined by laminin immunofluorescent staining was measured using Image J software. Measurements were taken from 5 sections from throughout the length of the muscle from one animal and averaged to generate a mean value for n=1, and this was done for 4 animals for each genotype.

For fiber type measurement, MY32 IHC was performed. Freshly frozen soleus muscle sections from male control and KO mice at 52 days of age were allowed to air-dry at room temperature for 30 min. Sections were fixed in 4% paraformaldehyde for 10 minutes, rinsed in PBS, and blocked in 3% normal goat serum in PBS for 1h at room temperature in a humid chamber. Sections were then incubated in mouse monoclonal anti-skeletal muscle myosin MY-32 (Sigma M4276) diluted 1:300 in 3% normal goat serum in PBS for 1h at room temperature in a humid chamber. Following incubation, the primary antibody was removed and sections were washed three times for 10 min in PBS. The secondary antibody, Alexa Fluor 594 anti-mouse (Molecular Probes, Invitrogen), was diluted 1:300 in 3% normal goat serum, and sections were incubated for 1h at room temperature in a humid chamber in the dark. Sections were then washed three times with

PBS for 20 min each at room temperature and mounted using Slow-Fade Gold antifade reagent with DAPI (Invitrogen) and photographed on a fluorescence microscope. Fast twitch fibers are positive for MY32 and appear red, whereas slow twitch fibers do not contain MY32 and therefore appear black. All fibers in a 10x field were counted, and the number of black/slow-twitch fibers was divided by the total number of fibers to yield of the percentage of slow-twitch fibers out of total fibers. Measurements were taken from 2 sections from throughout the length of the muscle from one animal and averaged to generate a mean value for n=1, and this was done for 5-9 animals for each genotype.

PAS stain and glycogen content quantification

PAS staining for glycogen was done on fresh frozen sections of quadriceps muscle (10µm thick) from male control or KO mice that were either exercised (run) or not exercised (no run) using the protocol as previously described (Sarnet, 1983). Sections were fixed in Carnoy's fixative (60% ethanol, 30% chloroform, 10% glacial acetic acid) for 5 min, followed by rinsing in tap water three times. Sections were immersed in 0.5% periodic acid (Sigma P7875) for 5 min, followed by rinsing in tap water four times. Sections were then transferred to Schiff's solution (Sigma 3952016) for 10 min, followed by rinsing in running tap water for 10 min. For mounting, sections were dehydrated in a series of ethanol washes, cleared in xylene, and mounted using Cytoseal 60 mounting medium (Richard-Allan Scientific 8310-16).

Total glycogen content in muscle was quantified using an adaptation of the protocol described by Hassid and Abraham (Hassid and Abraham, 1957). Approximately 30mg of frozen gastrocnemius tissue from male control or KO run or no run mice was

dissolved in 1ml 5N KOH in a boiling water bath with occasional shaking until dissolved. 0.2ml of saturated sodium sulfate and 1.5ml ethanol was added and mixed by vortexing. The mixture was heated until bubbles formed in a boiling water bath, approximately 1-2 min. After cooling on ice, samples were spun at 2000g for 10 min at 4°C and the supernatant was discarded. The pelleted material was resuspended in 0.5ml 2M HCl, vortexed, and incubated in a boiling water bath for 2-2.5 hours. After this incubation, samples were cooled and neutralized to pH 6-8 with 4N KOH, 0.1M triethanolamine. The glucose content of this solution was measured using the hexokinase method glucose assay kit as recommended by the manufacturer (Sigma GAHK20). The following mixtures were incubated for 15 min at room temperature: (1) 200µl extracted glycogen solution in 1ml of glucose assay reagent, (2) 200µl extracted glycogen solution in 1ml dH₂O and (3) 200µl dH₂O in 1ml of glucose assay reagent. The absorbance of these samples was measured at 340 nm versus a blank of deionized water. The total blank (A_{TB}) was calculated as the A_{340} of samples (2) + (3) above. The mg glucose/ml solution in the original sample was calculated as $(DA)(TV)(F)(0.029)/(SV)$, where $DA = A_{\text{sample}} - A_{TB}$, TV is the total assay volume (1ml assay reagent plus µl sample) in ml, F is the dilution factor of the added sample, and SV is the sample volume in ml. The mg glucose/ml solution value was normalized to the amount of starting tissue to yield mg glucose/g tissue.

Electron microscopy

Run male control or KO mice were exercised for 7 days, while no run male control or KO mice were housed in a cage containing no wheel for the duration of the

exercise assay, as described above. After 7 days of exercise, mice were injected with 10mg/ml pentobarbital at 100 μ l/10g body weight, and perfused with saline through the left ventricle to remove blood from the circulatory system. The right atrium was cut away from the heart to provide an outlet for perfused fluid. When the solution coming from the heart was clear, the perfusion was switched to a solution of 2% glutaraldehyde (EM grade, Sigma G5882) in 0.1M sodium cacodylate trihydrate pH 7.6 (Electron Microscopy Sciences 12310). Mice were perfused until rigid (approximately 8 min). The perfusions were performed by Ivo Cornelissen in the laboratory of Shaun Coughlin (UCSF). The soleus muscle was then removed and stored at 4°C in a solution of 2% glutaraldehyde and 0.1M sodium cacodylate trihydrate pH 7.6. After primary fixation, samples were dissected into 2% osmium tetroxide in PBS for 1.5 hours at room temperature. The samples were then dehydrated in a graded ethanol series and put into 2 changes of propylene oxide followed by a half and half mixture of propylene oxide and epoxy resin (EMbed 812, Electron Microscopy Sciences) overnight. The samples were then put into pure resin for 24 hours at room temperature before being embedded and baked at 60°C for 24 hours. Thin sections (100nm) were cut and stained with aqueous uranyl acetate followed by lead citrate. Sections were photographed using Kodak 4489 film and scanned. In addition, 1 μ m sections were cut and stained with 1% toluidine blue (Sigma 89640) in 1% sodium borate to check the quality of the sections for EM analysis. Dissection of the fixed tissue, processing, sectioning, EM analysis, and toluidine blue staining were all performed by Andrew Tauscher in the laboratory of Jennifer Lavail (UCSF).

Reverse-transcription PCR

Quadriceps muscle was dissected from control and KO mice, immediately placed in TRIzol (Invitrogen) at a concentration of 50-100mg tissue per 1ml TRIzol reagent, and stored at -80°C . For RNA isolation, tissue was homogenized on ice using a mechanical tissue homogenizer until all tissue was completely homogenized. The samples were then incubated for 5 min at room temperature to permit complete dissociation of nucleoprotein complex. 0.2ml of chloroform per 1ml TRIzol was then added and tubes were shaken vigorously by hand for 15 sec. Samples were allowed to incubate at room temperature for 10-15 min and then centrifuged for 10 min at 12,000rpm at 4°C . Following centrifugation, the top aqueous phase was removed and placed in a new tube and mixed with 0.5ml isopropanol per 1ml TRIzol to precipitate the RNA. Samples were incubated at room temperature for 10 min and then centrifuged for 10 min at 12,000rpm at 4°C . The supernatant was removed and the remaining pellet was washed in 70% ethanol and centrifuged at 9,000 rpm for 5 min at 4°C . The pellet was then resuspended in 30 μl RNase-free water and allowed to incubate for 10 min at 55°C . DNA was degraded by adding 3 μl DNase and 3 μl DNase buffer (Promega) to the resuspended RNA and incubating for 30 min at 37°C . The DNase-treated RNA was then phenol:chloroform extracted, ethanol precipitated, and resuspended in 30 μl RNase-free water. RNA was then cleaned-up using the RNeasy Mini Kit (Qiagen) RNA clean-up protocol according to the manufacturer's recommendations, eluted in 50 μl RNase-free water and stored at -80°C .

cDNA was synthesized using the Omniscript Reverse Transcriptase protocol (Qiagen). In brief, the RNA concentration was determined and 2 μg of total RNA was

used per cDNA reaction. The following components were mixed together for each reaction: 2µl 10x Buffer RT, 2µl dNTP mix, 3µl 50ng/ul random primers (Invitrogen 48190-011), 1µl RNase inhibitor (Roche 11787900), 1µl Omniscript Reverse Transcriptase, 2ng RNA, and up to 20µl RNase-free water. Reactions were incubated at 37°C for 1h and stored at -20°C.

For semi-quantitative RT-PCR, 1µl of cDNA sample was added to 2.5µl 10x buffer, 2.5µl 25mM MgCl₂, 0.5µl Taq polymerase (Allstar), 1µl 10mM dNTP, 1µl forward primer (25ng/µl), 1µl reverse primer (25ng/µl), and up to 25µl RNase-free water.

The following primers were used in the RT-PCR reactions:

Mef2c For: 5'-GGCCATGGTACACCGAGTACAACGAGC-3'

Mef2c Rev: 5'-GGGGATCCCTGTGTTACCTGCACTTGG-3'

Product size: 387bp (Martin et al, 1993)

L7 For: 5'-GGAGCTCATCTATGAGAAGGC-3'

L7 Rev: 5'-AAGACGAAGGAGCTGCAGAAC-3'

PCR product size: 202bp (Rawls et al, 1995)

The following program was used for both *Mef2c* and *L7* RT-PCR: 94°C 5', {94°C 30", 56°C 30", 72°C 45"} 30 cycles, 72°C 7'.

For quantitative real-time RT-PCR, 1µl of cDNA sample was added to 5µl SYBR Green PCR Master Mix (Applied Biosystems), 0.4µM forward primer, 0.4µM reverse primer, and 3µl RNase-free water. Quantitative real-time RT-PCR was performed on an ABI 7500 Real-Time PCR machine. The following program was used for both *Mef2c* and *L7* quantitative real-time RT-PCR: 50°C 2', 95°C 10', {95°C 15", 60°C 1'} 40 cycles, and a dissociation stage of 95°C 15", 60°C 15", and 95°C 15". The primers used for

Mef2c and *L7* detection by quantitative real-time RT-PCR were the same as those used for semi-quantitative RT-PCR (described above).

C2C12 differentiation assay

C2C12 cells were maintained in DMEM supplemented with 15% FBS, 1% L-glutamine, and 1% P/S. On day 1, the cells were seeded at 1×10^5 cells/well in a 6-well plate lined with coverslips coated with coating solution (20ml coating solution contains 23 μ l acetic acid, 2.64ml of 3.75mg/ml collagen, and up to 20ml autoclaved water; filter sterilize) and allowed to incubate overnight. On the morning of day 2, the growth media was removed and 2ml of differentiation media (DMEM with 2% horse serum and 1% P/S) was added. On day 4, 2ml of fresh differentiation media was added and the cells were treated with the appropriate drug (PBS, 100nM insulin + PBS, 10 μ M SB203580 + PBS, or 100nM insulin + 10 μ M SB203580) and allowed to incubate for 48 hours.

On day 6, IHC was performed on the cells while in the 6-well plate. Cells were washed 2 times in 1x cold PBS and fixed in 4% paraformaldehyde for 20 min at room temperature. They were rinsed in PBS and then permeabilized in 0.2% Triton X-100 for 20 min at room temperature. The cells were washed in PBS and then blocked in 3% normal goat serum in PBS for 1h at room temperature. Cells were then incubated with mouse monoclonal anti-MF20 (DSHB) diluted 1:200 in 3% normal goat serum in PBS overnight at 4°C. Following incubation, the primary antibody was removed and cells were washed four times for 5 min each in PBS. The secondary antibody, Alexa Fluor 594 anti-rabbit (Molecular Probes, Invitrogen), was diluted 1:300 in 3% normal goat serum in PBS, and cells were incubated for 1h at room temperature in the dark. Cells were then

washed four times for 5 min each in PBS at room temperature and coated with Slow-Fade Gold antifade reagent with DAPI (Invitrogen). The cover slips containing the stained cells were then removed from the 6-well plate and inverted onto a slide so that the cell-coated side of the cover slip faced down onto the slide and photographed on a fluorescence microscope.

For quantification of the diameter of C2C12 differentiated muscle fibers, 10 images were taken randomly at 10x magnification per condition. Within each 10x field, all multinucleated fibers were measured three times at equally spaced distances along the length of the fiber using Image J software and averaged.

Melissa Ehlers performed the cell culture differentiation, IHC, and imaging. I treated the cells with drug, then was blinded to the identification of the images and took the measurements so that there was no bias in the analysis.

Glucose tolerance and insulin resistance tests

For the glucose tolerance tests (GTT), 10-week old male control or KO mice were fasted overnight for 16 hours (6pm to 10am) in a clean cage with no food but full access to water. At 10am blood glucose measurements were first taken for a baseline reading (0 min) by nicking the tail with a razor blade and using a blood glucose meter (FreeStyle, Therasense, 99073-0110-01). The mice were then treated with glucose (1g glucose/kg body weight) for 2 hours. Blood glucose readings were then taken again at 15, 30, 60 and 120 minutes. Mice were then put back in cages with full access to food and water, and monitored for 24 hours after treatment to ensure full recovery from the GTT.

For the insulin resistance test (IRT), 10-week old male control or KO mice were allowed full access to food and water prior to treatment. At 10am blood glucose measurements were taken first taken for a baseline reading (0 min) and then they were treated with insulin (0.75 units/kg body weight) for 45 minutes. Blood glucose readings were then taken again at 15 and 45 minutes. Mice were monitored for 24 hours after treatment to ensure full recovery from the IRT.

Microarray

Microarray analysis was previously described by Analeah Heidt (Heidt, 2006). Gastrocnemius muscle was isolated from postnatal day 0 (P0) mice resulting from a cross between male *Mef2c*^{+/-}; *Myogenin*-1565-Cre^{Tg/0} and female *Mef2c*^{flox/flox} and immediately placed in 500µl TRIzol reagent (Invitrogen) and stored at -80°C until ready for processing. In the meantime, genotyping was performed for *Mef2c* and Cre as described above, as well as gender determination by PCR for the presence of the *Zfy* gene, for we only used males in the microarray analysis. For *Zfy* detection by PCR, the following primers and program were used:

Zfy For: 5'-GATAAGCTTACATAATCACATGGA-3'

Zfy Rev: 5'-CCTATGAAATCCTTTGCTGC -3'

95°C 5', {95°C 30", 55°C 1', 72°C 1'} 30 cycles, 72°C 10'

Product size: 600bp

Once gender and genotype were determined, the appropriate tissue samples were homogenized in TRIzol by repeated pipetting with a 1-20µl filter pipette tip. Once dissociated, the samples were processed as described in the RT-PCR section, except that

after the phenol:chloroform incubation they were placed in a Phase Lock Gel Tube (Eppendorf 955154045) to ensure clean separation between the aqueous and organic phases. Once the RNA was isolated and resuspended, it was cleaned-up using the RNeasy Micro Kit (Qiagen) according to the manufacturer's recommendations, including the on-column DNase treatment. RNA was checked for quantity using a spectrophotometer. Quality was determined using a BioAnalyzer Eukaryote RNA PicoChip (Gladstone Core Facility) loaded with total RNA at a concentration of 2000pg/μl. Total RNA samples were deemed of high quality if 2 distinct bands between 1000 and 2000 nucleotides (representing the 18S and 26S subunits) were detected.

For microarray hybridization, amplified RNA (aRNA) was generated using the MessageAmp II Biotin kit (Ambion #1791) according to the manufacturer's recommendations using 1μg of total RNA. Quality was determined using a BioAnalyzer Eukaryote RNA PicoChip (Gladstone Core Facility) loaded with aRNA at a concentration of 2000pg/μl. aRNA samples were deemed of high quality if a broad band between 250 and 5000 nucleotides was detected. The aRNA was then fragmented using the Ambion fragmentation kit (#8740) according to the manufacturer's recommendations. Fragmented, amplified, biotin-labeled RNA was stored at -80°C until further use.

Microarray hybridization was performed by the Gladstone Core Facility using Affymetrix Mouse Expression GeneChips. Three male control mice and three male KO mice were selected, and microarray analysis was performed individually on each of these mice. Statistical analysis was performed by Yuanyuan Xiao in the Gladstone Core Facility.

Statistical analyses

For statistical analysis on the quantification of *lacZ* expression in transgenic embryonic hearts, a one-way ANOVA analysis was performed followed by Newman-Keuls post-hoc test using the GraphPad Prism5 software program. For statistical analysis on the generation of *Mef2c*^{SkM-KO} mice, a chi square analysis was performed using the GraphPad online calculator (<http://www.graphpad.com/quickcalcs/chisquared1.cfm>). For all other statistical analyses, an unpaired t-test to compare two means was performed using the GraphPad online calculator (<http://www.graphpad.com/quickcalcs/ttest1.cfm>).

**All experiments using animals complied with federal and institutional guidelines and were reviewed and approved by the UCSF Institutional Animal Care and Use Committee.

Chapter 6: References

- Agarwal P.** 2009. Transcriptional Control of Neural Crest Development by MEF2C. Doctoral dissertation, University of California, San Francisco, USA.
- Al-Khalili L, AV Chibalin, M Yu, B Sjödin, C Nylén, JR Zierath, and A Krook.** 2004. MEF2 activation in differentiated primary human skeletal muscle cultures requires coordinated involvement of parallel pathways. *Am J Physiol Cell Physiol.* 286:C1410-6.
- Allen DL, BC Harrison, A Maass, ML Bell, WC Byrnes, and LA Leinwand.** 2001. Cardiac and skeletal muscle adaptations to voluntary wheel running in the mouse. *J Appl Physiol.* 90:1900-08.
- Altschul SF, W Gish, W Miller, EW Myers, and DJ Lipman.** 1990. Basic local alignment search tool. *J. Mol. Biol.* 215:403-410.
- Arad M, IP Moskowitz, VV Patel, F Ahmad, AR Perez-Atayde, DB Sawyer, M Walter, GH Li, PG Burgon, CT Maguire, D Stapleton, JP Schmitt, XX Guo, A Pizard, S Kupersmidt, DM Roden, CI Berul, CE Seidman, and JG Seidman.** 2003. Transgenic mice overexpressing mutant PRKAG2 define the cause of Wolff-Parkinson-White syndrome in glycogen storage cardiomyopathy. *Circulation.* 107:2850-6.
- Arad M, CE Seidman, and JG Seidman.** 2007. AMP-activated protein kinase in the heart: Role during health and disease. *Circ Res.* 100:474-488.
- Arany Z, N Lebrasseur, C Morris, E Smith, W Yang, Y Ma, S Chin, and BM Spiegelman.** 2007. The transcriptional coactivator PGC-1 β drives the formation of oxidative type IIX fibers in skeletal muscle. *Cell Metab.* 5:35-46.
- Asakura A, GE Lyons, and SJ Tapscott.** 1995. The regulation of MyoD gene expression: conserved elements mediate expression in embryonic axial muscle. *Dev Biol.* 171:386-98.
- Athéa Y, B Viollet, P Mateo, D Rousseau, M Novotova, A Garnier, S Vaulont, JR Wilding, A Grynberg, V Veksler, J Hoerter, and R Ventura-Clapier.** 2007. AMP-activated protein kinase $\alpha 2$ deficiency affects cardiac cardiolipin homeostasis and mitochondrial function. *Diabetes.* 56:786-94.
- Baron AD, G Brechtel, P Wallace, and SV Edelman.** 1988. Rates and tissue sites of non-insulin- and insulin-mediated glucose uptake in humans. *Am J Physiol.* 255:E769-74.
- Bartlett H, GJ Veenstra, and DL Weeks.** 2010. Examining the cardiac NK-2 genes in early heart development. *Pediatr Cardiol.* 31:335-41.

Bassel-Duby R and EN Olson. 2006. Signaling pathways in skeletal muscle remodeling. *Annu Rev Biochem.* 75:19-37.

Black BL and RM Cripps. 2010. Myocyte Enhancer Factor 2 Transcription Factors in Heart Development and Disease. *Heart Development and Regeneration.* 675-701.

Black BL, KL Ligon, Y Zhang, and EN Olson. 1996. Cooperative transcriptional activation by the neurogenic basic helix-loop-helix protein MASH1 and members of the myocyte enhancer factor-2 (MEF2) family. *J Biol Chem.* 271:26659-63.

Black BL and EN Olson. 1998. Transcriptional control of muscle development by myocyte enhancer factor-2 (MEF2) proteins. *Annu Rev Cell Dev Biol.* 14:167-96.

Bolster DR, LS Jefferson, and SR Kimball. 2004. Regulation of protein synthesis associated with skeletal muscle hypertrophy by insulin-, amino acid- and exercise-induced signalling. *Proc Nutr Soc.* 63:351-6.

Brewer A and J Pizzey. 2006. GATA factors in vertebrate heart development and disease. *Expert Rev Mol Med.* 8:1-20.

Buchberger A, N Nomokonova, and HH Arnold. 2003. Myf5 expression in somites and limb buds of mouse embryos is controlled by two distinct distal enhancer activities. *Development.* 130:3297-307.

Buckingham M. 2001. Skeletal muscle formation in vertebrates. *Curr Opin Genet Dev.* 11:440-8.

Buckingham M, L Bajard, T Chang, P Daubas, J Hadchouel, S Meilhac, D Montarras, D Rocancourt, and F Relaix. 2003. The formation of skeletal muscle: from somite to limb. *J Anat.* 202:59-68.

Buckingham M, S Meilhac, and S Zaffran. 2005. Building the mammalian heart from two sources of myocardial cells. *Nat Rev Genet.* 6:826-35.

Cai CL, X Liang, Y Shi, PH Chu, SL Pfaff, J Chen, and S Evans. 2003. Isl1 identifies a cardiac progenitor population that proliferates prior to differentiation and contributes a majority of cells to the heart. *Dev Cell.* 5:877-89.

Carvajal K, E Zarrinpashneh, O Szarszoi, F Joubert, Y Athea, P Mateo, B Gillet, S Vaultont, B Viollet, X Bigard, L Bertrand, R Ventura-Clapier, and JA Hoerter. 2007. Dual cardiac contractile effects of the α 2-AMPK deletion in low-flow ischemia and reperfusion. *Am J Physiol Heart Circ Physiol.* 292:H3136-47.

Chen CY and RJ Schwartz. 1995. Identification of novel DNA binding targets and regulatory domains of a murine tinman homeodomain factor, nkx-2.5. *J Biol Chem.* 270:15628-33.

- Cheng TC, TA Hanley, J Mudd, JP Merlie, and EN Olson.** 1992. Mapping of myogenin transcription during embryogenesis using transgenes linked to the myogenin control region. *J Cell Biol.* 119:1649-56.
- Cheung PC, IP Salt, SP Davies, DG Hardie, and D Carling.** 2000. Characterization of AMP-activated protein kinase gamma subunit isoforms and their role in AMP binding. *Biochem J.* 346:659-669.
- Chin ER, EN Olson, JA Richardson, Q Yang, C Humphries, JM Shelton, H Wu, W Zhu, R Bassel-Duby, and RS Williams.** 1998. A calcineurin-dependent transcriptional pathway controls skeletal muscle fiber type. *Genes Dev.* 12:2499-509.
- Choi SJ, SY Park, and TH Han.** 2001. 14-3-3tau associates with and activates the MEF2D transcription factor during muscle cell differentiation. *Nucleic Acids Res.* 29:2836-42.
- Christensen TH, H Prentice, R Gahlmann, and L Kedes.** 1993. Regulation of the human cardiac/slow-twitch troponin C gene by multiple, cooperative, cell-type-specific, and MyoD-responsive elements. *Mol Cell Biol.* 13:6752-65.
- Chung S, PP Dzeja, RS Faustino, C Perez-Terzic, A Behfar, and A Terzic.** 2007. Mitochondrial oxidative metabolism is required for the cardiac differentiation of stem cells. *Nat Clin Pract Cardiovasc Med.* 4 Suppl 1:S60-7.
- Chung S, DK Arrell, RS Faustino, A Terzic, and PP Dzeja.** 2010. Glycolytic network restructuring integral to the energetics of embryonic stem cell cardiac differentiation. *J Mol Cell Cardiol.* 48:725-34.
- Coleman ME, F DeMayo, KC Yin, HM Lee, R Geske, C Montgomery, and RJ Schwartz.** 1995. Myogenic vector expression of insulin-like growth factor I stimulates muscle cell differentiation and myofiber hypertrophy in transgenic mice. *J Biol Chem.* 270:12109-16.
- Crabtree GR.** 1999. Generic signals and specific outcomes: signaling through Ca²⁺, calcineurin, and NF-AT. *Cell.* 96:611-4.
- Creemers EE, LB Sutherland, J Oh, AC Barbosa, and EN Olson.** 2006. Coactivation of MEF2 by the SAP domain proteins myocardin and MASTR. *Mol Cell.* 23:83-96.
- Cserjesi P, B Lilly, C Hinkley, M Perry, and EN Olson.** 1994. Homeodomain protein MHox and MADS protein myocyte enhancer-binding factor-2 converge on a common element in the muscle creatine kinase enhancer. *J Biol Chem.* 269:16740-5.

- Czubryt MP, J McAnally, GI Fishman, and EN Olson.** 2003. Regulation of peroxisome proliferator-activated receptor γ coactivator 1 α (PGC-1 α) and mitochondrial function by MEF2 and HDAC5. *Proc Natl Acad Sci USA.* 100:1711-1716.
- DeFronzo RA, E Ferrannini, Y Sato, P Felig, and J Wahren.** 1981. Synergistic interaction between exercise and insulin on peripheral glucose uptake. *J Clin Invest.* 68:1468-74.
- De Val S, NC Chi, SM Meadows, S Minovitsky, JP Anderson, IS Harris, ML Ehlers, P Agarwal, A Visel, SM Xu, LA Pennacchio, I Dubchak, PA Krieg, DY Stainier, and BL Black.** 2008. Combinatorial regulation of endothelial gene expression by ets and forkhead transcription factors. *Cell.* 135:1053-64.
- Dodou E, SM Xu, and BL Black.** 2003. *mef2c* is activated directly by myogenic basic helix-loop-helix proteins during skeletal muscle development in vivo. *Mech Dev.* 120:1021-32.
- Dodou E, MP Verzi, JP Anderson, SM Xu, and BL Black.** 2004. *Mef2c* is a direct transcriptional target of ISL1 and GATA factors in the anterior heart field during mouse embryonic development. *Development.* 131:3931-42.
- Dolinsky VW and JR Dyck.** 2006. Role of AMP-activated protein kinase in healthy and diseased hearts. *Am J Physiol Heart Circ Physiol.* 291:H2557-H2569.
- Edmondson DG, TC Cheng, P Cserjesi, T Chakraborty, and EN Olson.** 1992. Analysis of the myogenin promoter reveals an indirect pathway for positive autoregulation mediated by the muscle-specific enhancer factor MEF-2. *Mol Cell Biol.* 12:3665-77.
- Edmondson DG, GE Lyons, JF Martin, and EN Olson.** 1994. *Mef2* gene expression marks the cardiac and skeletal muscle lineages during mouse embryogenesis. *Development.* 120:1251-1263.
- Freeman H and RD Cox.** 2006. Type-2 diabetes: a cocktail of genetic discovery. *Hum Mol Genet.* 15 Spec No 2:R202-9.
- Gallagher EJ, D Leroith, and E Karnieli.** 2010. Insulin resistance in obesity as the underlying cause for the metabolic syndrome. *Mt Sinai J Med.* 77:511-23.
- Garry DJ, RS Bassel-Duby, JA Richardson, J Grayson, PD Neuffer, and RS Williams.** 1996. Postnatal development and plasticity of specialized muscle fiber characteristics in the hindlimb. *Dev Genet.* 19:146-56.
- Glass DJ.** 2005. Skeletal muscle hypertrophy and atrophy signaling pathways. *Int J Biochem Cell Biol.* 37:1974-84.

- Goldhamer DJ, BP Brunk, A Faerman, A King, M Shani, and CP Emerson Jr.** 1995. Embryonic activation of the *myoD* gene is regulated by a highly conserved distal control element. *Development*. 121:637-49.
- Gollnick PD, B Sjödin, J Karlsson, E Jansson, and B Saltin.** 1974. Human soleus muscle: a comparison of fiber composition and enzyme activities with other leg muscles. *Pflugers Arch*. 348:247-55.
- Gundersen K.** 2010. Excitation-transcription coupling in skeletal muscle: the molecular pathways of exercise. *Biol Rev Camb Philos Soc*. Epub ahead of print.
- Habara-Ohkubo A.** 1996. Differentiation of beating cardiac muscle cells from a derivative of P19 embryonal carcinoma cells. *Cell Struct Funct*. 21:101-10.
- Hadchouel J, JJ Carvajal, P Daubas, L Bajard, T Chang, D Rocancourt, D Cox, D Summerbell, S Tajbakhsh, PW Rigby, and M Buckingham.** 2003. Analysis of a key regulatory region upstream of the *Myf5* gene reveals multiple phases of myogenesis, orchestrated at each site by a combination of elements dispersed throughout the locus. *Development*. 130:3415-26.
- Han J, Y Jiang, Z Li, VV Kravchenko, and RJ Ulevitch.** 1997. Activation of the transcription factor MEF2C by the MAP kinase p38 in inflammation. *Nature*. 386:296-9.
- Hargreaves M.** 2004. Muscle glycogen and metabolic regulation. *Proc Nutr Soc*. 63:217-20.
- Hassid WZ and S Abraham.** 1957. Chemical procedures for analysis of polysaccharide I. Determination of glycogen and starch – Determination of glycogen with the anthron reagent. *Methods Enzymol* 3:35-36.
- Heidt AB and BL Black.** 2005. Transgenic mice that express Cre recombinase under control of a skeletal muscle-specific promoter from *mef2c*. *Genesis*. 42:28-32.
- Heidt A.** 2006. Transcriptional Regulation Skeletal Muscle Development. Doctoral dissertation, University of California, San Francisco, USA.
- Hickey MS, JO Carey, JL Azevedo, JA Houmard, WJ Pories, RG Israel, and GL Dohm.** 1995. Skeletal muscle fiber composition is related to adiposity and in vitro glucose transport rate in humans. *Am J Physiol*. 268:E453-7.
- Himits Y and SM Hughes.** 2007. Mef2s are required for thick filament formation in nascent muscle fibres. *Development*. 134:2511-9.
- Hogan B, R Beddington, F Constantini, and E Lacy.** 1994. *Manipulating The Mouse Embryo*. Plainview, NY: Cold Spring Harbor Laboratory Press.

Holloszy JO and EF Coyle. 1984. Adaptations of skeletal muscle to endurance exercise and their metabolic consequences. *J Appl Physiol.* 56:831-8.

Holmes BF, DP Sparling, AL Olson, WW Winder, and GL Dohm. 2005. Regulation of muscle GLUT4 enhancer factor and myocyte enhancer factor 2 by AMP-activated protein kinase. *Am J Physiol Endocrinol Metab.* 289:E1071-6.

Horton RM, HD Hunt, SN Ho, JK Pullen, and LR Pease. 1989. Engineering hybrid genes without the use of restriction enzymes: gene splicing by overlap extension. *Gene.* 77:61-68.

Izumiya Y, T Hopkins, C Morris, K Sato, L Zeng, J Viereck, JA Hamilton, N Ouchi, NK LeBrasseur, and K Walsh. 2008. Fast/Glycolytic muscle fiber growth reduces fat mass and improves metabolic parameters in obese mice. *Cell Metab.* 7:159-72.

Kelley DE, MA Mintun, SC Watkins, JA Simoneau, F Jadali, A Fredrickson, J Beattie, and R Thériault. 1996. The effect of non-insulin-dependent diabetes mellitus and obesity on glucose transport and phosphorylation in skeletal muscle. *J Clin Invest.* 97:2705-13.

Keren A, Y Tamir, and E Bengal. 2006. The p38 MAPK signaling pathway: a major regulator of skeletal muscle development. *Mol Cell Endocrinol.* 252:224-30.

Khiem D, JG Cyster, JJ Schwarz, and BL Black. 2008. A p38 MAPK-MEF2C pathway regulates B-cell proliferation. *Proc Natl Acad Sci USA.* 105:17067-72.

Knight JB, CA Eyster, BA Griesel, and AL Olson. 2003. Regulation of the human GLUT4 gene promoter: interaction between a transcriptional activator and myocyte enhancer factor 2A. *Proc Natl Acad Sci USA.* 100:14725-30.

Kothary R, S Clapoff, S Darling, MD Perry, LA Moran, and J Rossant. 1989. Inducible expression of an hsp68-lacZ hybrid gene in transgenic mice. *Development.* 105:707-714.

Krook A, M Björnholm, D Galuska, XJ Jiang, R Fahlman, MG Myers Jr, H Wallberg-Henriksson, and JR Zierath. 2000. Characterization of signal transduction and glucose transport in skeletal muscle from type 2 diabetic patients. *Diabetes.* 49:284-92.

Lai KM, M Gonzalez, WT Poueymirou, WO Kline, E Na, E Zlotchenko, TN Stitt, AN Economides, GD Yancopoulos, and DJ Glass . 2004. Conditional activation of akt in adult skeletal muscle induces rapid hypertrophy. *Mol Cell Biol.* 24:9295-304.

Latinkic BV, B Cooper, N Towers, D Sparrow, S Kotecha, and TJ Mohun. 2002. Distinct enhancers regulate skeletal and cardiac muscle-specific expression programs of the cardiac alpha-actin gene in *Xenopus* embryos. *Dev Biol.* 245:57-70.

- Laverriere AC, C MacNeill, C Mueller, RE Poelmann, JB Burch, and T Evans.** 1994. GATA-4/5/6, a subfamily of three transcription factors transcribed in developing heart and gut. *J Biol Chem.* 269:23177-84.
- Li L, Z Liu, B Mercer, P Overbeek, and EN Olson.** 1997. Evidence for serum response factor-mediated regulatory networks governing SM22 α transcription in smooth, skeletal, and cardiac muscle cells. *Dev Biol.* 187:311-321.
- Lilly B, EN Olson, and MC Beckerle.** 2001. Identification of a CArG box-dependent enhancer within the cysteine-rich protein 1 gene that directs expression in arterial but not venous or visceral smooth muscle cells. *Dev Biol.* 240:531-547.
- Lin J, H Wu, PT Tarr, CY Zhang, Z Wu, O Boss, LF Michael, P Puigserver, E Isotani, EN Olson, BB Lowell, R Bassel-Duby, and BM Spiegelman.** 2002. Transcriptional co-activator PGC1 alpha drives the formation of slow-twitch muscle fibres. *Nature.* 418:797-801.
- Lin Q, J Schwarz, C Bucana, and EN Olson.** 1997. Control of mouse cardiac morphogenesis and myogenesis by transcription factor MEF2C. *Science.* 276:1404-1407.
- Linder CC and MT Davisson.** 2004. Strains, Stocks, and Mutant Mice. In H. Hedrich (Ed.), *The Laboratory Mouse* (pp. 25-46). London: Elsevier Academic Press.
- Liu ML, AL Olson, NP Edgington, WS Moye-Rowley, and JE Pessin.** 1994. Myocyte enhancer factor 2 (MEF2) binding site is essential for C2C12 myotube-specific expression of the rat GLUT4/muscle-adipose facilitative glucose transporter gene. *J Biol Chem.* 269:28514-21.
- Lopaschuk GD, JR Ussher, CDL Folmes, JS Jaswal, and WC Stanley.** 2010. Myocardial fatty acid metabolism in health and disease. *Physiol Rev.* 90:207-258.
- Lopaschuk GD and JS Jaswal.** 2010. Energy metabolic phenotype of the cardiomyocyte during development, differentiation, and postnatal maturation. *J Cardiovasc Pharmacol.* 56:130-140.
- Lu J, TA McKinsey, RL Nicol, and EN Olson.** 2000a. Signal-dependent activation of the MEF2 transcription factor by dissociation from histone deacetylases. *Proc Natl Acad Sci USA.* 97:4070-5.
- Lu J, TA McKinsey, CL Zhang, and EN Olson.** 2000b. Regulation of skeletal myogenesis by association of the MEF2 transcription factor with class II histone deacetylases. *Mol Cell.* 6:233-44.
- Lyons GE and ME Buckingham.** 1992. Developmental regulation of myogenesis in the mouse. *Semin Dev Biol.* 3:243-253.

Lyons I, LM Parsons, L Hartley, R Li, JE Andrews, L Robb, and RP Harvey. 1995. Myogenic and morphogenetic defects in the heart tubes of murine embryos lacking the homeo box gene *Nkx2-5*. *Genes Dev.* 9:1654-66.

Manabe I and GK Owens. 2001. CArG elements control smooth muscle subtype specific expression of smooth muscle myosin in vivo. *J Clin Invest.* 107:823-834.

Martin JF, JJ Schwarz, and EN Olson. 1993. Myocyte enhancer factor (MEF) 2C: A tissue-restricted member of the MEF-2 family of transcription factors. *Biochemistry.* 90: 5282-5286.

Mayor C, M Brudno, JR Schwartz, A Poliakov, EM Rubin, KA Frazer, LS Pachter, and I Dubchak. 2000. VISTA: visualization global DNA sequence alignments of arbitrary length. *Bioinformatics.* 16:1046-1047.

McKinsey TA, CL Zhang, and EN Olson. 2000. Activation of the myocyte enhancer factor-2 transcription factor by calcium/calmodulin-dependent protein kinase-stimulated binding of 14-3-3 to histone deacetylase 5. *Proc Natl Acad Sci USA.* 97:14400-5.

McKinsey TA, CL Zhang, and EN Olson. 2001. Identification of a signal-responsive nuclear export sequence in class II histone deacetylases. *Mol Cell Biol.* 21:6312-21.

Miano JM, JM Carlson, JA Spencer, and RP Misra. 2000. Serum response factor-dependent regulation of the smooth muscle calponin gene. *J Biol Chem.* 275:9814-9822.

Michael LF, Z Wu, RB Cheatham, P Puigserver, G Adelmant, JJ Lehman, DP Kelly, and BM Spiegelman. 2001. Restoration of insulin-sensitive glucose transporter (GLUT4) gene expression in muscle cells by the transcriptional coactivator PGC-1. *Proc Natl Acad Sci USA.* 98:3820-5.

Miska EA, C Karlsson, E Langley, SJ Nielsen, J Pines, and T Kouzarides. 1999. HDAC4 deacetylase associates with and represses the MEF2 transcription factor. *EMBO J.* 18:5099-107.

Moelling K, K Schad, M Bosse, S Zimmermann, and M Schweneker. 2002. Regulation of Raf-Akt Cross-talk. *J Biol Chem.* 277:31099-106.

Muñoz JP, A Collao, M Chiong, C Maldonado, T Adasme, L Carrasco, P Ocaranza, R Bravo, L Gonzalez, G Díaz-Araya, C Hidalgo, and S Lavandero. 2009. The transcription factor MEF2C mediates cardiomyocyte hypertrophy induced by IGF-1 signaling. *Biochem Biophys Res Commun.* 388:155-60.

Musarò A, KJ McCullagh, FJ Naya, EN Olson, and N Rosenthal. 1999. IGF-1 induces skeletal myocyte hypertrophy through calcineurin in association with GATA-2 and NF-ATc1. *Nature.* 400:581-5.

- Nagy A.** 2000. Cre recombinase: the universal reagent for genome tailoring. *Genesis*. 26:99-109.
- Naya FJ, C Wu, JA Richardson, P Overbeek, and EN Olson.** 1999. Transcriptional activity of MEF2 during mouse embryogenesis monitored with a MEF2-dependent transgene. *Development*. 126:2045-52.
- Naya FJ, B Mercer, J Shelton, JA Richardson, RS Williams, and EN Olson.** 2000. Stimulation of slow skeletal muscle fiber gene expression by calcineurin in vivo. *J Biol Chem*. 275:4545-8.
- Naya FJ, BL Black, H Wu, R Bassel-Duby, JA Richardson, JA Hill, and EN Olson.** 2002. Mitochondrial deficiency and cardiac sudden death in mice lacking the MEF2A transcription factor. *Nat Med*. 8:1303-1309.
- Ontell M and K Kozeka.** 1984. The organogenesis of murine striated muscle: a cytoarchitectural study. *Am J Anat*. 171:133-48.
- Orkin SH.** 1992. GATA-binding transcription factors in hematopoietic cells. *Blood*. 80:575-81.
- Ornatsky OI, DM Cox, P Tangirala, JJ Andreucci, ZA Quinn, JL Wrana, R Prywes, YT Yu, and JC McDermott.** 1999. Post-translational control of the MEF2A transcriptional regulatory protein. *Nucleic Acids Res*. 27:2646-54.
- Parsons SA, BJ Wilkins, OF Bueno, and JD Molkentin.** 2003. Altered skeletal muscle phenotypes in calcineurin A α and A β gene-targeted mice. *Mol Cell Biol*. 23:4331-43.
- Pette D and C Spamer.** 1986. Metabolic properties of muscle fibers. *Fed Proc*. 45:2910-4.
- Pipes GC, EE Creemers, and EN Olson.** 2006. The myocardin family of transcriptional coactivators: versatile regulators of cell growth, migration, and myogenesis. *Genes Dev*. 20:1545-56.
- Plum L, FT Wunderlich, S Baudler, W Krone, and JC Brüning.** 2005. Transgenic and knockout mice in diabetes research: novel insights into pathophysiology, limitations, and perspectives. *Physiology (Bethesda)*. 20:152-61.
- Potthoff MJ and EN Olson.** 2007a. MEF2: a central regulator of diverse developmental programs. *Development*. 134:4131-40.
- Potthoff MJ, H Wu, MA Arnold, JM Shelton, J Backs, J McAnally, JA Richardson, R Bassel-Duby, and EN Olson.** 2007b. Histone deacetylase degradation and MEF2 activation promote the formation of slow-twitch myofibers. *J Clin Invest*. 117:2459-67.

Potthoff MJ, MA Arnold, J McAnally, JA Richardson, R Bassel-Duby, and EN Olson. 2007c. Regulation of skeletal muscle sarcomere integrity and postnatal muscle function by *Mef2c*. *Mol Cell Biol.* 27:8143-51.

Puigserver P, Z Wu, CW Park, R Graves, M Wright, and BM Spiegelman. 1998. A cold-inducible coactivator of nuclear receptors linked to adaptive thermogenesis. *Cell.* 92:829-39.

Rawls A, JH Morris, M Rudnicki, T Braun, HH Arnold, WH Klein, and EN Olson. 1995. Myogenin's functions do not overlap with those of MyoD or Myf-5 during mouse embryogenesis. *Dev Biol.* 172:37-50.

Reecy JM, X Li, M Yamada, FJ DeMayo, CS Newman, RP Harvey, and RJ Schwartz. 1999. Identification of upstream regulatory regions in the heart-expressed homeobox gene *Nkx2-5*. *Development.* 126:839-49.

Rojas A, S De Val, AB Heidt, SM Xu, J Bristow, and BL Black. 2005. *Gata4* expression in lateral mesoderm is downstream of BMP4 and is activated directly by Forkhead and GATA transcription factors through a distal enhancer element. *Development.* 132:3405-17.

Rommel C, BA Clarke, S Zimmermann, L Nuñez, R Rossman, K Reid, K Moelling, GD Yancopoulos, and DJ Glass. 1999. Differentiation stage-specific inhibition of the Raf-MEK-ERK pathway by Akt. *Science.* 286:1738-41.

Russell B, D Motlagh, and WW Ashley. 2000. Form follows function: how muscle shape is regulated by work. *J Appl Physiol.* 88:1127-32.

Russell RR 3rd, J Li, DL Coven, M Pypaert, C Zechner, M Palmeri, FJ Giordano, J Mu, MJ Birnbaum, and LH Young. 2004. AMP-activated protein kinase mediates ischemic glucose uptake and prevents postischemic cardiac dysfunction, apoptosis, and injury. *J Clin Invest.* 114:495-503.

Ryder JW, J Yang, D Galuska, J Rincón, M Björnholm, A Krook, S Lund, O Pedersen, H Wallberg-Henriksson, JR Zierath, and GD Holman. 2000. Use of a novel impermeable biotinylated photolabeling reagent to assess insulin- and hypoxia-stimulated cell surface GLUT4 content in skeletal muscle from type 2 diabetic patients. *Diabetes.* 49:647-54.

Sarnat HB. 1983. *Muscle Pathology and Histochemistry*. Chicago, IL: American Society of Clinical Pathologists Press.

Sauer B and N Henderson. 1988. Site-specific DNA recombination in mammalian cells by the Cre recombinase of bacteriophage P1. *Proc Natl Acad Sci USA.* 85:5166-70.

- Schiaffino S and C Reggiani.** 1996. Molecular diversity of myofibrillar proteins: gene regulation and functional significance. *Physiol Rev.* 76:371-423.
- Schrauwen P and ML Hesselink.** 2004. Oxidative capacity, lipotoxicity, and mitochondrial damage in type 2 diabetes. *Diabetes.* 53:1412-7.
- Searcy RD, EB Vincent, CM Liberatore, and KE Yutzey.** 1998. A GATA-dependent *nkx-2.5* regulatory element activates early cardiac gene expression in transgenic mice. *Development.* 125:4461-70.
- Shimizu RT, RS Blank, R Jervis, SC Lawrenz-Smith, and GK Owens.** 1995. The smooth muscle actin gene promoter is differentially regulated in smooth muscle versus non-smooth muscle cells. *J Biol Chem.* 270:7631-7643.
- Shyu KG, WH Ko, WS Yang, BW Wang, and P Kuan.** 2005. Insulin-like growth factor-1 mediates stretch-induced upregulation of myostatin expression in neonatal rat cardiomyocytes. *Cardiovasc Res.* 68:405-14.
- Slot JW, HJ Geuze, S Gigengack, DE James, and GE Lienhard.** 1991. Translocation of the glucose transporter GLUT4 in cardiac myocytes of the rat. *Proc Natl Acad Sci USA.* 88:7815-9.
- Smith AG and GE Muscat.** 2005. Skeletal muscle and nuclear hormone receptors: implications for cardiovascular and metabolic disease. *Int J Biochem Cell Biol.* 37:2047-63.
- Soriano P.** 1999. Generalized *lacZ* expression with the ROSA26 Cre reporter strain. *Nat Genet.* 21:70-1.
- Stitt TN, D Drujan, BA Clarke, F Panaro, Y Timofeyva, WO Kline, M Gonzalez, GD Yancopoulos, and DJ Glass.** 2004. The IGF-1/PI3K/Akt pathway prevents expression of muscle atrophy-induced ubiquitin ligases by inhibiting FOXO transcription factors. *Mol Cell.* 14:395-403.
- Stump CS, EJ Henriksen, Y Wei, and JR Sowers.** 2006. The metabolic syndrome: role of skeletal muscle metabolism. *Ann Med.* 38:389-402.
- Sweeney G, R Somwar, T Ramlal, A Volchuk, A Ueyama, and A Klip.** 1999. An inhibitor of p38 mitogen-activated protein kinase prevents insulin-stimulated glucose transport but not glucose transporter translocation in 3T3-L1 adipocytes and L6 myotubes. *J Biol Chem.* 274:10071-8.
- Taha M and GD Lopaschuk.** 2007. Alterations in energy metabolism in cardiomyopathies. *Ann Med.* 39:594-607.

- Thai MV, S Guruswamy, KT Cao, JE Pessin, and AL Olson.** 1998. Myocyte enhancer factor 2 (MEF2)-binding site is required for GLUT4 expression in transgenic mice. Regulation of MEF2 DNA binding activity in insulin-deficient diabetes. *J Biol Chem.* 273:14285-14292.
- Thompson JD, DG Higgins, and TJ Gibson.** 1994. CLUSTAL W: improving the sensitivity of progressive multiple sequence alignment through sequence weighting, position-specific gap penalties and weight matrix choice. *Nucleic Acids Res.* 22:4673-4680.
- Viollet B, Y Athes, R Mounier, B Guigas, E Zarrinpashneh, S Horman, L Lantier, S Hebrard, J Devin-Leclerc, C Beauloye, M Foretz, F Andreelli, R Ventura-Clapier, and L Bertrand.** 2009. AMPK: Lessons from transgenic and knockout animals. *Front Biosci.* 14:19-44.
- Vong LH, MJ Ragusa, and JJ Schwarz.** 2005. Generation of conditional *Mef2c^{loxP/loxP}* mice for temporal- and tissue-specific analyses. *Genesis.* 43:43-8.
- Wang LH, R Chmelik, and M Nirenberg.** 2002. Sequence-specific DNA binding by the *vnd/NK-2* homeodomain of *Drosophila*. *Proc Natl Acad Sci USA.* 99:12721-6.
- Wang YX, CL Zhang, RT Yu, HK Cho, MC Nelson, CR Bayuga-Ocampo, J Ham, H Kang, and RM Evans.** 2004. Regulation of muscle fiber type and running endurance by PPARdelta. *PLoS Biol.* 2:e294.
- Wang Z, DZ Wang, GC Teg Pipes, and EN Olson.** 2003. Myocardin is a master regulator of smooth muscle gene expression. *Proc Natl Acad Sci USA.* 100:7129-7134.
- Wilkinson DG and MA Nieto.** 1993. Detection of messenger RNA by in situ hybridization to tissue sections and whole mounts. *Methods Enzymol.* 225:361-373.
- Wright WE, DA Sassoon, and VK Lin.** 1989. Myogenin, a factor regulating myogenesis, has a domain homologous to MyoD. *Cell.* 56:607-17.
- Wu H, FJ Naya, TA McKinsey, B Mercer, JM Shelton, ER Chin, AR Simard, RN Michel, R Bassel-Duby, EN Olson, and RS Williams.** 2000. MEF2 responds to multiple calcium-regulated signals in the control of skeletal muscle fiber type. *EMBO J.* 19:1963-73.
- Xing Y, N Musi, N Fujii, L Zou, I Luptak, MF Hirshman, LJ Goodyear, and R Tian.** 2003. Glucose metabolism and energy homeostasis in mouse hearts overexpressing dominant negative $\alpha 2$ subunit of AMP-activated protein kinase. *J Biol Chem.* 278:28372-7.
- Yang SH, A Galanis, and AD Sharrocks.** 1999. Targeting of p38 mitogen-activated protein kinases to MEF2 transcription factors. *Mol Cell Biol.* 19:4028-38.

Yee SP and PW Rigby. 1993. The regulation of *myogenin* gene expression during the embryonic development of the mouse. *Genes Dev.* 7:1277-1289.

Zarrinpashneh E, K Carjaval, C Beauloye, A Ginion, P Mateo, AC Pouleur, S Horman, S Vaulont, J Hoerter, B Viollet, L Hue, JL Vanoverschelde, and L Bertrand. 2006. Role of the $\alpha 2$ -isoform of AMP-activated protein kinase in the metabolic response of the heart to no-flow ischemia. *Am J Physiol Heart Circ Physiol.* 291:H2875-83.

Zarrinpashneh E, C Beauloye, A Ginion, AC Pouleur, X Havaux, L Hue, B Viollet, JL Vanoverschelde, and L Bertrand. 2008. AMPK $\alpha 2$ counteracts the development of cardiac hypertrophy induced by isoproterenol. *Biochem Biophys Res Commun.* 376:677-81.

Zetser A, E Gredinger, and E Bengal. 1999. p38 mitogen-activated protein kinase pathway promotes skeletal muscle differentiation. Participation of the Mef2c transcription factor. *J Biol Chem.* 274:5193-200.

Zhang CL, TA McKinsey, S Chang, CL Antos, JA Hill, and EN Olson. 2002. Class II histone deacetylases act as signal-responsive repressors of cardiac hypertrophy. *Cell.* 110:479-88.

Zhao M, L New, VV Kravchenko, Y Kato, H Gram, F di Padova, EN Olson, RJ Ulevitch, and J Han. 1999. Regulation of the MEF2 family of transcription factors by p38. *Mol Cell Biol.* 19:21-30.

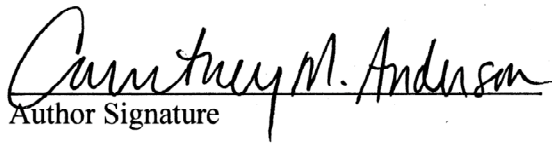
Zon LI, C Mather, S Burgess, ME Bolce, RM Harland, and SH Orkin. 1991. Expression of GATA-binding proteins during embryonic development in *Xenopus laevis*. *Proc Natl Acad Sci USA.* 88:10642-6.

Publishing Agreement

It is the policy of the University to encourage the distribution of all theses, dissertations, and manuscripts. Copies of all UCSF theses, dissertations, and manuscripts will be routed to the library via the Graduate Division. The library will make all theses, dissertations, and manuscripts accessible to the public and will preserve these to the best of their abilities, in perpetuity.

Please sign the following statement:

I hereby grant permission to the Graduate Division of the University of California, San Francisco to release copies of my thesis, dissertation, or manuscript to the Campus Library to provide access and preservation, in whole or in part, in perpetuity.


Author Signature

1/3/11
Date